MULTIFUNCTIONAL CARBON NANOTUBE THIN FILM COMPOSITES BY LAYER-BY-LAYER ASSEMBLY TECHNIQUE

by

Bong Sup Shim

A dissertation submitted in partial fulfillment
of the requirements for the degree of
Doctor of Philosophy
(Chemical Engineering)
in The University of Michigan
2009

Doctoral Committee:

Professor Nicholas A. Kotov, Chair

Professor Erdogan Gulari

Professor John Kieffer

Professor David Martin

To my LORD, Jesus

And

To my beloved wife, Jae Won

Acknowledgements

As a non-native English writer, I am getting used to express my thinking and knowledge, but still feel very poor at showing my thankful heart. With my best, "Thank you, Professor Nicholas A. Kotov. You are wonderful". Without Professor Kotov, this quality of thesis may not exist. He was always helpful, kind, and patient to me during the studies. He also provided me a full of great opportunities as much as I can handle. His guidance was so much advanced and his ideas were always brilliant. Definitely, he is my best advisor, mentor, leader, motivator, and model. I respect him sincerely as my Professor.

Secondly, I'd like to show my best gratitude to Professor Erdogan Gulari, Dr. Zhiyong Tang, Dr. Paul Podsiadlo. They were not just excellent, but also helped me greatly to finish my Ph D studies in many situations. I also want to thank members of my committee: Professor John Kieffer, Professor David Martin for helpful comments. Working with Professor Jerome Lynch and his group was also great experience to me. Professor Joerg Lahann and Professor Max Shtein also suggested me many helpful advices.

All of Kotov group members are the direct contributors on this thesis. Jian Zhu, Edward Jan, Dr. Jaebeom Lee, Dr. Sudhanshu Srivastava, Jungwoo Lee, Peter Ho, Dr. Kevin Critchley, Dr. Vladimir Sinani, Ashish Agarwal, Dr. Christ Doty, Meghan Cuddihy, Daniel Lilly, Joong Bahng, Dr. Soo-hwan Jeong, Ming Qin, Christine Andreas, Dr. Marc Michel, Dr. Ying Wang, Dr. Alex Sinyagin, Dr. Shan Wickramanayake, Darren Lee, Dr. Ki-Sub Kim, Dr. Vincent Ball, and all the undergraduate students who worked with me in the lab should be acknowledged as contributors to this thesis.

I also like to share my thanks to other U-M people. Dr. Onnop Srivannavit, Dr. Yongmei Xia, and Woog Hee Lee in Gulari Lab. Dr. Kyung-Ho Roh, Dr. Hsien-Yeh Chen, and Himabindu Nandivada in Lahann Lab. Dr. Jihua Chen, Charles Shaw, and Jinghang Wu in Martin Lab. Dr. Haiping Sun, and Kai Sun in EMAL. Lang Sui in Kieffer Lab. Dr. Paddy Chan, Kwang Hyup An and Abhishek Yadav in Pipe Lab. Hyun Joon Kim in Green Lab. They are all my research collaborators. I also want to thank Ms. Ruby Sowards and Susan Hamlin for their assistance.

I'd like to also thank Rev. Hwang. You are very special to me. KPCAA members including Dong Jun Seo, Young Jae Kang, and everyone else were also good supporters during my Ph. D Studies.

I also want to share this Joy with my parents and my parent-in-laws who brought me up and supported me all the time. My two kids, Rebecca Yejin and Esther Yeeun, were also wonderful gifts to me in AA.

My wife, Jaewon, should be mentioned properly, but I don't know how. I will never forget your encouragements, cares, and supports during this studies. Indeed, I am one of the luckiest husbands in the world.

Finally, I'd like to thank my Lord, Jesus Christ. The Creator of this wonderful universe directed me to U-M six years ago and provided me everything generously. During my Ph. D. studies, amazing God also let me know what is 'Truth' and what is 'Love'. I'll pursue this 'Truth & Love' for all my life. Thanks.

Preface

Polymeric layer-by-layer (LBL) assembly offers a pathway for multifunctional / multicomponent materials with molecular-scale control of stratified structures. Among the wide variety nanoscale building blocks such as nanowires and nanodots, single-walled carbon nanotubes (SWNTs) are regarded as one of the most versatile because of their superior mechanical and electrical properties as well as geometrical perfection. In this thesis, LBL assembled SWNT thin film nanocomposites with high mechanical strength/toughness and with high electrical/optical properties are presented. Exceptional exfoliation state of SWNTs and controlled nm-thick layered structures are the basis for achieving tunable physical properties. Highly anisotropic features of SWNTs are translated into 2 dimensional alignments by meniscus combing technique during LBL assemblies. Advanced LBL assemblies by dewetting methods are also introduced, which significantly accelerate the process with improved lateral organization of nanowires. Furthermore, SWNT composite coating on commodity cotton yarns produced intelligent electronic textiles (e-textiles) with intrinsic humidity sensibility. This e-textile has been further combined with antigen/antibody sensing capability in order to develop a selective albumin biosensor which provides a direct route for the application of these materials as wearable biomonitoring and telemedicine sensors.

Table of Contents

List of Figures

List of Tables

Chapter I

Introduction

A. Layer-by-Layer Nano-Scale Assembly

Our modern era is now experiencing new materials revolution initiated by nano-science. Among many dimensions of nanosciences, nano-scale assemblies provide one of the most practical tools to improve our daily life by providing advanced nano-scale functional materials. Nanoscale materials, although finding their new properties is still under active research, allow us to select materials with functional continuity and with new exclusive functionality. This nanoscale assembly covers wide spectrums of chemical and physical processes. Top-down and bottom-up classification are also used by the construction methods of nanoscale objects. There are many reviews[1-5] on the classification of nanoscale process. Here, as the nanoprocess already becomes a big general term, we focus on 'layer-by-layer assembly' which is one of two-dimensional bottom-up chemical nano-assembly techniques driven by supra-molecular interactions.

Layer-by-layer (LBL) assembly has been introduced since early 1990s.[6] The assembly has been systematically built as collective nanofabrication tools by a few pioneers such as G. Decher,[7] M. Rubner,[8-11] and N. Kotov[12, 13] during mid 1990s. This

LBL assembly is currently one of the most dynamic nanofabrication techniques because of its versatility, simplicity, robustness, and nanostructural controllability. First, LBL is versatile in materials selection and combination. Ideally, perfect monolayers of organic and inorganic macromolecules such as quantum-dots (QDs),[14] nanowires (NWs),[15] nanoplatelets,[16] complex nanomaterials,[17] polymers, proteins,[18] and even viruses[19, 20] can be coated on a desired substrate such as silicon, glass, metal, polymers, biological soft materials, and even micro-/nano- objects. Second, LBL is simple in operating process. The LBL process is generally consisted with three steps of dipping, rinsing, and drying. Thus, the whole process can be easily automated and scaled-up. Third, LBL assembly is robust by its reproducible material structures and qualities. Forth, LBL has unique nanostructural controllability because the thickness of each layers can be tuned in 1 ~ 100 nm ranges by varying LBL process conditions. More details about the advantages of LBL assemblies for materials structures, molecular characteristics, functional properties, and applications are discussed in the following chapters.

The original LBL assembly was introduced as a preparation technique of ultrathin multilayer films of two polymers: polyanion and polycation. Thus, this electrostatic attraction provides mechanistic understanding of LBL assembly although the actual driving forces of LBL assembly are the combinations of all exerting weak forces such as van der Waals, hydrogen, and hydrophobic interactions. Schematics in figure 1 summarize the operating procedures of LBL assemblies. Generally, this LBL assembly builds nano-architecture layers of at least two components and more. The unique features of LBL structures are originated from (a) strong molecular binding between adjacent

layers and to whole LBL structures because each layering adsorption happens by overcoming stabilization forces of a solution and (b) nano-thin layers whose qualities are guaranteed by rinsing steps. This traditional concept of LBL assembly developed to fabrication of molecularly organized nanocomposites by substituting one polymeric component to other functional materials such as carbon nanotubes (CNTs), aluminosilicate platelets, semiconducting nanoparticles, and inorganic NWs. Recently, a new processing techniques have been introduced as advanced LBL assemblies, which include the dewetting mode LBL assembly without rinsing steps[17] or the inorganic-only LBL assembly with nanoparticles.[21]

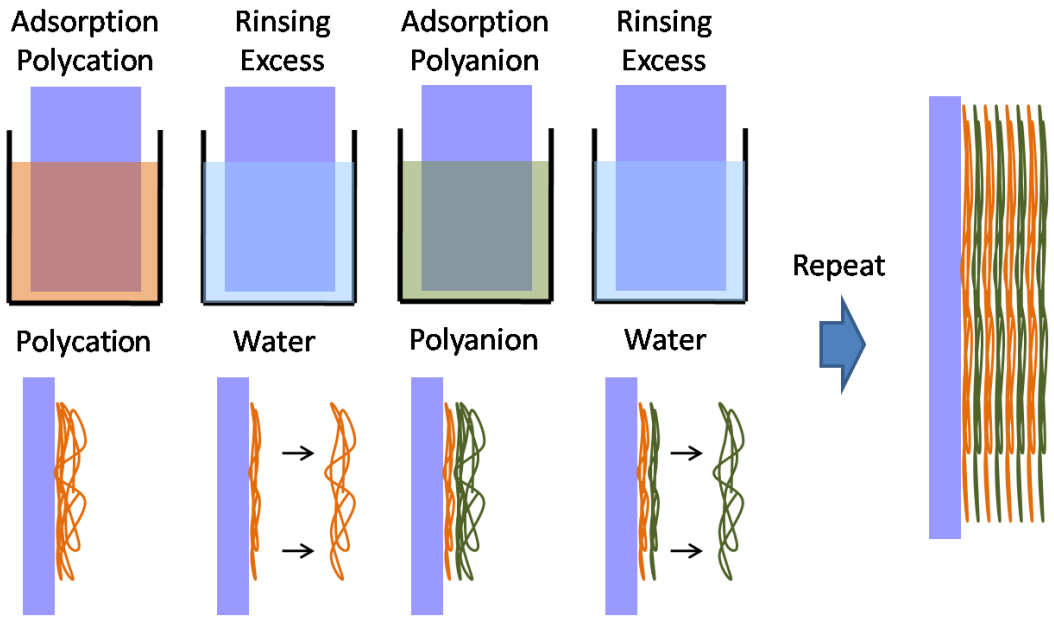

Figure 1 Schematic representations of the traditional layer-by-layer assembly. One complete LBL cycle consists of adsorption of polycation, rinsing of excess polycation, adsorption of polyanion, and rinsing of excess polyanion. Repeating this cycle forms LBL multi-layers.

The functional materials by LBL assembly were developed to fill the challenges in conventional nanocomopsite applications and to open a new novel complex material utilization. First, engineering materials provide continuous research opportunities for the current industrial applications. The particular interest of these polymeric nanocomposite research focuses on the elemental structural properties: physical/chemical, electrical,[22] thermal, and mechanical.[23] Example lists of these specific properties for the current industrial applications are summarized in table 1. Among them, strong,[15] tough, stiff,[24] electrically conductive,[22] anti-corrosive[25] thin films have been introduced or are now being actively prepared by LBL assembly of structural nanocomposites. Second, exceptional structural advantages of LBL assembled nanocomposites, however, drove more researches to focus on novel, complex, and smart materials applications such as sensor,[26] fuel cell,[27] transducer,[28] drug delivery,[29] tissue engineering scaffolds,[30] and next generation electronic materials.[31]

Among all the nano functional materials, CNTs are the frontiers of these researches because of significantly improved and unusual properties. Besides having been one of the most widely used nano-fillers in LBL functional nanocomposites, the CNTs are available with commercialized standard qualities, which is one of the most crucial challenges for emerging technologies like nano-science. It allows general comparative standards about the efficiencies of transferring the properties of nanoblocks into organized LBL composites because of the large quantity availability with widely known materials performances unlike laboratory prepared nanomaterials. From the

subsection, the detailed information of these CNT nanocomposites and their functional properties is presented and matched with real-world potential applications.

Table 1. List of multicomponent composite properties for current industrial applications

Elemental property	Specific property for industrial applications
Physical / Chemical	Controlling gas permeability, Anti-corrosion, Oxidation resistance
Electrical	Electrostatic discharge (ESD), Electromagnetic interference (EMI) shielding, Lightening strike protection, Conducting adhesives
Thermal	Thermal conductivity, Thermal expansion, Thermal protection
Mechanical	Toughness, Modulus, Tensile strength, Shear strength, Compression strength,

B. Carbon Nanotubes as Nano-Building Blocks

CNTs are rolled-up structures of a perfect hexagonal carbon crystal molecular sheet as a tubular cylinder. As the carbon crystal sheet, a graphene, is the strongest known material and a zero-band gap semiconductor, CNTs have shown many unique mechanical and electrical properties by the rolling direction types and the number of walls: single-walled and multi-walled carbon nanotubes (SWNTs, MWNTs). Stiffness and toughness of CNTs are arguably known as about up to 1 TPa and 300 GPa, respectively.[32] SWNTs are tough due to inward-collapse and plastic deformation,[33] whereas MWNTs have shown unique 'sword-in-sheath' breakage pattern.[32]

Electrically, a SWNT can be either semiconducting or metallic, which can be calculated by the chiral vecter indices (*n, m*) of graphene layer.[34] Although separation of each type and production techniques of one structural kind are actively under development, overall one-third of bulk SWNTs are metallic and the rest are semiconducting. Besides the properties of each CNT, the type distribution of CNTs collectively affects the macro-scale performance of composites. Thus, the identification of CNTs type as well as controlling the distribution ratio is critical research factors for the assembly of CNT multilayers. Raman spectroscopy is widely used to extract the information of individual CNT structures and types.[35, 36] Furthermore, theoretical predictions of each type of CNTs were well documented for such as electronic, photonic and phonon dispersion states in a single CNT.[34, 37, 38]

Usually, the length of CNTs varies μm to cm ranges so that the extremely high aspect ratios of CNTs in nano-scale dimensions further enrich the application potentials. However, given the hydrophobic graphene and smooth crystalline walls, dispersion of CNTs still remains as grand challenges. Collective van der Waals forces, which exert in a CNT bundle and preventing exfoliation, dramatically increase as the length increases. Thus, currently only limited lengths under 100 μm long CNTs are employed as solution processing of CNT, which is the pre-requirements of LBL assemblies. Furthermore, two typical dispersion techniques of CNTs, which are oxidation of CNTs and interfacing with stabilizers, severely degrade, or at least modify, the properties of CNTs. Overall, tipping point of LBL assembly of CNTs originate from the widespread difficulties of uniform dispersion as well as precise controlled structural casting into a solid composite by

conventional composite processing techniques. Before we elaborate on the details of CNT LBL assembled nanocomposites, common materials principles and significant structural factors of CNT nanocomposites are briefly analyzed in two physical dimensions- mechanical and electrical properties.

1. Structural Factors of Strong CNT Nanocomposites

High mechanical properties are usually originated from high loading, uniform, and controlled dispersion of CNTs, and enhanced molecular interactions. For examples, Vigolo *et al*. developed a strong fiber with oriented SWNTs along its axis by means of flow induced spinning process.[39] They improved understanding of surfactant / SNWT / water mixture system in order to optimize the amount of surfactant to produce stable dispersion of SWNTs. With re-condensation of dispersed SWNTs in PVA solution and efficient introduction of CNT alignments, they could achieve SWNT – PVA composite fiber with exceptional orientation and loading of SWNTs. Following this spinning method, Dalton *et al.* achieved a super tough carbon nanotube fiber which has $\boldsymbol{\sigma}_{ult}$ = 1.8 GPa and $\boldsymbol{K}$ = 570 J/g with 60 wt% of SWNT loading.[40, 41]

Although high content of organized CNTs is the crucial clues of successful transfer of nano-scale CNTs' properties to macro-scale composites, however, the derivation to SWNT-polymer matrix interfacial bonding and the compositional impurities have been very poorly presented in the previous examples. To understand these effects, we need to search other classes of CNT reinforced composites, randomly oriented bulk

composites whose particular interests are how to achieve improved interfacial bonding and homogeneous distribution between CNTs and a matrix polymer. To this, many tried a load-transfer analysis[42] by observing fracture behavior in CNT composites[43-45] and by measuring energy of CNT pull-out from matrix.[46-48] Molecular simulation of CNT-polymer interaction reveals that just 1% of chemical bond formation can improve the modulus of a composite by over an order of magnitude.[49, 50] Cadek *et al.* suggested that the increased surface area[51] and crystallization of matrix polymer[52] can further improve the reinforcement efficiency of a CNT filled composite. Shortly, the factors to affect the mechanical properties of a composite are loading ratio of CNTs, organization of CNTs, interfacial bonding between CNTs and matrix, properties of polymer matrix, and exfoliation of CNTs. The more details of this mechanical strength topic are presented in the chapter II.

2. Basic Principles of Electrically Conductive CNT Nanocomposites

The most basic concept of electrical conductivities of a CNT composite is percolation theory in which the volume scalar ratio of conductive CNTs predicts the electrical conductivity of composites[53, 54] because the series of these CNTs form interconnected transport routes through insulating matrix. With advanced tools to control the nano-morphology of CNT networks, however, the recent efforts to improve electrical properties of CNT materials are more focusing on the physical/chemical states and the distribution structures of CNTs in a composites such as porosity,[55] distances between

CNTs,[56] shapes,[57] exfoliation,[22] and types of CNTs,[58, 59] than the volume of CNTs.[60] For example, controlled morphology of CNT distribution throughout the polymer matrix can dramatically reduce the percolation threshold,[57, 61] which is the minimum CNT volume ratio to make a composite to be an electrical conductor. The more details of this electrical property of CNT composites are further discussed in the chapter III.

Although specific factor optimization to the desired properties needs to be varied as shown in the brief survey, the common requirements of advanced CNT nanocomposites are (1) uniform or controlled CNT dispersion, (2) modulated interfaces between CNTs and matrix, (3) proper selection of polymer matrix, (4) directional organization of CNTs, and (5) the ability to tune nano-structures precisely. Layer-by-Layer (LBL) assembly, which satisfies almost all of these desirable processing requirements, provides one of the most efficient manipulation tools of CNTs in precise nano-scale organized structures. In addition to this molecular manipulation of CNTs, the unique advantages of LBL assembly of CNT suggest anisotropic layered organization with well-known structure controlling factors, unprecedented uniform and dense loading of CNTs, and high quality ultrathin film with conformable structure even on a complex geometry substrate.

C. Review of LBL Assembly with CNTs

The primary advantages of LBL assembly of CNTs include (1) uniform dispersion of CNTs into a composite which is enabled by direct adsorption of CNTs from

a solution to a solid state without phase segregation, (2) tunable multi-functional properties of a composite which is enabled by accurately controlled multi-component nano-layers, and (3) simple, robust, and versatile processibility of CNT nano-thin composite coating. The early pioneering work of CNT LBL assembly is the introduction of successful conquest over dispersion challenges of CNTs in polymer composites. Mamedov et al.[15] reported that exceptionally uniform dispersion of SWNTs in nano-thin layered structures showed great potential in their mechanical properties even with weak polymers, which has drawn broad attention from various disciplines. Notable mechanical functionalities of the SWNT LBL composite are originated by not just uniform dispersion, but also high loading of CNTs and functional activated interfacial bondings between CNTs and polyelectrolyte matrix, poly(ethylene imine) (PEI). Successive experimental reports confirmed that LBL assembly of SWNTs indeed allowed exceptional exfoliation and homogeneous dispersion in a polymeric composite[62] and nano-scale stepwise deposition of CNTs showed tremendous potential promise for development of a wide range of functional materials.[63-66] The loading of CNTs in LBL assembled composites can be controlled in the range of 10 %[22] to 75 %[67], which depends on many variables of LBL assembly such as LBL polymer matrix, stabilizer of CNTs, process conditions, and so forth. The layered growth by dipping is usually linear with constant slope[68, 69] and the surface roughness of each layers rely on the layer growth rate and the thickness of each layer[69] although it is limited within nano-scale ranges, which allow precise organization controls during CNT LBL assembly. The adsorption interaction between CNTs and polymers can be either conventional electrostatic force,[70] hydrogen bonds,[68] or van der

Waals interactions[71] and later modified to strong covalent bonds[68]. The features of LBL assembly were also effective to various sizes of carbon nanomaterials including MWNTs,[63] vapor grown hollow carbon fibers with diameter size of 50~150nm,[72] and exfoliated graphene nanoplatelet.[73]

The unusual properties of CNTs are modulated in LBL assembled nanocomposites by mix-matching with complementary polymeric LBL partners. For their uses as sensors, cell scaffolds, drug delivery carrier, fuel cell membranes, and sesnsors, the judicial selection of polymeric matrix in LBL assembly is required for enhancing the performances in the field of application. The scopes of macromolecules as a CNT's LBL counter partner are extended from conventional LBL polymers such as poly(vinyl alcohol) (PVA),[22] poly(allylamine hydrocholoride) (PAH),[29] poly(ethylene imine) (PEI),[15, 74] poly(diallyldimethyl ammonium choloride) (PDDA), poly(acrylic acid) (PAA),[30] to functional materials like poly(3,4-ethylenedioxythiphene)/poly(styrene sulfonate) (PEDOT/PSS),[75] poly(anilne) (PANI),[76] polypyrrole (PPy),[77, 78] light sensitive diazoresin (DR),[68] poly(viologen) derivatives,[79, 80] porphyrin,[80] prussian blue (PB)[81, 82] and to bio related materials such as blood compatible poly(lactic acid-co-glycolic acid) (PLGA),[83] biopolymer chitosan,[82] antimicrobial lysozyme (LSZ),[84] antisense oligodeoxynucleotide (ASODN) enzymes.[85] In the following subsections, detailed examples of CNT LBL assembly classified by applications are introduced.

1. Electrical Conductor Applications

The combination of exceptional nano-organization of LBL assembly and unique electrical properties of CNTs has opened wide research opportunities. In 2005, Kovtyukhova et al. reported that LBL composites of densely distributed SWNTs have highly anisotropic electrical properties because of layered structures.[64] The conductivity differences between in-plane and out-of-plane directions are more than factor of three so that great potential to property modulation were suggested with ultrathin film thickness controls.[64, 86] The same research team further demonstrated p-n hetero junction diodes on Au nanowires with high rectifying efficiency, which was fabricated by mixed LBL assembly of SWNTs, conductive polymer (PANI), and semiconducting nanoparticles on Au nanowires.[65] In this research, the features of SWNT LBL films were highly p-type conductive, ultrathin to coat over Au nanowires, and stable to provide junction performances even after alumina membreanes dissolution. As a way to improve the electrical properties of LBL assembled CNT nanocomposites, Shim *et al*. reported that electrical conductivities are depended on micro-/nano-scale continuous conductive path by the analysis specific to molecular structures of LBL composites[22] Following this analysis, heat treatment techniques at 200^{o}C and 300^{o}C were suggested to form tighter SWNT connections whose in-situ measurements of nano-structural changes during treatments were demonstrated. These treatments improved the electrical conductivities of SWNT LBL film by two orders of magnitude. Furthermore, they revealed that LBL assembled SWNT composites were up to 10 times stronger than SWNT-only mats. The films were suggested to be used as high performance transparent conductors (TCs),

which justified the advantages of SWNT LBL composites as new class electronic materials.[22] These high electrical properties of SWNT LBL films were further demonstrated as low cost, high efficient polymeric thin film transistor (TFT) by Xue *et al*.[87] The same team further suggested that these micro-patterned electronic devices could be fabricated on a highly flexible substrate by LBL assembly.[88]

Among the applications of these properties, TCs provide direct commercialization opportunities utilizing precise nano-scale organization of LBL assembly of SWNTs. Yu et al. reported a SWNT/PDDA LBL composite with 2.5 kohm/sq at 86.5% light transmittance[89] and they further formed the similar LBL coating as a transparent surface electrode on a PVDF actuator whose audio speaker performances were demonstrated as excellent.[90] Ham *et al.* utilized conductive PEDOT/PSS with SWNTs to form TCs by LBL assembly[75] although the TC performances are lower than SWNT-only mats, Bucky papers. The competitive TC performances of SWNT LBL composites compared to conventional ITOs were reported by Shim et al., whose TC coating with vigorous acid doping demonstrated lower than 100 ohm/sq at 80% light transmittance.[91] Unlike other processes for SWNT nanomats- bucky-papers, simple and easy to scale-up processibilty of LBL assembly and the high mechanical integrity of SWNT LBL composites make them to be a viable alternative option of TC materials of choice. As extension of TC properties, Jain *et al.* reported that durable electrochromic devices, which usually require high transparency, high contrast, low surface roughness, accurate thickness control, and fast ion conductivity, were fabricated by LBL assembly of poly[2-(3-thienyl) ethoxy-4-butylsulfonate / poly(allylamine hydrochloride) on SWNT electrodes.[92]

2. Sensor applications

A great deal of SWNT nanocomposites fabricated LBL assembly techniques were applied to physical/chemical sensors by utilizing (1) electrical property change of CNTs by chemical species, (2) electrochemical responses of counter LBL partner of CNTs, (3) structural deformation induced electrical resistance changes of a composite, or (4) specially designed micro-/nano-electrical mechanical system (MEMS/NEMS) devices. Typical examples of monitoring physical and chemical states by CNT LBL composites are demonstrated by Loh *et al.* They reported that a strain sensor by tailored piezoresistive response[26] and a pH sensing strips sensitive enough to monitor environment changes caused by corrosion of metal structures[76] were constructed by SWNT/PVA and SWNT/PANI LBL composites, respectively. Detection targets of SWNT LBL composites are only limited by our imagination. Biological materials such as DNA,[93] glucose,[77, 78, 82, 94-99] dopamine,[100, 101] uric acid,[100] and toxic materials such as arsenic,[102] phenols[78] were often detected by amperometric measurements of CNT LBL nanocomposites utilizing the combinations of electrocatalytic activities, electrochemical sensitivities of CNTs and various materials immobilization given by versatile selections of LBL assembly. Environmental changes like humidity are easily monitored by CNT LBL composites.[103]

The integration of LBL assembled composites into MEMS/NEMS devices are new fusion technology of top-down and bottom-up nano-process.[104] CNTs are also leading these frontiers owing to their unique electrical and mechanical properties. The LBL assembled SWNT nanocomposites were patterned as flexible micro-cantilever

arrays whose movements were demonstrated by Xue et al.[105] This CNT LBL micro-cantilever can find future applications in biosensors and micro-valve for microfluidic structure channels. As another recent important progress, highly efficient nanomembrane micro-sensor platforms by MEMS devices were developed by SWNT LBL composites[28] following ultrathin membrane design concepts.[106] The thickness of freely suspended sensors could be varied from 7 to 26 nm due to strong mechanical properties of SWNT LBL composites. Kang et al. claims that this freely suspended nanomembrane array open a breakthrough path to new nano-membrane micro-sonsors by exceptional sensitivity, versatile multi-component functionality, and extreme stability.[28]

3. Fuel Cell Applications

Combined with unique merit of LBL assemblies such as nano-thin orgarnized structures, controlled porosity, and free selection of ionic matrix, fuel cell proton exchange membranes (PEMs) were constructed by LBL assembled CNT nanocomposites as highly conductive and chemically durable electrodes.[27, 107-109] Michel et al. reported that CNTs wrapped with Nafion and Pt catalysts showed unusual fuel cell performances when they are LBL assembled to a fuel cell PEM, which is featured with nano-scale optimized electron/proton movements, simple, low cost production, and efficient utilization of Pt catalysts as well as with mechanical strength, high electrical, high thermal conductivities, and stable chemical durability.[27] This LBL scheme is further adapted as blending techniques between proton exchange Nafion and CNTs to nano-layer

controlled structures, whose aim is to improve proton conduction efficiency at high operating temperature.[110] Interestingly, biofuel cell applications were also developed by CNT/poly-l-(lysine)/fungal laccase LBL assembly, which features electrical potential generation by stable enzyme immobilization.[111]

4. Nano-/Micro-shell LBL Coatings and Biomedical Applications

These LBL assembly principles are effective not only on bulk planar surfaces but also on micro-/nano- complex objects which may have potential applications such as in biomedicine and biocompatible micro-prosthetic devices. For these complex coatings, two design schemes associated with CNTs are introduced. The first is assembling CNT LBL films over microspheres. Starting from Sano et al.'s initial success reports of hollow carbon micro-vessels in 2002,[112] the efforts have been directed to improve the properties micro-spherical shells such as strength, permeability, and porosity,[113, 114] and to modify production process by changing types of microsphere template[113, 115] or by adding calcination to remove polymers.[114] Various types of micro-objects by desires can be used as templates for LBL assemblies. Coating over soft-microcapsules were developed to protect liposome by CNT reinforced LBL composites.[29] Pan et al. reported that electrospun polystyrene (PS) microfibers were employed as a template of MWNT LBL composites.[116] By dissolving of PS, hollow micro-tubular structures of MWNT LBL nanocompsites were obtained easily.

The other types of nanoshell designs are direct LBL assemblies over CNT strands like templates. Artyukhin et al. reported that SWNTs attached with ionic pyrene derivatives were successfully wrapped by polymeric LBL assemblies.[117] This technique has been further applied to produce porous indium oxide nanotubes which may be useful as toxic gas detectors.[118] Du *et al.* reported that nano-tubular structures of indium oxide produced by LBL assembly over CNT strands and purified by calcinations greatly expand their active surface areas and simultaneous improved sensitivity over NH_3 gas.[118] As other examples, stable bio-molecule coatings over MWNTs were demonstrated by *Liu et al*.[119] They formed a thick and molecular brick like rigid β-cyclodextrin layers over a MWNT by LBL assembly techniques. Certainly, this biomolecule wrapping of CNTs were proved to be effective tools to intracellular delivery of biomedicine.[85] Jia *et al,* reported that anti-cancer enzymes, ASODNs, and fluorescent labeling quantum dots coated on MWNTs by LBL assembly were successfully injected into tumor cells.[85] Thus, further developments of LBL assembly over CNT nano-objects may be needed for the future biomedicine or tissue engineering application.

Along with above structural controls, biomedical functionality and cell interface compatibility tests were performed with CNT LBL nanocomposites. Following cellular adhesion experiments,[120] Gheith *et al.* reported that neural cells and their neurite growth were enhanced by electrical stimulus through CNT LBL composites,[30] which was the first observation of cellular interactions to CNT materials by electrical potential. Furthermore, these neural cell tests were extended to the differentiation of embryonic neural stem cells on CNT LBL nanocomposites.[74] These live cell interface experiments

corroborate that CNT LBL composites are indeed one of viable functional materials options for biomedical implant, prosthetic devices, and stem cell growth platforms.

Another type of biocompatible, blood-compatible surface tests were performed on LBL assembled CNT/PLGA nanocomposites for the aim of thromboresistance suppression to foreign artificial blood prostheses.[83] In contrast to this biocompatible, anti-fouling or antimicrobial coating provides also good application examples of LBL assembly. Nepal et al. designed LBL assembly of antimicrobial lysozyme (LSZ) with CNTs for the aim of improving mechanical properties of surfaces.[84] The nanoindentation measurement, however, needs to be careful to determine the Young's modulus and hardness of LBL film, because the substrate effect is so significant in a thin film. The suggestion of valid measurement condition is no dipper than 10% of total thickness as indicated by Pavoor et al.[121]

D. Research Overview

As presented in the previous discussion, the LBL assembly of CNT – polymer hybrid composites has unique abilities to transfer many useful physicochemical properties of SWNTs into macro-scale thin films. Some of the key features include (1) preservation of the exfoliated state of SWNTs from solution to solid state, (2) controllable molecularly-thin layered organization of SWNTs and polymer, (3) exceptionally high loading of SWNTs in a composite.

Following the first introduction of CNT LBL assembly from our group, I studied the nanostructures, chemical compositions, and post-assembly optimization treatments for the application of the ultra-strong and tough materials as well as the next generation flexible transparent conductive thin films. The high mechanical strength of a SWNT-PVA LBL composite is a result of strong interfacial molecular bonding from chemical cross-linking treatment, and high and uniform SWNT loading with 2-dimensional architectures.

High-loading of SWNTs with molecularly thin PVA binder provided high electrical conductivity integrated with mechanical strength and flexibility. I also found that super-acid treated thin LBL coating of SWNTs demonstrated exceptional transparency and electrical conductivity as well as flexibility, unlike weakly bound SWNT-only networks. The combination of high mechanical and electrical properties tailored by nano-scale hybrid architectures and optimization chemistries are the fundamental elements of numerous potential applications.

I also introduced a three dimensional CNT nanocomposite coating process that transformed ordinary cotton threads into intelligent material for electronic textiles (e-textiles). Important characteristics of e-textiles include weavablity, wearability, light weight, and “smart” functionalities as well as chemical/mechanical durability and high electrical conductivity. Efficient charge transport through the network of nanotubes and the possibility to engineer tunneling junctions make them promising materials for many high knowledge-content garments. Along with integrated humidity sensing, I

demonstrated that CNT/cotton threads can be used to detect albumin, the most abundant protein in blood, with high sensitivity and selectivity.

Although traditional LBL assembly has many features including nano-scale hierarchical structures, the deposition process is slow and it is difficult to control the in-plane structure. To overcome these shortcomings, I introduced two new advanced LBL assembly techniques: *'dewetting LBL'*, which dramatically increases and simplifies the LBL process by eliminating the rinsing steps and features unique lateral organizations, and *'SWNT combing'*, which efficiently aligns SWNTs during LBL assemblies. The nano-scale lateral organizations from both processes are governed by the surface tension of the dewetting meniscus and the hydrodynamic drag forces of near-wall microflows. These techniques are useful for designing sophisticated molecular architectures as well as improving material performances of SWNT nanocomposites.

Reference

1. Gates, B. D.; Xu, Q. B.; Stewart, M.; Ryan, D.; Willson, C. G.; Whitesides, G. M., New approaches to nanofabrication: Molding, printing, and other techniques. *Chemical Reviews* **2005,** 105, (4), 1171-1196.
2. Whitesides, G. M.; Mathias, J. P.; Seto, C. T., Molecular self-assembly and nanochemistry - A chemical strategy for the synthesis of nanostructures. . *Science* **1991,** 254, (5036), 1312-1319.
3. Ozin, G. A., Nanochemistry - Synthesis in diminishing dimensions. *Advanced Materials* **1992,** 4, (10), 612-649.
4. Lehn, J. M., Toward complex matter: Supramolecular chemistry and self-organization. *Proceedings of the National Academy of Sciences of the United States of America* **2002,** 99, (8), 4763-4768.
5. Quake, S. R.; Scherer, A., From micro- to nanofabrication with soft materials. *Science* **2000,** 290, (5496), 1536-1540.
6. Fuchs, H.; Ohst, H.; Prass, W., Ultrathin orgnaic films - Molecular architectures for advanced optical, electronic and bio-related systems. *Advanced Materials* **1991,** 3, (1), 10-18.
7. Decher, G., Fuzzy nanoassemblies: toward layered polymeric multicomposites. *Science* **1997,** 277, (5330), 1232-1237.
8. Ferreira, M.; Rubner, M. F., Molecular-level processing of conjugated polymers. 1. Layer-by-layer manipulation of conjugated polyions. *Macromolecules* **1995,** 28, (21), 7107-7114.
9. Fou, A. C.; Rubner, M. F., Molecular-level processing of conjugated polymers. 2. Layer-by-layer manipulation of in-situ polymerized p-type doped conducting polymers. *Macromolecules* **1995,** 28, (21), 7115-7120.
10. Cheung, J. H.; Stockton, W. B.; Rubner, M. F., Molecular-level processing of conjugated polymers .3. Layer-by-layer manipulation of polyaniline via electrostatic interactions. *Macromolecules* **1997,** 30, (9), 2712-2716.
11. Stockton, W. B.; Rubner, M. F., Molecular-level processing of conjugated polymers .4. Layer-by-layer manipulation of polyaniline via hydrogen-bonding interactions. *Macromolecules* **1997,** 30, (9), 2717-2725.
12. Kotov, N. A.; Dekany, I.; Fendler, J. H., Layer-by-layer self-assembly of polyelectrolyte-semiconductor nanoparticle composite films. *Journal of Physical Chemistry* **1995,** 99, (35), 13065-13069.
13. Kotov, N. A.; Magonov, S.; Tropsha, E., Layer-by-layer self-assembly of alumosilicate-polyelectrolyte composites: Mechanism of deposition, crack resistance, and perspectives for novel membrane materials. *Chemistry of Materials* **1998,** 10, (3), 886-895.
14. Mamedov, A. A.; Belov, A.; Giersig, M.; Mamedova, N. N.; Kotov, N. A., Nanorainbows: Graded semiconductor films from quantum dots. *Journal of the American Chemical Society* **2001,** 123, (31), 7738-7739.

15. Mamedov, A. A.; Kotov, N. A.; Prato, M.; Guldi, D. M.; Wicksted, J. P.; Hirsch, A., Molecular design of strong single-wall carbon nanotube/polyelectrolyte multilayer composites. *Nature Materials* **2002,** 1, (3), 190-194.
16. Tang, Z.; Kotov, N. A.; Magonov, S.; Ozturk, B., Nanostructured artificial nacre. *Nature Materials* **2003,** 2, (6), 413-418.
17. Shim, B. S.; Podsiadlo, P.; Lilly, D. G.; Agarwal, A.; Lee, J.; Tang, Z.; Ho, S.; Ingle, P.; Paterson, D.; Lu, W.; Kotov, N. A., Nanostructured Thin Films Made by Dewetting Method of Layer-By-Layer Assembly. *Nano Lett.* **2007,** 7, (11), 3266-3273.
18. Lvov, Y.; Ariga, K.; Ichinose, I.; Kunitake, T., ASSEMBLY OF MULTICOMPONENT PROTEIN FILMS BY MEANS OF ELECTROSTATIC LAYER-BY-LAYER ADSORPTION. *Journal of the American Chemical Society* **1995,** 117, (22), 6117-6123.
19. Nam, K. T.; Kim, D. W.; Yoo, P. J.; Chiang, C. Y.; Meethong, N.; Hammond, P. T.; Chiang, Y. M.; Belcher, A. M., Virus-enabled synthesis and assembly of nanowires for lithium ion battery electrodes. *Science* **2006,** 312, (5775), 885-888.
20. Yoo, P. J.; Nam, K. T.; Qi, J. F.; Lee, S. K.; Park, J.; Belcher, A. M.; Hammond, P. T., Spontaneous assembly of viruses on multilayered polymer surfaces. *Nature Materials* **2006,** 5, (3), 234-240.
21. Lee, D.; Rubner, M. F.; Cohen, R. E., All-nanoparticle thin-film coatings. *Nano Letters* **2006,** 6, (10), 2305-2312.
22. Shim, B. S.; Tang, Z. Y.; Morabito, M. P.; Agarwal, A.; Hong, H. P.; Kotov, N. A., Integration of Conductivity, Transparency, and Mechanical Strength into Highly Homogeneous Layer-by-Layer Composites of Single-Walled Carbon Nanotubes for Optoelectronics. *Chemistry of Materials* **2007,** 19, 5467-5474.
23. Ear, Y.; Silverman, E., Challenges and opportunities in multifunctional nanocomposite structures for aerospace applications. *Mrs Bulletin* **2007,** 32, (4), 328-334.
24. Podsiadlo, P.; Kaushik, A. K.; Arruda, E. M.; Waas, A. M.; Shim, B. S.; Xu, J. D.; Nandivada, H.; Pumplin, B. G.; Lahann, J.; Ramamoorthy, A.; Kotov, N. A., Ultrastrong and stiff layered polymer nanocomposites. *Science* **2007,** 318, (5847), 80-83.
25. Westcott, S. L.; Kotov, N. A.; Ostrander, J. W.; Mamedov, A. A.; Reust, D. K.; Roark, J. P. In *Corrosion protection by multifunctional stratified coatings*, Nanotechnology Conference and Trade Show (Nanotech 2004), Boston, MA, Mar 07-11, 2004; Laudon, M. R. B., Ed. Boston, MA, 2004; pp 288-291.
26. Loh, K. J.; Lynch, J. P.; Shim, B. S.; Kotov, N. A., Tailoring piezoresistive sensitivity of multilayer carbon nanotube composite strain sensors. *Journal of Intelligent Material Systems and Structures* **2008,** 19, (7), 747-764.
27. Michel, M.; Taylor, A.; Sekol, R.; Podsiadlo, P.; Ho, P.; Kotov, N.; Thompson, L., High-performance nanostructured membrane electrode, assemblies for fuel cells made by layer-by-layer assembly of carbon nanocolloids. *Advanced Materials* **2007,** 19, (22), 3859-+.
28. Kang, T. J.; Cha, M.; Jang, E. Y.; Shin, J.; Im, H. U.; Kim, Y.; Lee, J.; Kim, Y. H., Ultra-thin and conductive nanomembrane arrays for nanomechanical transducers. *Advanced Materials* **2008,** 20, (16), 3131-3137.

29. Angelini, G.; Boncompagni, S.; De Maria, P.; De Nardi, M.; Fontana, A.; Gasbarri, C.; Menna, E., Layer-by-layer deposition of shortened nanotubes or polyethylene glycol-derivatized nanotubes on liposomes: A tool for increasing liposome stability. *Carbon* **2007,** 45, (13), 2479-2485.
30. Gheith, M. K.; Pappas, T. C.; Liopo, A. V.; Sinani, V. A.; Shim, B. S.; Motamedi, M.; Wicksted, J. R.; Kotov, N. A., Stimulation of neural cells by lateral layer-by-layer films of single-walled currents in conductive carbon nanotubes. *Advanced Materials* **2006,** 18, (22), 2975-+.
31. Sekitani, T.; Noguchi, Y.; Hata, K.; Fukushima, T.; Aida, T.; Someya, T., A rubberlike stretchable active matrix using elastic conductors. *Science* **2008,** 321, (5895), 1468-1472.
32. Yu, M. F.; Lourie, O.; Dyer, M. J.; Moloni, K.; Kelly, T. F.; Ruoff, R. S., Strength and breaking mechanism of multiwalled carbon nanotubes under tensile load. *Science* **2000,** 287, (5453), 637-640.
33. Calvert, P., Nanotube composites: A recipe for strength. *Nature* **1999,** 399, (6733), 210-211.
34. Dresselhaus, M. S.; Dresselhaus, G.; Jorio, A., Unusual properties and structure of carbon nanotubes. *Annual Review of Materials Research* **2004,** 34, 247-278.
35. Jorio, A.; Saito, R.; Hafner, J. H.; Lieber, C. M.; Hunter, M.; McClure, T.; Dresselhaus, G.; Dresselhaus, M. S., Structural (n, m) determination of isolated single-wall carbon nanotubes by resonant Raman scattering. *Physical Review Letters* **2001,** 86, (6), 1118-1121.
36. Rao, A. M.; Richter, E.; Bandow, S.; Chase, B.; Eklund, P. C.; Williams, K. A.; Fang, S.; Subbaswamy, K. R.; Menon, M.; Thess, A.; Smalley, R. E.; Dresselhaus, G.; Dresselhaus, M. S., Diameter-selective Raman scattering from vibrational modes in carbon nanotubes. *Science* **1997,** 275, (5297), 187-191.
37. Fantini, C.; Jorio, A.; Souza, M.; Strano, M. S.; Dresselhaus, M. S.; Pimenta, M. A., Optical transition energies for carbon nanotubes from resonant Raman spectroscopy: Environment and temperature effects. *Physical Review Letters* **2004,** 93, (14).
38. Dresselhaus, M. S.; Eklund, P. C., Phonons in carbon nanotubes. *Advances in Physics* **2000,** 49, (6), 705-814.
39. Vigolo, B.; Penicaud, A.; Coulon, C.; Sauder, C.; Pailler, R.; Journet, C.; Bernier, P.; Poulin, P., Macroscopic fibers and ribbons of oriented carbon nanotubes. *Science* **2000,** 290, (5495), 1331-1334.
40. Dalton, A. B.; Collins, S.; Munoz, E.; Razal, J. M.; Ebron, V. H.; Ferraris, J. P.; Coleman, J. N.; Kim, B. G.; Baughman, R. H., Super-tough carbon-nanotube fibres. *Nature* **2003,** 423, (6941), 703.
41. Dalton, A. B.; Collins, S.; Razal, J.; Munoz, E.; Ebron, V. H.; Kim, B. G.; Coleman, J. N.; Ferraris, J. P.; Baughman, R. H., Continuous carbon nanotube composite fibers: properties, potential applications, and problems. *J.Mater.Chem.* **2004,** 14, (1), 1-3.
42. Schadler, L. S.; Giannaris, S. C.; Ajayan, P. M., Load transfer in carbon nanotube epoxy composites. *Applied Physics Letters* **1998,** 73, (26), 3842-3844.

43. Qian, D.; Dickey, E. C.; Andrews, R.; Rantell, T., Load transfer and deformation mechanisms in carbon nanotube-polystyrene composites. *Applied Physics Letters* **2000,** 76, (20), 2868-2870.
44. Ajayan, P. M.; Schadler, L. S.; Giannaris, C.; Rubio, A., Single-walled carbon nanotube-polymer composites: Strength and weakness. *Advanced Materials* **2000,** 12, (10), 750-+.
45. Lourie, O.; Wagner, H. D., Evidence of stress transfer and formation of fracture clusters in carbon nanotube-based composites. *Composites Science and Technology* **1999,** 59, (6), 975-977.
46. Barber, A. H.; Cohen, S. R.; Wagner, H. D., Measurement of carbon nanotube-polymer interfacial strength. *Applied Physics Letters* **2003,** 82, (23), 4140-4142.
47. Barber, A. H.; Cohen, S. R.; Wagner, H. D., Static and Dynamic Wetting Measurements of Single Carbon Nanotubes. *Physical Review Letters* **2004,** 92, (18), 186103/1-186103/4.
48. Ding, W.; Eitan, A.; Fisher, F. T.; Chen, X.; Dikin, D. A.; Andrews, R.; Brinson, L. C.; Schadler, L. S.; Ruoff, R. S., Direct observation of polymer sheathing in carbon nanotube-polycarbonate composites. *Nano Letters* **2003,** 3, (11), 1593-1597.
49. Frankland, S. J. V.; Caglar, A.; Brenner, D. W.; Griebel, M., Molecular Simulation of the Influence of Chemical Cross-Links on the Shear Strength of Carbon Nanotube-Polymer Interfaces. *Journal of Physical Chemistry B* **2002,** 106, (12), 3046-3048.
50. Frankland, S. J. V.; Harik, V. M., Analysis of carbon nanotube pull-out from a polymer matrix. *Surface Science* **2003,** 525, (1-3), L103-L108.
51. Cadek, M.; Coleman, J. N.; Ryan, K. P.; Nicolosi, V.; Bister, G.; Fonseca, A.; Nagy, J. B.; Szostak, K.; Beguin, F.; Blau, W. J., Reinforcement of Polymers with Carbon Nanotubes: The Role of Nanotube Surface Area. *Nano Letters* **2004,** 4, (2), 353-356.
52. Cadek, M.; Coleman, J. N.; Barron, V.; Hedicke, K.; Blau, W. J., Morphological and mechanical properties of carbon-nanotube-reinforced semicrystalline and amorphous polymer composites. *Applied Physics Letters* **2002,** 81, (27), 5123-5125.
53. Shaffer, M. S. P.; Windle, A. H., Fabrication and characterization of carbon nanotube/poly(vinyl alcohol) composites. *Advanced Materials* **1999,** 11, (11), 937-941.
54. Coleman, J. N.; Curran, S.; Dalton, A. B.; Davey, A. P.; McCarthy, B.; Blau, W.; Barklie, R. C., Percolation-dominated conductivity in a conjugated-polymer-carbon-nanotube composite. *Physical Review B-Condensed Matter* **1998,** 58, (12), R7492-R7495.
55. Lyons, P. E.; De, S.; Blighe, F.; Nicolosi, V.; Pereira, L. F. C.; Ferreira, M. S.; Coleman, J. N., The relationship between network morphology and conductivity in nanotube films. *Journal of Applied Physics* **2008,** 104, (4).
56. Vigolo, B.; Coulon, C.; Maugey, M.; Zakri, C.; Poulin, P., An Experimental Approach to the Percolation of Sticky Nanotubes. *Science* **2005,** 309, (5736), 920-923.
57. Grunlan, J. C.; Mehrabi, A. R.; Bannon, M. V.; Bahr, J. L., Water-based single-walled-nanotube-filled polymer composite with an exceptionally low percolation threshold. *Advanced Materials* **2004,** 16, (2), 150-153.

58. Blackburn, J. L.; Barnes, T. M.; Beard, M. C.; Kim, Y. H.; Tenent, R. C.; McDonald, T. J.; To, B.; Coutts, T. J.; Heben, M. J., Transparent conductive single-walled carbon nanotube networks with precisely tunable ratios of semiconducting and metallic nanotubes. *Acs Nano* **2008,** 2, (6), 1266-1274.
59. Green, A. A.; Hersam, M. C., Colored semitransparent conductive coatings consisting of monodisperse metallic single-walled carbon nanotubes. *Nano Letters* **2008,** 8, (5), 1417-1422.
60. Blighe, F. M.; Hernandez, Y. R.; Blau, W. J.; Coleman, J. N., Observation of percolation-like scaling - Far from the percolation threshold - In high volume fraction, high conductivity polymer-nanotube composite films. *Advanced Materials* **2007,** 19, (24), 4443-+.
61. Potschke, P.; Bhattacharyya, A. R.; Janke, A., Carbon nanotube-filled polycarbonate composites produced by melt mixing and their use in blends with polyethylene. *Carbon* **2004,** 42, (5-6), 965-969.
62. Rouse, J. H.; Lillehei, P. T., Electrostatic assembly of polymer/single walled carbon nanotube multilayer films. *Nano Letters* **2003,** 3, (1), 59-62.
63. Olek, M.; Ostrander, J.; Jurga, S.; Mohwald, H.; Kotov, N.; Kempa, K.; Giersig, M., Layer-by-layer assembled composites from multiwall carbon nanotubes with different morphologies. *Nano Letters* **2004,** 4, (10), 1889-1895.
64. Kovtyukhova, N. I.; Mallouk, T. E., Ultrathin Anisotropic Films Assembled from Individual Single-Walled Carbon Nanotubes and Amine Polymers. *Journal of Physical Chemistry B* **2005,** 109, (7), 2540-2545.
65. Kovtyukhova, N. L.; Mallouk, T. E., Nanowire p-n heterojunction diodes made by templated assembly of multilayer carbon-nanotube/polymer/semiconductor-particle shells around metal nanowires. *Advanced Materials* **2005,** 17, (2), 187-+.
66. Rouse, J. H.; Lillehei, P. T.; Sanderson, J.; Siochi, E. J., Polymer/Single-Walled Carbon Nanotube Films Assembled via Donor-Acceptor Interactions and Their Use as Scaffolds for Silica Deposition. *Chemistry of Materials* **2004,** 16, (20), 3904-3910.
67. Xue, W.; Cui, T. H., Characterization of layer-by-layer self-assembled carbon nanotube multilayer thin films. *Nanotechnology* **2007,** 18, (14).
68. Shi, J. H.; Qin, Y. J.; Luo, H. X.; Guo, Z. X.; Woo, H. S.; Park, D. K., Covalently attached multilayer self-assemblies of single-walled carbon nanotubols and diazoresins. *Nanotechnology* **2007,** 18, (36).
69. Paloniemi, H.; Lukkarinen, M.; Aaritalo, T.; Areva, S.; Leiro, J.; Heinonen, M.; Haapakka, K.; Lukkari, J., Layer-by-layer electrostatic self-assembly of single-wall carbon nanotube polyelectrolytes. *Langmuir* **2006,** 22, (1), 74-83.
70. Shen, J. F.; Hu, Y. Z.; Qin, C.; Ye, M. X., Layer-by-layer self-assembly of multiwalled carbon nanotube polyelectrolytes prepared by in situ radical polymerization. *Langmuir* **2008,** 24, (8), 3993-3997.
71. Moya, S. E.; Ilie, A.; Bendall, J. S.; Hernandez-Lopez, J. L.; Ruiz-Garcia, J.; Huck, W. T. S., Assembly of polyelectrolytes on CNTs by Van der Waals interactions and fabrication of LBL polyelectrolyte/CNT composites. *Macromolecular Chemistry and Physics* **2007,** 208, (6), 603-608.

72. Shim, B. S.; Starkovich, J.; Kotov, N., Multilayer composites from vapor-grown carbon nano-fibers. *Composites Science and Technology* **2006,** 66, (9), 1174-1181.
73. Hendricks, T. R.; Lu, J.; Drzal, L. T.; Lee, I., Intact pattern transfer of conductive exfoliated graphite nanoplatelet composite films to polyelectrolyte multilayer platforms. *Advanced Materials* **2008,** 20, (10), 2008-+.
74. Jan, E.; Kotov, N. A., Successful differentiation of mouse neural stem cells on layer-by-layer assembled single-walled carbon nanotube composite. *Nano Letters* **2007,** 7, (5), 1123-1128.
75. Ham, H. T.; Choi, Y. S.; Chee, M. G.; Cha, M. H.; Chung, I. J., PEDOT-PSS/singlewall carbon nanotubes composites. *Polymer Engineering and Science* **2008,** 48, (1), 1-10.
76. Loh, K. J.; Kim, J.; Lynch, J. P.; Kam, N. W. S.; Kotov, N. A., Multifunctional layer-by-layer carbon nanotube-polyelectrolyte thin films for strain and corrosion sensing. *Smart Materials & Structures* **2007,** 16, (2), 429-438.
77. Shirsat, M. D.; Too, C. O.; Wallace, G. G., Amperometric glucose biosensor on layer by layer assembled carbon nanotube and polypyrrole multilayer film. *Electroanalysis* **2008,** 20, (2), 150-156.
78. Korkut, S.; Keskinler, B.; Erhan, E., An amperometric biosensor based on multiwalled carbon nanotube-poly(pyrrole)-horseradish peroxidase nanobiocomposite film for determination of phenol derivatives. *Talanta* **2008,** 76, (5), 1147-1152.
79. Wang, X.; Huang, H. X.; Liu, A. R.; Liu, B.; Wakayama, T.; Nakamura, C.; Miyake, J.; Qian, D. J., Layer-by-layer assembly of single-walled carbon nanotube-poly(viologen) derivative multilayers and their electrochemical properties. *Carbon* **2006,** 44, (11), 2115-2121.
80. Wang, X.; Huang, H. X.; Liu, A. R.; Liu, B.; Chen, M.; Qian, D. J., Multilayer assembly and characterization of zinc porphyrin-carbon nanotubes-poly(viologen) derivative. *Thin Solid Films* **2008,** 516, (10), 3244-3250.
81. Wang, L.; Guo, S. J.; Hu, X. O.; Dong, S. J., Layer-by-layer assembly of carbon nanotubes and Prussian blue nanoparticles: A potential tool for biosensing devices. *Colloids and Surfaces a-Physicochemical and Engineering Aspects* **2008,** 317, (1-3), 394-399.
82. Zou, Y. J.; Xian, C. L.; Sun, L. X.; Xu, F., Amperometric glucose biosensor prepared with biocompatible material and carbon nanotube by layer-by-layer self-assembly technique. *Electrochimica Acta* **2008,** 53, (12), 4089-4095.
83. Koh, L. B.; Rodriguez, I.; Zhou, J. J., Platelet adhesion studies on nanostructured poly(lactic-co-glycolic-acid)-carbon nanotube composite. *Journal of Biomedical Materials Research Part A* **2008,** 86A, (2), 394-401.
84. Nepal, D.; Balasubramanian, S.; Simonian, A. L.; Davis, V. A., Strong antimicrobial coatings: Single-walled carbon nanotubes armored with biopolymers. *Nano Letters* **2008,** 8, (7), 1896-1901.
85. Jia, N. Q.; Lian, Q.; Shen, H. B.; Wang, C.; Li, X. Y.; Yang, Z. N., Intracellular delivery of quantum dots tagged antisense oligodeoxynucleotides by functionalized multiwalled carbon nanotubes. *Nano Letters* **2007,** 7, 2976-2980.

86. Palumbo, M.; Lee, K. U.; Ahn, B. T.; Suri, A.; Coleman, K. S.; Zeze, D.; Wood, D.; Pearson, C.; Petty, M. C., Electrical investigations of layer-by-layer films of carbon nanotubes. *Journal of Physics D-Applied Physics* **2006,** 39, (14), 3077-3085.
87. Xue, W.; Liu, Y.; Cui, T. H., High-mobility transistors based on nanoassembled carbon nanotube semiconducting layer and SiO2 nanoparticle dielectric layer. *Applied Physics Letters* **2006,** 89, (16).
88. Xue, W.; Cui, T. H. In *Electrical and electromechanical characteristics of self-assembled carbon nanotube thin films on flexible substrates*, 14th International Conference on Solid-State Sensors, Actuators and Microsystems, Lyon, FRANCE, Jun 10-14, 2007; Lyon, FRANCE, 2007; pp 330-335.
89. Yu, X.; Rajamani, R.; Stelson, K. A.; Cui, T., Fabrication of carbon nanotube based transparent conductive thin films using layer-by-layer technology. *Surface & Coatings Technology* **2008,** 202, (10), 2002-2007.
90. Yu, X.; Rajamani, R.; Stelson, K. A.; Cui, T., Carbon nanotube-based transparent thin film acoustic actuators and sensors. *Sensors and Actuators a-Physical* **2006,** 132, (2), 626-631.
91. Shim, B. S.; Zhu, J.; Chritchley, K.; Ho, S.; Kotov, N. A., Single-Walled Carbon Nanotube Polymeric Layer-By-Layer Nanocomposites for Flexible Transparent Conductive Film Applications. *In preparation*.
92. Jain, V.; Yochum, H. M.; Montazami, R.; Heflin, J. R.; Hu, L. B.; Gruner, G., Modification of single-walled carbon nanotube electrodes by layer-by-layer assembly for electrochromic devices. *Journal of Applied Physics* **2008,** 103, (7).
93. Ma, H. Y.; Zhang, L. P.; Pan, Y.; Zhang, K. Y.; Zhang, Y. Z., A novel electrochemical DNA biosensor fabricated with layer-by-layer covalent attachment of multiwalled carbon nanotubes and gold nanoparticles. *Electroanalysis* **2008,** 20, (11), 1220-1226.
94. Yan, X. B.; Chen, X. J.; Tay, B. K.; Khor, K. A., Transparent and flexible glucose biosensor via layer-by-layer assembly of multi-wall carbon nanotubes and glucose oxidase. *Electrochemistry Communications* **2007,** 9, (6), 1269-1275.
95. Wu, B. Y.; Hou, S. H.; Yin, F.; Zhao, Z. X.; Wang, Y. Y.; Wang, X. S.; Chen, Q., Amperometric glucose biosensor based on multilayer films via layer-by-layer self-assembly of multi-wall carbon nanotubes, gold nanoparticles and glucose oxidase on the Pt electrode. *Biosensors & Bioelectronics* **2007,** 22, (12), 2854-2860.
96. Sun, Y. Y.; Wang, H. Y.; Sun, C. Q., Amperometric glucose biosensor based on layer-by-layer covalent attachment of AMWNTs and IO4--oxidized GOx. *Biosensors & Bioelectronics* **2008,** 24, (1), 22-28.
97. Liu, Y.; Wu, S.; Ju, H. X.; Xu, L., Amperometric glucose biosensing of gold nanoparticles and carbon nanotube multilayer membranes. *Electroanalysis* **2007,** 19, (9), 986-992.
98. Qu, F. L.; Yang, M. H.; Chen, J. W.; Shen, G. L.; Yu, R. Q., Amperometric biosensors for glucose based on layer-by-layer assembled functionalized carbon nanotube and poly (neutral red) multilayer film. *Analytical Letters* **2006,** 39, (9), 1785-1799.

99. Zhang, J.; Feng, M.; Tachikawa, H., Layer-by-layer fabrication and direct electrochemistry of glucose oxidase on single wall carbon nanotubes. *Biosensors & Bioelectronics* **2007,** 22, (12), 3036-3041.
100. Zhang, Y. Z.; Pan, Y.; Sit, S.; Zhang, L. P.; Li, S. P.; Shao, M. W., A novel functionalized single-wall carbon nanotube modified electrode and its application in determination of dopamine and uric acid in the presence of high concentrations of ascorbic acid. *Electroanalysis* **2007,** 19, 1695-1701.
101. Zhang, M. N.; Gong, K. P.; Zhang, H. W.; Mao, L. Q., Layer-by-layer assembled carbon nanotubes for selective determination of dopamine in the presence of ascorbic acid. *Biosensors & Bioelectronics* **2005,** 20, (7), 1270-1276.
102. Liu, Y. X.; Wei, W. Z., Layer-by-layer assembled DNA functionalized single-walled carbon nanotube hybrids for arsenic(III) detection. *Electrochemistry Communications* **2008,** 10, (6), 872-875.
103. Yu, H. H.; Cao, T.; Zhou, L. D.; Gu, E. D.; Yu, D. S.; Jiang, D. S., Layer-by-layer assembly and humidity sensitive behavior of poly(ethyleneimine)/multiwall carbon nanotube composite films. *Sensors and Actuators B-Chemical* **2006,** 119, (2), 512-515.
104. Hua, F.; Cui, T. H.; Lvov, Y. M., Ultrathin cantilevers based on polymer-ceramic nanocomposite assembled through layer-by-layer adsorption. *Nano Letters* **2004,** 4, (5), 823-825.
105. Xue, W.; Cui, T. H. In *Carbon nanotube micropatterns and cantilever arrays fabricated with layer-by-layer nano self-assembly*, Workshop on Solid-State Sensors, Actuators and Microsystems, Hilton Head Isl, SC, Jun 04-08, 2006; Hilton Head Isl, SC, 2006; pp 510-517.
106. Jiang, C. Y.; Markutsya, S.; Pikus, Y.; Tsukruk, V. V., Freely suspended nanocomposite membranes as highly sensitive sensors. *Nature Materials* **2004,** 3, (10), 721-728.
107. Yuan, J. H.; Wang, Z. J.; Zhang, Y. J.; Shen, Y. F.; Han, D. X.; Zhang, Q.; Xu, X. Y.; Niu, L., Electrostatic layer-by-layer a of platinum-loaded multiwall carbon nanotube multilayer: A tunable catalyst film for anodic methanol oxidation. *Thin Solid Films* **2008,** 516, (18), 6531-6535.
108. Shi, J.; Hu, Y. Q.; Hua, Y. X., Self-assembly of platinum nanoparticle/multiwalled carbon nanotube multilayer film on Au substrate electrode. *Electroanalysis* **2008,** 20, (13), 1483-1489.
109. Wang, L.; Guo, S. J.; Huang, L. J.; Dong, S. J., Alternate assemblies of polyelectrolyte functionalized carbon nanotubes and platinum nanoparticles as tunable electrocatalysts for dioxygen reduction. *Electrochemistry Communications* **2007,** 9, (4), 827-832.
110. Chen, W. F.; Wu, J. S.; Kuo, P. L., Poly(oxyalkylene)diamine-functionalized carbon nanotube/perfluorosulfonated polymer composites: Synthesis, water state, and conductivity. *Chemistry of Materials* **2008,** 20, (18), 5756-5767.
111. Deng, L.; Shang, L.; Wang, Y. Z.; Wang, T.; Chen, H. J.; Dong, S. J., Multilayer structured carbon nanotubes/poly-L-lysine/laccase composite cathode for glucose/O-2 biofuel cell. *Electrochemistry Communications* **2008,** 10, (7), 1012-1015.

112. Sano, M.; Kamino, A.; Okamura, J.; Shinkai, S., Noncovalent self-assembly of carbon nanotubes for construction of "cages". *Nano Letters* **2002,** 2, (5), 531-533.
113. Ji, L. J.; Ma, J.; Zhao, C. G.; Wei, W.; Ji, L. J.; Wang, X. C.; Yang, M. S.; Lu, Y. F.; Yang, Z. Z., Porous hollow carbon nanotube composite cages. *Chemical Communications* **2006**, (11), 1206-1208.
114. Shi, J. H.; Chen, Z. Y.; Qin, Y. J.; Guo, Z. X., Multiwalled carbon nanotube microspheres from layer-by-layer assembly and calcination. *Journal of Physical Chemistry C* **2008,** 112, (31), 11617-11622.
115. Kim, B. S.; Kim, B.; Suh, K. D., Electrorheological properties of carbon nanotube/polyelectrolyte self-assembled polystyrene particles by layer-by-layer assembly. *Journal of Polymer Science Part a-Polymer Chemistry* **2008,** 46, (3), 1058-1065.
116. Pan, C.; Ge, L. Q.; Gu, Z. Z., Fabrication of multi-walled carbon nanotube reinforced polyelectrolyte hollow nanofibers by electrospinning. *Composites Science and Technology* **2007,** 67, 3271-3277.
117. Artyukhin, A. B.; Bakajin, O.; Stroeve, P.; Noy, A., Layer-by-layer electrostatic self-assembly of polyelectrolyte nanoshells on individual carbon nanotube templates. *Langmuir* **2004,** 20, (4), 1442-1448.
118. Du, N.; Zhang, H.; Chen, B. D.; Ma, X. Y.; Liu, Z. H.; Wu, J. B.; Yang, D. R., Porous indium oxide nanotubes: Layer-by-layer assembly on carbon-nanotube templates and application for room-temperature NH3 gas sensors. *Advanced Materials* **2007,** 19, (12), 1641-+.
119. Liu, K. S.; Fu, H. G.; Xie, Y.; Zhang, L. L.; Pan, K.; Zhou, W., Assembly of beta-cyclodextrins acting as molecular bricks onto multiwall carbon nanotubes. *Journal of Physical Chemistry C* **2008,** 112, (4), 951-957.
120. Gheith, M. K.; Sinani, V. A.; Wicksted, J. P.; Matts, R. L.; Kotov, N. A., Single-walled carbon nanotube polyelectrolyte multilayers and freestanding films as a biocompatible platformfor neuroprosthetic implants. *Advanced Materials* **2005,** 17, (22), 2663-+.
121. Pavoor, P. V.; Bellare, A.; Strom, A.; Yang, D. H.; Cohen, R. E., Mechanical characterization of polyelectrolyte multilayers using quasi-static nanoindentation. *Macromolecules* **2004,** 37, (13), 4865-4871.

Chapter II

Mechanical Properties of CNT LBL Composites

A. Survey of Mechanical Characteristics of Carbon Nanotube Composites

Single-walled carbon nanotubes (SWNTs) are the rolled-up form of graphene sheets, the strongest currently known materials.[1] The Young's modulus (stiffness) and ultimate strength of SWNTs are theoretically estimated to be $\boldsymbol{E}$ ~1 TPa, $\boldsymbol{\sigma}_{ult}$ ~ 300 GPa[2] , and experimentally determined to be $\boldsymbol{E}$ ~0.64 TPa, $\boldsymbol{\sigma}_{ult}$ ~ 37 GPa.[1] SWNTs are also extremely tough due to their hollow structures which allow energy to be absorbed by making inward collapse and plastic deformation.[3] These exceptional mechanical properties of SWNTs as well as multi-walled carbon nanotubes (MWNTs) have attracted significant research attention for their potential use as reinforcing fillers for polymeric composites. However, macro-scale composites made from carbon nanotubes (CNTs) have not yet fully produced the impressive mechanical characteristics possessed by their nanoscale constituents. The individual nanoscale building blocks underperform when they are incorporated into composites due to inefficient stress transfer with the polymer matrix. This represents one of the most challenging problems in materials science, and its resolution has signification implications from both fundamental and practical perspectives.

The road to practical realization of such composites lies through careful structural design of the materials and control of the polymer-nanotube interface. Molecular and nanoscale engineering of different hybrid organic–inorganic materials can be accomplished by using the layer-by-layer assembly (LBL) technique of composite manufacturing. Compared to the traditional extrusion, mixing, supercritical liquid processing, and other methods of bulk composite preparation, LBL possesses key advantages for nano-scale organization, such as high degree of structural control, ability to incorporate different nanomaterials in one structure leading to multifunctional composites, and the possibility to produce coatings and free-standing films on 2D and 3D surfaces and topologies. This LBL technique presents another unique advantage in terms of nanoscale mechanics. Intermediate rinsing stages of the LBL process stimulate efficient interfacial bonding between the components of the composites by removal of polymeric chains loosely attached to SWNTs. The LBL composites have also shown unusually high loadings of SWNTs and excellent homogeneity of the resulting material. Orientation of nanotubes along one direction has been demonstrated during the LBL processing.[4, 5] Alignment of reinforcing fillers should help to distribute the stress in the material better than randomly oriented fillers, as was recently demonstrated for clay platelets.[6]

As CNT nanocomposites have been made by a large variety of techniques, it is desirable to extract the principles determining the organization of various nanocomposites from the large amount of available data. As the first step toward this goal, we provide here a brief survey of the mechanical parameters reported for nanocomposites

produced from different manufacturing methods. In this effort we avoid extensive discussion of theoretical approaches which can be found in several recent reviews,[7-9] but rather focus on simple numerical descriptors. In addition to ultimate strength and stiffness, particular attention is given to toughness ***(K)*** which, in many cases, we calculated for the reported materials when sufficient data are available in the corresponding publications. In our opinion, ***K*** is probably the most critical parameter in many applications, ranging from fuel cells[10] to aviation.[11, 12] We want to acknowledge that methods of improving ***K*** in CNT nanocomposite systems are not well understood[13] and have been achieved in the past mostly by rather accidental discoveries.

CNT-polymer nanocomposite can be divided into two major categories: unidirectional fibers and fairly random bulk composites. There are significant differences in the properties, material design factors, manufacturing approaches, and potential areas of use between the two categories as well as similarities, such as necessity of strong matrix-nanotube bonding, dense packing of CNT fillers, and the well-known challenge of full exfoliation of CNTs. Furthermore, monodispersity of SWNT structures are receiving growing attention in both directions.[14] The importance of the monodispersity and the exfoliation of SWNTs can be illustrated by a simple example. The fillers with 10 nm and 1 nm in diameter have an order of magnitude difference in the interfacial area between fillers and matrix,[15] which significantly affects the efficiency of load transfer from matrix to nanotubes.[16] Analytical methods used to establish the degree of exfoliation can also be employed to probe the size variations of SWNTs. It include the indirect optical measurements by UV-Vis-NIR spectroscopy (van Hove transitions),[17] Raman

spectroscopy[18], band-gap fluorescence microscopy,[19] and direct observations by transmission electron microscopy (TEM) and atomic force microscopy (AFM). A combination of these methods should be applied to characterize nanocomposites.

1. Unidirectional CNT Nanocomposite Fibers

One of the most obvious and efficient ways to introduce alignment of CNTs is the utilization of shear dynamic forces. Ribbons with significant degree of alignment were formed by injecting SWNTs dispersed in poly(vinyl alcohol) (PVA) into a vigorously stirred solution. The mechanical properties of the produced fiber were $\boldsymbol{\sigma}_{ult}$ = 150 MPa, $\boldsymbol{E}$ = 15 GPa, and $\boldsymbol{K}$ ~ 2 J/g. [20] Improvements were made with similar solution spinning techniques, yielding fibers of $\boldsymbol{\sigma}_{ult}$ = 1.8 GPa and $\boldsymbol{K}$ = 570 J/g with 60 wt% of SWNT loading.[21, 22] These measurements were rivaled by those of fibers made by the hot drawing approach which produced $\boldsymbol{\sigma}_{ult}$ = 1.8 GPa for SWNTs, and $\boldsymbol{\sigma}_{ult}$ = 1.4 GPa for MWNTs.[23] The toughness measurements for the same materials were reported to be $\boldsymbol{K}$ = 870 J/g for SWNTs and $\boldsymbol{K}$ = 690 J/g for MWNTs, holding the record for the aligned fiber composites. The high toughness of these CNT fibers was explained by the partial crystalinity of PVA, efficient alignment, and interactions between SWNTs and PVA chains, but no information was disclosed regarding the CNT to PVA ratio and kinds of interactions involved.[24]

Although most solution spinning techniques for fiber production have revealed efficient alignment of SWNTs, very few of them have produced equally impressive

performance. We can infer from this observation that specific interactions between CNTs with PVA must have a key role in the mechanical properties. The importance of the matrix is illustrated by SWNT fibers made from sulfuric acid dispersion without polymer matrix.[16] The fibers yielded $\boldsymbol{\sigma_{ult}}$ = 116 MPa and $\boldsymbol{E}$ = 120 GPa (data were insufficient for calculation of $\boldsymbol{K}$). Without a polymer binder, the ultimate strength of solution processed SWNT fibers cited here is an order of magnitude lower than those from polymer containing fibers.

Spinning of gels with SWNTs was realized for polyacrylonitrile composites and resulted in 5~10% SWNT loaded fibers with $\boldsymbol{\sigma_{ult}}$ = 360 MPa, $\boldsymbol{E}$ = 16.2 GPa and $\boldsymbol{K}$ ~ 20.[25] The authors pointed out that the exfoliated state of SWNTs in the solution was not preserved in the fibers as indicated by the disappearance of van Hove transitions.[26] PVA gels can also be spun with SWNTs producing fibers yielding noticeably better performance with $\boldsymbol{\sigma_{ult}}$ = 1.1 GPa, $\boldsymbol{E}$ = 35.8 GPa, and $\boldsymbol{K}$ ~ 32 J/g, although the SWNT content was fairly low – only 3%.[27] Wet spinning of SWNT fiber with poly(p-phenylene-2,6-benzoxazole) (PBO) displayed $\boldsymbol{\sigma_{ult}}$ = 4.2 GPa, $\boldsymbol{E}$ = 167 GPa, and $\boldsymbol{K}$ ~ 45 J/g with 10% SWNT content.[28]

Multi-walled carbon nanotubes (MWNTs) can be synthesized in an aligned fashion (i.e. nanotube forest),[29] making dry spinning of CNT fibers possible without an intermediate dispersion stage.[30] Dry spinning was first developed to produced twisted CNT yarns and was later incorporated with polymer infiltration[31] and solvent densification[32] to increase yarn strength. The earlier reports on dry spinning showed density-normalized ultimate strength of $\boldsymbol{\sigma_{ult}/\rho}$ = $\boldsymbol{\sigma_{ult}^{d}}$ = 500 MPa· cm^3/g.[33] The best

performance from such process is an aerogel type spun fiber showing $\boldsymbol{\sigma_{ult}}$ = 8.8 GPa, $\boldsymbol{E}$ = 357 GPa and $\boldsymbol{K}$ = 121 J/g.[34] Recently, similarly respectable measurements have been reported for a dry spun fiber having $\boldsymbol{\sigma_{ult}}$ = 3.3 GPa, $\boldsymbol{E}$ = 263 GPa and $\boldsymbol{K}$ = 975 J/g.[35] We, however, will not include this toughness measurement in our discussion because in the experiment most of the energy absorption took place after the highest stress peaks. Overall, dry spinning improves both strength and stiffness by efficient alignment of intact and long MWNTs, as well as by densification to optimize stress transfer between nanotubes. However, the toughness of matrix-free fibers still suffers compared to those made by solution spinning.

Micro/nanofibrilar sheets have also been made by aligned CNT fibers. The density-normalized strength of transparent sheets woven from CNT yarns was reported to be $\boldsymbol{\sigma_{ult}^{d}}$ =175 MPa· cm^3/g, which exceeds the density-normalized strength of steel $\boldsymbol{\sigma_{ult}^{d}}$ ~125 MPa· cm^3/g. For comparison, one can also recall the density-normalized strength of Mylar or Kapton films $\boldsymbol{\sigma_{ult}^{d}}$ ~ 160 MPa· cm^3/g and aluminum $\boldsymbol{\sigma_{ult}^{d}}$ ~250 MPa· cm^3/g.[36] Another unique example is CNTs growth on a SiC fabric. The flexural mechanical properties of the SiC-MWNT fabric were $\boldsymbol{\sigma_{Flexural}}$ = 150 MPa, $\boldsymbol{E_{Flexural}}$ = 24 GPa and $\boldsymbol{K_{Flexural}}$ = 30.4 Nmm.[37]

Electrospinning (e-spinning) is also a popular method in preparation of nanofiber-based sheets. Polystyrene, polyurethane[38], nylon 6,[39] PVA,[40] and polyacrylonitrile[41-43] have been employed as a polymer matrix for electrospun fibers. Polyurethane-SWNT e-spun nanofiber sheets showed $\boldsymbol{\sigma_{ult}}$ = 15 MPa, $\boldsymbol{E}$ = 25 MPa and $\boldsymbol{K}$ ~29 J/g.[38] E-spun

polyacrylonitrile composite mats showed a different behavior. With 20% MWNT loading, the e-spun sheets yielded $\boldsymbol{\sigma_{ult}}$ = 285 MPa, $\boldsymbol{E}$ = 14.5 GPa and $\boldsymbol{K}$ ~ 5.4 J/g.[42]

It must be brought to attention that most of the CNT-based fibers described so far do not possess mechanical characteristics sufficiently higher than those of commercialized long carbon fibers. For example, the mechanical parameters of the strong Torayca carbon fibers made by Toray Inc. have $\boldsymbol{\sigma_{ult}}$ = 6.4 GPa, $\boldsymbol{E}$ = 294 GPa, $\boldsymbol{\varepsilon}$ = 2.2%, while the stiff Torayca carbon fibers have $\boldsymbol{\sigma_{ult}}$ = 3.9 GPa, $\boldsymbol{E}$ = 588 GPa, $\boldsymbol{\varepsilon}$ = 0.8%. Their bulk composites with 60% fiber and epoxy resin claim to achieve $\boldsymbol{\sigma_{ult}}$ = 3.0 GPa, $\boldsymbol{E}$ = 165 GPa, $\boldsymbol{\varepsilon}$ = 1.7% and $\boldsymbol{\sigma_{ult}}$ = 2.0 GPa, $\boldsymbol{E}$ = 365 GPa, and $\boldsymbol{\varepsilon}$ = 0.6%, respectively for the strong and stiff fibers. These composites are now industrially used in sporting goods, aerospace components, pressure vessels, and so forth.

2. Homogeneous bulk composites

If we comparing the data for bulk composites and unidirectional fibers, it is easy to see that mechanical parameters of the bulk composites are significantly lower than those for the fibers, often by an order of magnitude. This is related to several factors. (1) The key structural difference between the two types of composites is the need for nanotubes to stretch and reorganize during the deformation of the bulk nanocomposites, while the stress in the aligned fibers is transferred to the nanoscale “reinforcing bars” in a more efficient manner. (2) Mixtures in kinetically frozen states such as drawn fibers have intrinsically lower degree of phase separation. Segregation of components even at the

nanoscale creates local defects, which is detrimental for mechanical properties. This process has far greater propensity to take place in thermodynamically equilibrated bulk phases. (3) The CNT loading of aligned fibers is significantly higher than those of the bulk composites in a same volume. We must emphasize that despite structural advantages, fibrous materials still cannot replace bulk materials for a variety of applications, especially when continuity, flatness, uniformity of heat/electrical/gas transport, or isotropic distribution of stress are required. Furthermore, unidirectional fibers still need secondary macro-scale processing to prepregs, fabrics, braids, etc.

Keeping these issues in mind, let us survey some of the bulk composites with the best mechanical characteristics reported so far. Typically more impressive mechanical properties of materials in this class are obtained after chemical cross-linking between the CNTs and the matrix, which can be realized by in-situ polymerization[44] and direct polymer functionalization of CNTs.[45] It was also proven theoretically that cross-linking significantly improves the overall composite strength[46-48] and toughness.[49] These predictions[50] were confirmed by a series of pull-out experiments of CNTs from polymer matrix with various interfaces[51, 52] showing that more efficient load transfer to fibers takes place after cross-linking. One representative example is an SWNT-Nylon 6 composite fiber with $\boldsymbol{\sigma_{ult}}$ = 109 MPa, $\boldsymbol{E}$ = 790 MPa and $\boldsymbol{K}$ ~ 146 J/g.[53] Direct funtionalization with polyurethanes also produced encouraging bulk composites with $\boldsymbol{\sigma_{ult}}$ = 45 MPa, $\boldsymbol{E}$ = 9.6 MPa, and $\boldsymbol{\sigma_{ult}}$ = 38 MPa, $\boldsymbol{E}$ = 22 MPa for mixed and grafted composites respectively.[54] The strain of these materials were as high as $\boldsymbol{s}$ = 969% (mixed) and $\boldsymbol{s}$ = 852% (grafted) which corresponded to toughness of $\boldsymbol{K}$ ~ 124~167 J/g. Although

the strain of elastomeric materials is usually high, the stiffness of these materials, however, is typically fairly low.[55] Analogous results were also obtained for chlorinated polypropylene: $\boldsymbol{\sigma_{ult}}$ = 49 MPa, $\boldsymbol{E}$ = 0.68 GPa, $\boldsymbol{K}$ = 108 J/g.[56] As expected, the same process for epoxy resins gave even stronger and stiffer materials but with lower toughness: $\boldsymbol{\sigma_{ult}}$ = 104 MPa, $\boldsymbol{E}$ = 2.65 GPa, $\boldsymbol{K}$ ~ 3.4 J/g.[57]

Cross-linking is a logical approach to improving mechanical characteristics, but recent data suggests that it is not the only answer and probably not the best answer to load transfer.[58] Composites from CNTs with non-covalently attached poly(p-phenylene ethynylenes), which are often used in luminescent sensors,[59, 60] were demonstrated to yield competitive mechanical properties of $\boldsymbol{\sigma_{ult}}$ = 250 MPa, $\boldsymbol{E}$ = 5 GPa,and $\boldsymbol{K}$ ~ 25 J/g.[61] Crystalized poly(vinylalcohol) (PVA) composites with 0.6% MWNT loading were reported to produce $\boldsymbol{\sigma_{ult}}$ = 348 MPa, $\boldsymbol{E}$ = 7.04 GPa and $\boldsymbol{K}$ ~ 6.7 J/g.[62] Therefore, one may also choose utilize polymers with strong physical adsorption on the nanotubes. Such polymer chains may order and crystallize around CNTs,[63, 64] which can strongly affect the mechanics at the CNT-polymer interface.

Layer-by-layer (LBL) assembled nanotube materials have more similarities with bulk CNT composites than fibers because the nanotubes in LBL multilayers also undergo substantial restructuring during deformation. With a fairly non-optimal polymer such as poly(ethyleneimine) (PEI), the hybrid composites displayed $\boldsymbol{\sigma_{ult}}$ = 220 MPa, $\boldsymbol{E}$ = 16 GPa, $\boldsymbol{K}$ ~ 0.85 J/g[65] and $\boldsymbol{\sigma_{ult}}$ = 150 MPa, $\boldsymbol{E}$ = 4.5 GPa, $\boldsymbol{K}$ ~ 3.7 J/g[66] for SWNT and MWNT multilayers respectively. The impressive strength performance with weak polymer compared to other previously mentioned materials is attributed to the uniform CNT

dispersion, kinetic thresholds for phase separation, and high loading of CNT fillers. Recently, ordered packing of strong fillers, such as clay nano-platelets, by LBL assembly with PVA and appropriate cross-linking between constituents showed exceptionally strong and stiff mechanical properties in the resulting composite films.[6]

B. Increasing Strength and Toughness of CNT LBL Composites

1. Summary

Carbon nanotubes (CNT) – polymer hybrid materials are expected to produce unusual mechanical properties when their hybrid coupling structures are organized at the molecular level. Here, we report strong and tough SWNT-PVA nanocomposites fabricated by layer-by-layer (LBL) assembly techniques which enables these structural requirements to improve the stress transfer at the nano-scale. The typical mechanical properties of known SWNT composites, such as strength, stiffness, and toughness, are assessed in an introductory survey where we conclude that nanoscale organization, SWNT loading, and bonding with the matrix are important parameters in structural engineering of SWNT composites. By optimizing these parameters within the framework of LBL technique, the resulting SWNT-PVA composites demonstrated ultimate tensile strength ($\boldsymbol{\sigma_{ult}}$) = 504.5±67.3 MPa, stiffness ($\boldsymbol{E}$) = 15.6±3.8 GPa, and toughness ($\boldsymbol{K}$) = 121.2±19.2 J/g with maximum values recorded at $\boldsymbol{\sigma_{ult}}$ = 600.1 MPa, $\boldsymbol{E}$ = 20.6 GPa, and $\boldsymbol{K}$ = 152.1 J/g. This represents one of the strongest, stiffest, and toughest non-fibrous SWNT composites made to date. Our observation suggests that the strengthening and toughening

mechanism originate from the synergistic combination of SWNT exfoliation, efficient SWNT-PVA binding, crack surface roughening, and multiple micro-crazing. In addition, the tough composite displays a pseudo-textile breaking behavior unlike other bulk composites.

2. Experimental Procedure

Purified HiPco SWNTs were purchased from Carbon Nanotechnologies Inc. (CNI). In order to incorporate various amounts of functional groups on SWNTs, SWNTs were treated with 15.8M HNO_3 for 2 hrs and, 7.9M HNO_3 for 1 hr in an ultrasonic bath. These functionalized SWNTs were filtered with PTFE membrane, rinsed with deionized water, and collected as solid powder. We denote $SWNT_{-COOH}$(15.8) and $SWNT_{-COOH}$(7.9) respectively by the concentration of HNO_3. Non-treated SWNTs were denoted as $SWNT_{-COOH}$ (0). The relative amounts of oxygen incorporated in SWNT-COOH were estimated by EDAX analysis. (Figure 2) This powder was re-dispersed in a poly(sodium 4-styrene-sulfonate) (PSS, MW 1,000,000, Sigma-Aldrich Co.) solution in ultrasonic bath for three days. The weight ratio of SWNTs and PSS was 1:2 and the concentration of SWNTs was adjusted to 0.05wt%. Poly(vinyl alcohol) (PVA, MW 195,000, Mowiol 56-98, Kuraray and Fluka) solution was prepared as a counter LBL partner of SWNTs.

LBL assembly was carried out on cleaned glass substrates. First, the glass slide was dipped in a PVA solution (pH 1.5, 0.25 wt%, 20^{o}C) for 10 min, then rinsed in deionized water (pH 5~7), and dried in compressed air. The slide was again dipped in a

SWNT dispersion solution (pH 12, 1 wt%, 20^{o}C) for 10 min, which was followed by rinsing and drying. This cycle was repeated *n* times producing a coating with a cumulative structure [PVA/SWNT$_{-COOH}$(15.8, 7.9, 0) + PSS]$_n$. We used automated LBL deposition robots to minimize the variability of manufacturing parameters.

Bonding of SWNT functional groups to matrix was done by two methods: (1) thermal cross-linking annealing at 220^{o}C for 10 min, (2) chemical cross-linking by immersion in 5% glutaraldehyde (GA) GA solution in water for 1 hr and subsequent drying in vacuum. Subsequently, the films were easily peeled off from the substrate by immersing in 1% HF solution.

The mechanical properties of the SWNT composites were obtained by stretching test in an Instron Q systems model 100 (Test Resources). The free-standing sample strips were cut by 1±0.3 mm of width. The rate of stretching and the initial gap between grips were 0.01 mm/s and 4±1 mm respectively. For accuracy, all the testing dimensions were directly measured by precision calipers and the measurements were reproduced and averaged 3 ~ 5 times.

Scanning electron microscopy (SEM) images were taken by a FEI Nova Nanolab dualbeam FIB and scanning electron microscope. Atomic force microscopy (AFM) imaging was performed with a Nanoscope III atomic force microscope (Digital Instruments/Veeco Metrology Group). X-ray photoelectron spectroscopy (XPS) results were obtained uaing a Kratos Axis Ultra X-ray Photoelectron Spectrometer. UV-vis absorption measurements were taken using an Agilent 8453E UV-visible spectrometer.

Thermo gravimetric analysis (TGA) was performed by a PerkinElmer Pyris 1 TGA. Ellipsometric measurements were obtained from an M-44 IR Spectroscopic Ellipsometer (J. A. Woollam Co., Inc.).

3. SWNT LBL Assembly and Film Characterization

The dissolution is PSS allowed the HiPCo SWNTs to be almost perfectly exfoliated.[67, 68] The SWNT colloids were negatively charged due to PSS wrapping and oxidation, while the PVA is neutral at the assembly conditions. Thus, the traditional understanding of LBL as alternation of positive/negative components is not applicable to these multilayers. The adsorption driving force of SWNT-PSS on PVA is a manifold of fairly weak interactions which include hydrogen bonding, van der Waals attraction, dipolar electrostatic forces, and hydrophobic interaction.[69] The repetition of LBL cycles resulted in linear film growth, which was identified by UV-vis absorption spectra (Figure 2 A, B). The growth rates depended on pH and temperature (Figure 2 C, D). After the initial stage of layering optimization, we chose PVA solution with pH 1.5 and SWNT dispersion with pH 12 as the LBL processing conditions for the preparation of thick free-standing films for mechanical testing. These conditions gave the densest SWNT adsorption per deposition cycle (Figure 2 C-E) compared to other conditions.

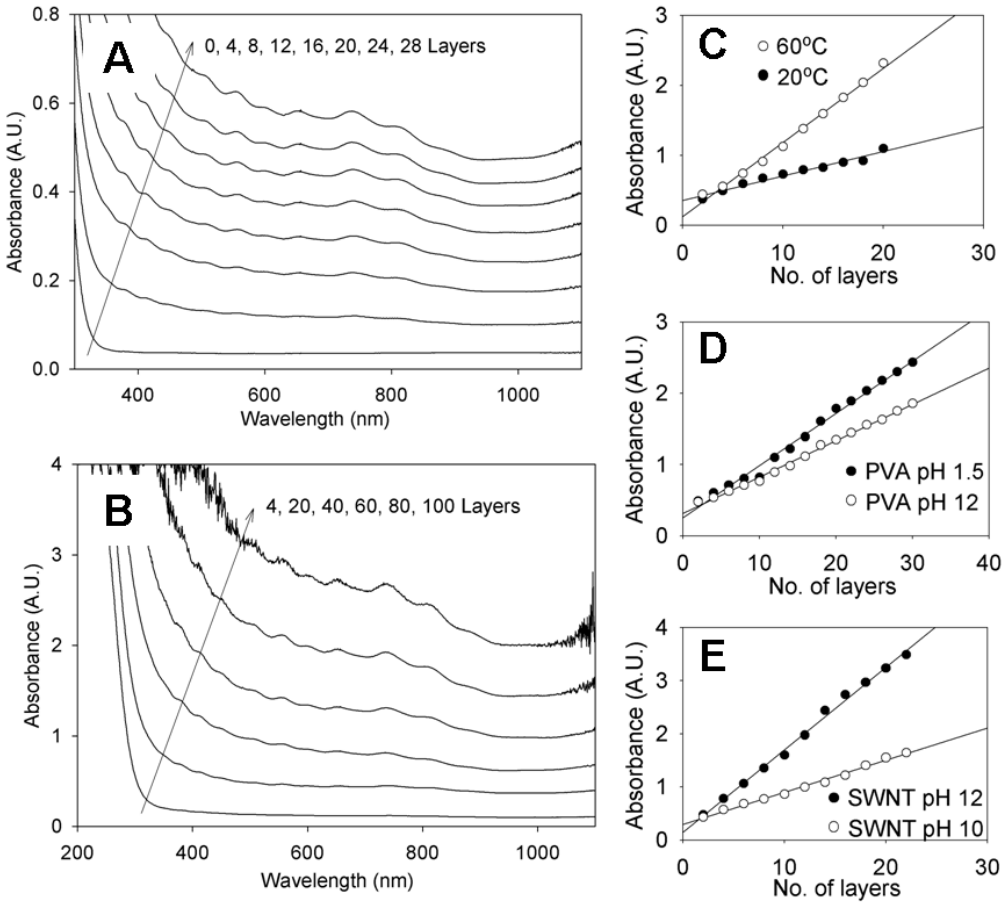

Figure 2 (A-B) UV-vis absorbance spectra of [PVA / $SWNT_{-COOH}$ (15.8)]$_n$ LBL assembly. The values of *n* are indicated in the graphs. (C-E) UV-vis absorbance at 300 nm trend of LBL assembly with various solution conditions: (C) processing temperature, (D) pH of a PVA solution, and (D) pH of a SWNT solution.

The optical properties of nanomaterials are characterized by discrete excitonic transitions from valence electronic bands to conduction bands. For SWNTs, they are observed in UV-Vis-NIR spectra as a series of peaks and shoulders also known as van Hove singularities. These peaks and shoulders are not observed from powdered or highly bundled SWNTs because of electronic broadening of energy states, but only from well separated or exfoliated SWNTs according to their size and structural distributions.

Importantly, for LBL films of SWNTs, the van Hove transitions are easily observed and do not change as the number of SWNT cycles increases (Figure 2 A, B). This indicates that the exfoliation of SWNTs in the solution state can be preserved during LBL assembly and that little electronic coupling with adjacent SWNTs occurs as the film becomes thicker. We would like to point out that the spectral characteristics of SWNT multilayers are in contrast to LBL films made from metal particles, in which the plasmon peak shifts strongly with increasing LBL deposition cycles.[70]

To confirm the exfoliated state of adsorbed SWNTs, film topography was observed by tapping mode atomic force microscopy (AFM). The degree of exfoliation of SWNTs was assessed using the height differences obtain in section analysis (Figure 3 A, B) as an indicator. Even though very few agglomerates were observed, the height of the majority of long strands associated with SWNTs was less than 2 nm, which is indicative of high degree of exfoliation. Furthermore, few thick strands, having cross-sections above 2 nm, could due to both localized thick polymer coverage on individual SWNTs and occasional bundles of long and short tubes.

Thick film samples prepared by hundreds of LBL cycles were characterized to examine their structures, dimensions, and compositions. SEM images of cross-sections indicate that the resulting LBL films are dense non-porous materials (Figure 4 A-C). The thickness of a 200-bilayer LBL nancomposite ranged between 300 and 400 nm, which corresponds to 1.5~2 nm of adsorption in each deposition cycle. Film morphologies reminiscent of combed hair that originated from stretched SWNTs were observed at edges cut by a razor blade (Figure 4 D, E).

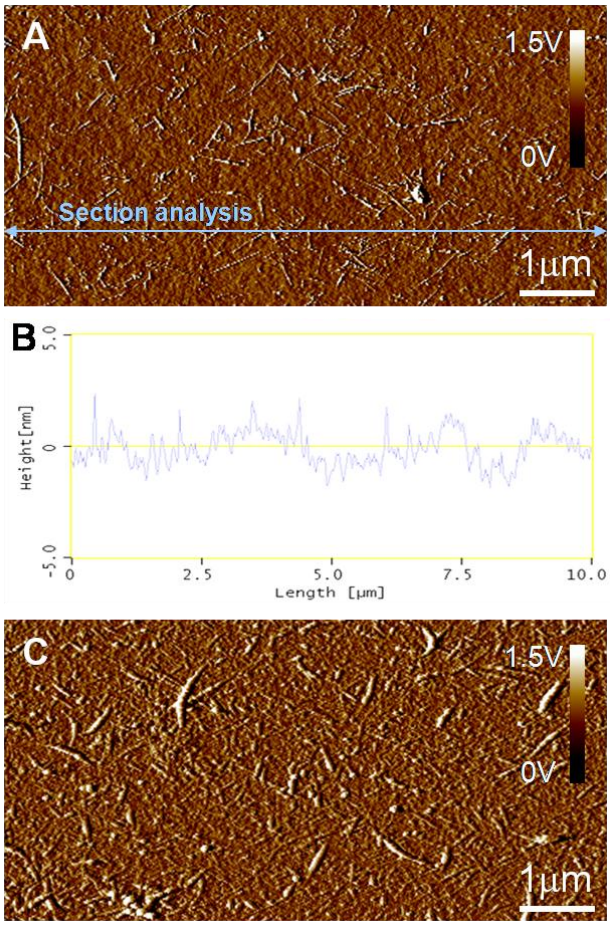

Figure 3 (A) AFM image of [PVA/SWNT-$_{COOH}$(15.8) + PSS]$_1$ and B) Height information of section analysis following blue arrows in (A). (C) AFM image of [PVA/SWNT-$_{COOH}$(15.8) + PSS]$_2$

Carbon nanotube contents in the film were varied by changing the surface charge of SWNTs and adsorption of polymer during LBL processing. Overall, the SWNT loading in the LBL films were estimated by TGA to be 47 % with SWNT-$_{COOH}$(0), 60 % with SWNT-$_{COOH}$(7.9), 72 % with SWNT-$_{COOH}$(15.8) when we compared the tests in air and N_2 environment.[68] (Figure 5)

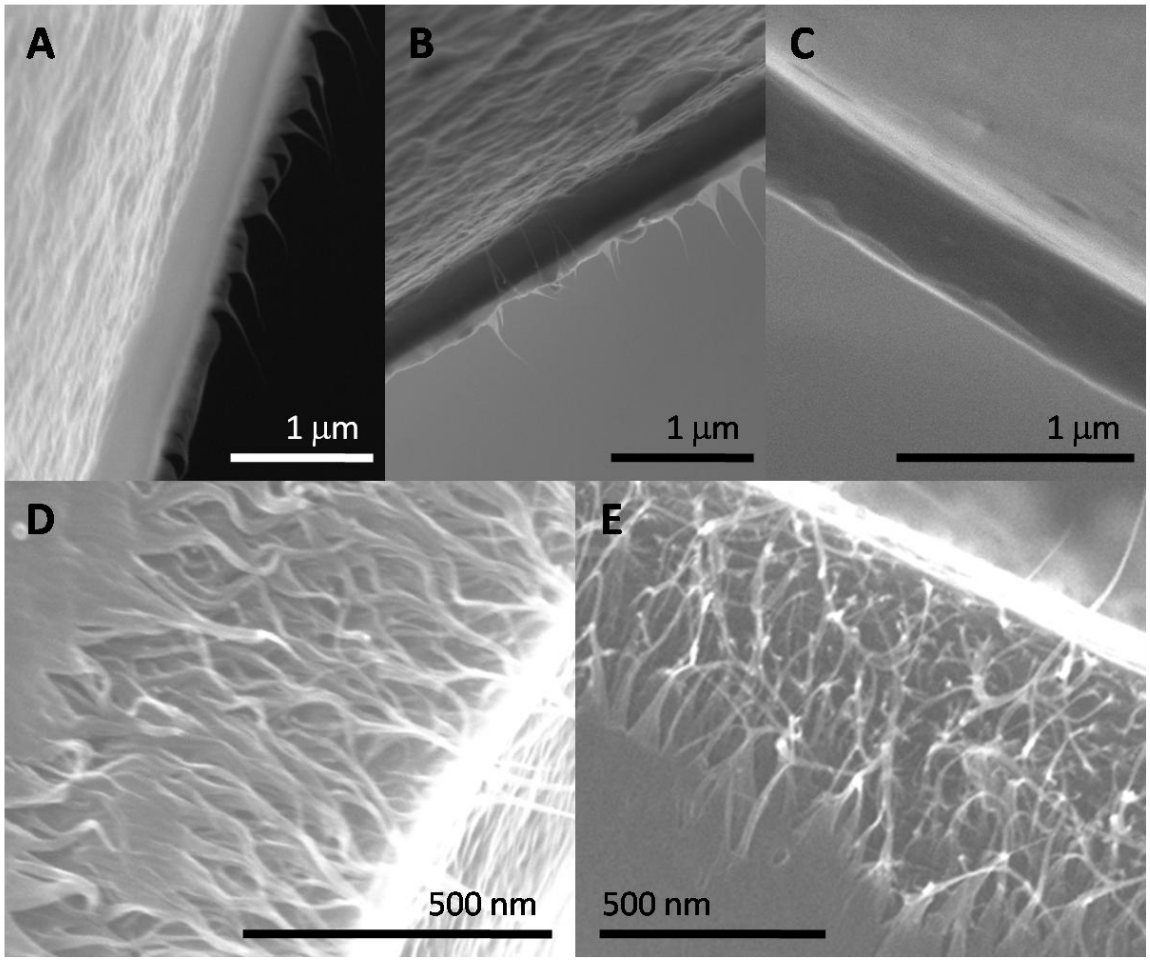

Figure 4 SEM images of LBL film cross-sections cut by a razor blade: (A) [PVA / $SWNT_{-COOH}(0)$ + PSS]$_{200}$ with GA treatment, (B) a [PVA / $SWNT_{-COOH}(7.9)$ + PSS]$_{200}$ with GA treatment, and (C) a [PVA / $SWNT_{-COOH}(15.8)$ + PSS]$_{200}$ with GA treatment. Close-up images showing combed SWNTs by a razor blade action in (D) [PVA / $SWNT_{-COOH}(7.9)$ + PSS]$_{600}$ and (E) [PVA / $SWNT_{-COOH}(15.8)$ + PSS]$_{215}$.

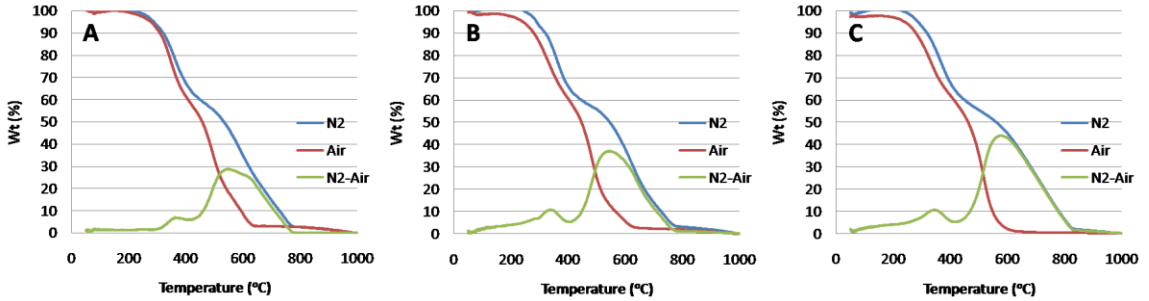

Figure 5 TGA analysis of (A) [[PVA/SWNT-COOH(0) +PSS] LBL, (B) [PVA/SWNT-COOH(7.9) +PSS] LBL, and (C) [PVA/SWNT-COOH(15.8) +PSS] LBL nanocomposite films.

Table 2 XPS analysis of SWNT LBL nanocomposite films

Samples	Cross-linkage	Amt. %			Ratio
		C	O	S	C/O
[PVA/SWNT-COOH(15.8) +PSS] LBL film	-	76.0	23.8	0.2	3.2
	Heat	77.3	22.5	0.2	3.4
	GA	77.5	22.3	0.2	3.5
PVA/SWNT-COOH(7.9) +PSS] LBL film	-	80.3	18.7	0.9	4.3
	Heat	77.9	21.8	0.3	3.6
	GA	78.4	21.2	0.3	3.7
[PVA/SWNT-COOH(0) +PSS] LBL film	-	78.8	20.8	0.3	3.8
	Heat	80.8	19.0	0.2	4.3
	GA	80.7	18.7	0.6	4.3

Based on the C, O, and S composition in the composites as determined by XPS (Table 2), the estimated contents of PSS in the LBL films were 1.1±0 % with SWNT-COOH(0), 2.9±2.0 % with SWNT-COOH(7.9), 2.1±1.2 % with SWNT-COOH(15.8). Even considering the potential inaccuracy of XPS, the measured amount of PSS in the composites was unexpectedly low. Originally from 1:2 mass ratio of SWNT:PSS in the

dipping solutions, 20~40 times more SWNTs were actually transferred to the solid composites by LBL assembly than PSS.

4. Mechanical Properties of SWNT LBL Composites

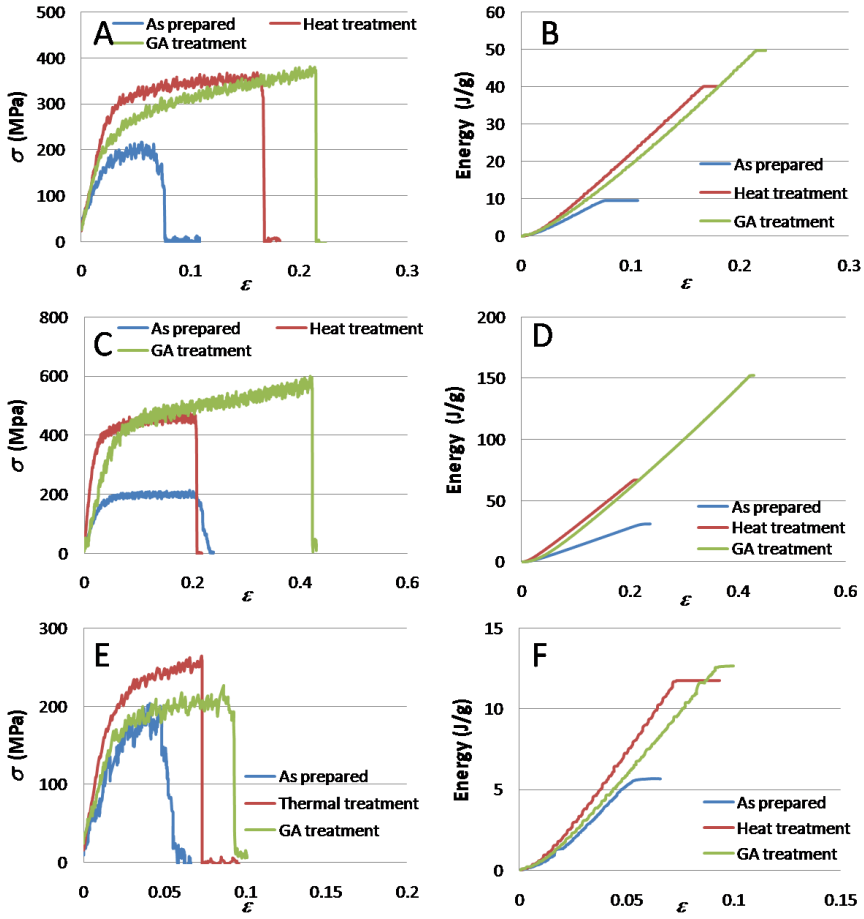

Figure 6 Tension test results of SWNT LBL nanocomposites. (A, C, E) Stress-strain and (B, D, F) toughness-strain curves of (A, B) $[PVA / SWNT_{-COOH}(15.8) + PSS]_{200}$, (C, D) $[PVA / SWNT_{-COOH}(7.9) + PSS]_{200}$, and (E, F) $[PVA / SWNT_{-COOH}(0) + PSS]_{200}$. Additional processing steps of the composites are indicated in the graphs.

Table 3 Comparison table of ultimate tensile strength (σ_{ult}), stiffness (***E***), toughness (***K***), strain (ε), and CNT loading for LBL composites and other materials.

Samples (estimated CNT loading)	Cross-linkage	σ_{ult} (MPa)	E (GPa)	K (J/g)	ε (%)
[PVA/SWNT$_{-COOH}$(15.8) +PSS] LBL (70%)	GA	391.5±36.8	13.2±2.4	42.8±10.5	18±4
	Heat	359.9±41.5	15.1±2.8	41.4±7.4	18±3
	-	257.2±24.6	11.9±2.5	13.8±3.8	11±1
PVA/SWNT$_{-COOH}$(7.9) +PSS] LBL (60%)	GA	504.5±67.3	15.6±3.8	121.2±19.2	39±3
	Heat	452.6±30.1	23.0±2.4	47.9±16.9	16±4
	-	224.5±15.1	11.6±2.0	26.9±10.5	19±7
[PVA/SWNT$_{-COOH}$(0) +PSS] LBL (47%)	GA	233.4±25.7	11.3±2.0	11.3±5.0	8±3
	Heat	262.57±2.1	10.9±0.8	12.8±1.5	8±1
	-	196.6±30.2	14.2±1.7	5.8±3.8	6±2
[PVA/Clay] LBL[6]	GA	400±40	106±11	~ 0.5	0.3±0.04
PVA[6]	-	40±4	1.7±0.2	~ 7.7	35±4
High performance CNT fiber[34] (100%)	-	8800	357	121	~8
SWNT Nylon composite fiber[53] (0.5%)	-	109	0.79	146	350
Kevlar fiber[71]	-	3600	90	33	5
Spider silk[71]	-	1150±200	7.9±1.8	165±30	39
Aluminum alloy (7075-T6)	-	572	71.7	29	11

Mechanical tests of these samples were performed by direct stretching using a standard Instron equipment and protocol. Because one of the goals of this measurement was to identify parameters that significantly affect the mechanical strength, stiffness, and toughness, the stress-strain and toughness-strain curves and the data results of the various SWNT composites were shown in Figure 6 and Table 3. As two principal parameters determining materials performances here, we selected (1) the density of sticky functional

groups on a SWNT and (2) effective conversion of functional groups to strong covalent interfaces in a composite structure. Optimizations of other processing factors are less crucial and rather intuitive. Thinner PVA layers and longer PVA molecular chains are preferable to improve the mechanical properties.

First, we varied the density of sticky functional sites on SWNTs. More functionalization causes benefit to the interfacial interactions between PVA and SWNTs but loss to the crystal perfectness in SWNTs. Furthermore, creations of functional sites on a SWNT are not uniform at all; end-caps first and side-wall later. Although this non-linear functionalization may not be identified, the overall variations could be achieved by adjusting acid treatment conditions of SWNTs; HNO_3 concentration and treatment time. We employed fairly mild conditions like no oxidation (0M), 7.9M / 1 hr, and 15.8M / 2 hr at room temperature. Figure 7 shows that the densities of functional sites were successfully varied on SWNTs. By the auto-coupling LBL assembly, this variation affected not only stress transfer function but also the overall contents of SWNTs in the composites. Let's compare the blue lines in Figure 6 A, C, E, which are as-prepared LBL composites without covalent bonding modification. Only very marginal deviations in tensile strength and modulus were observed by adding sticky groups on SWNTs toward PVA matrix. The changes in the toughness, however, were notable. Starting from 7.7 J/g for pure PVA, the toughness of the LBL composites shifted to 5.5 J/g for $SWNT_{\text{-COOH}}(0)$, to 26.9 J/g for $SWNT_{\text{-COOH}}(7.9)$, and then to 13.8 J/g for $SWNT_{\text{-COOH}}(15.8)$. This variation in toughness was a consequence of the simultaneous changes in SWNT contents and the energy transfer efficiencies by introducing sticky interface between SWNTs and

PVA. Although toughness changes are extrmely difficult to predict as seen in our survey, this hypothesis is supported by some previous reports. Firstly, the toughness could be improved by simply increasing the CNT content..[62, 72] Coleman et al. reported toughness improvements by 1.7 times for crystalline PVA reinforced by addition of MWNTs and 4.4 times for cross-linking of PVA – MWNT composites.[62] The toughness was gradually improved by increasing MWNT's contents up to 0.6 % although the CNT contents were much lower than our LBL composites here. Secondly, traits of surface conditions of CNTs are also crucial to improving the toughness both of homogeneous bulk composites[49, 73] and of aligned fibers.[20, 21, 23, 24] Particularly, the increase in the toughness of the PVA-SWNT fibers, which was observed over time from 2 J/g[20], to 570 J/g,[21] and to 870 J/g,[23] was attributed to the special binding roles of PVA, namely its affinity[75] and chain stretch,[24]as well as the alignment of CNTs. Therefore, effectively long SWNTs with sticky functional groups might help to improve overall toughness in LBL composites.

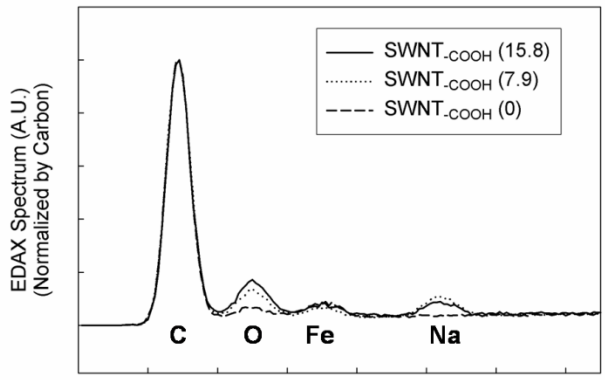

Figure 7 EDAX measurements for $SWNT_{-COOH}$ treated with varied HNO_3 concentrations. Averaged O/C ratio of $SWNT_{-COOH}$ (15.8), (7.9) and (0) were 0.23±0.01, 0.199±0.006, and 0.133±0.02 respectively. There are residual amounts of Fe catalysis from SWNT production and Na from acid filtration process.

Second, we demonstrated that effective cross-linking conversion of sticky sites further improved the mechanical properties. The two cross-linking methodologies used here were thermal ester bond formation between –COOH in SWNTs and –OH in PVA and glutraraldehyde (GA) treatment which forms a complex branched matrix by grafting PVA chains. We found that the LBL composite with $SWNT_{-COOH}(7.9)$ demonstrated the most dramatic cross-linking effect from both heat and GA treatments, possibly due to attainment of the optimal molecular interactions. After cross-linking the $[PVA/ SWNT_{-COOH}(7.9) +PSS]_{200}$ film, the mechanical properties changed from the original values of $\boldsymbol{\sigma_{ult}}$ = 224.5 MPa, $\boldsymbol{E}$ = 11.6 GPa and $\boldsymbol{K}$ = 26.9 J/g to $\boldsymbol{\sigma_{ult}}$ = 452.6 MPa, $\boldsymbol{E}$ = 23.0 GPa and $\boldsymbol{K}$ = 47.9 J/g for the heat treated samples and to $\boldsymbol{\sigma_{ult}}$ = 504.5 MPa, $\boldsymbol{E}$ = 15.6 GPa and $\boldsymbol{K}$ = 121.2 J/g for samples after GA treatment. The maximum measurements were recorded at $\boldsymbol{\sigma_{ult}}$ = 600.1 MPa, $\boldsymbol{E}$ = 20.6 GPa, and $\boldsymbol{K}$ = 152.1 J/g in a GA treated sample. As we surveyed, these combinations of high strength, modulus, and toughness are unusual among all types of homogeneous bulk composites.

The thermal treatment effects of LBL composites find a close analogy in hot drawing of PVA – CNT fibers.[23] The mechanical parameters of these fibers before and after heat treatment were $\boldsymbol{\sigma_{ult}}$ = 600 MPa and $\boldsymbol{K}$ = 870 J/g, and $\boldsymbol{\sigma_{ult}}$ = 1.8 GPa, $\boldsymbol{E}$ = 45 GPa and $\boldsymbol{K}$ = 60 J/g, respectively.[23] According to the same study, an improved stress transfer between PVA and CNTs resulted in approximately 3 times increase in tensile strength while the drop in toughness was less than 1/10 of the original value, which the authors credited to the partial crystallinity of PVA. This partial crystallinity in our LBL

composites was also observed only by heat treatments. Therefore, crystalline PVA phase significantly enhance stress transfer between PVA and SWNT from heat treatment.

Besides crystallinity of polymer matrix, it is surprising but well established that the toughness of a composite can be greatly improved by chemically grafting CNTs and polymer matrix.[49, 74-76] Even 0.5 ~ 1 % of CNT loading could produce 3 ~ 6 times increase in tensile strength, modulus, strain, and toughness, resulted altogether from a chemical cross-linkage. However, systematic understanding of improvements made by cross-linking is beyond the surveyed information. Here, we try to suggest the effects separately in chemical and physical dimensions.

5. Mechanistic Analysis of Strength and Toughness of SWNT LBL Composites

In molecular level interactions, the allowable maximum interfacial shear strength is only limited by the SWNT's fracture strength.[77] The interplay of these molecular level strengths ultimately determines the strength of a nanocomposite. Thus, the strength of our LBL composites is a function of the degree of CNT functionalization and efficiency of cross-linking. We should point out here that different cross-linking techniques result in different density and length of covalent bonds. This length variation is a crucial clue to understanding the toughness improvement of LBL composites.[49] So, we rationalize that the toughness of our LBL composites should be dictated by the length of cross-linked bonds. According to previously published data,[78] ester bonds are formed by heat treatment between –COOH in SWNTs and –OH in PVA. Such bonds are mostly limited

to the edges of SWNTs and short in molecular length. In contrast, the long GA molecules can be inserted between two PVA chains and form ester bridges between –(OH) in PVA and –CHO in GA,[79] producing bonds that are longer and more flexible than the former type. Furthermore, the density of chemical bonds formed by GA is dependent on the duration, concentration, and temperature of the treatment. Thus in this study, optimized GA cross-linking at mild conditions showed great enhancement in toughness and strain, whereas substantial effects from heat cross-linking were confined to strength and modulus with only marginal changes in strain. It is logical that the toughness of GA treated samples increased more dramatically than the heat treated one as toughness is calculated from the area underneath the stress-strain curve. (Table 3) Although the effects from cross-linking are well exemplified, it is worth recalling that pure PVA tend to lose their flexibility upon GA cross-linking.[80]

Unlike chemical analysis, the physical toughening mechanism is still unexplored. Articles which reported both successful demonstration of toughness enhancement in CNT composites and suggestion of viable toughening models are extremely rare. As a rule of thumb, observation of physically torn interfaces of a composite and extrusion behavior of SWNTs is useful for understanding the strengthening and toughening mechanisms. In this study, interesting fracture behavior resembling that of textiles was observed in the toughest [PVA/ $SWNT_{\text{-COOH}}$(7.9) +PSS]$_{200}$ LBL film treated with GA using high resolution SEM (Figure 8 AB). One may instantly notice that the SWNTs are densely interweaved together in the LBL strata. These dense SWNTs have sticky functional groups that interact with the interdigitated PVA matrix which is evenly and

homogeneously distributed over the SWNT network by LBL assembly, and thus, allows the transfer of external stress to high surface area SWNT webs. Therefore, large forces and energies are required to untie this strongly bound hybrid matrix, indicating the high strength and toughness of the composite. Again, high strain is a result of evenly spread stress over a large area, producing numerous parallel cracks along the stretched SWNTs extending up to 3 μm and allowing large amount of energy to be dissipated upon deformation. The exceptional mechanical properties of the [PVA/ $SWNT_{-COOH}$(7.9) +PSS]$_{200}$ LBL composites with GA cross-linking are the combination of highly precise nanoscale structural controls as well as optimal surface chemistry.

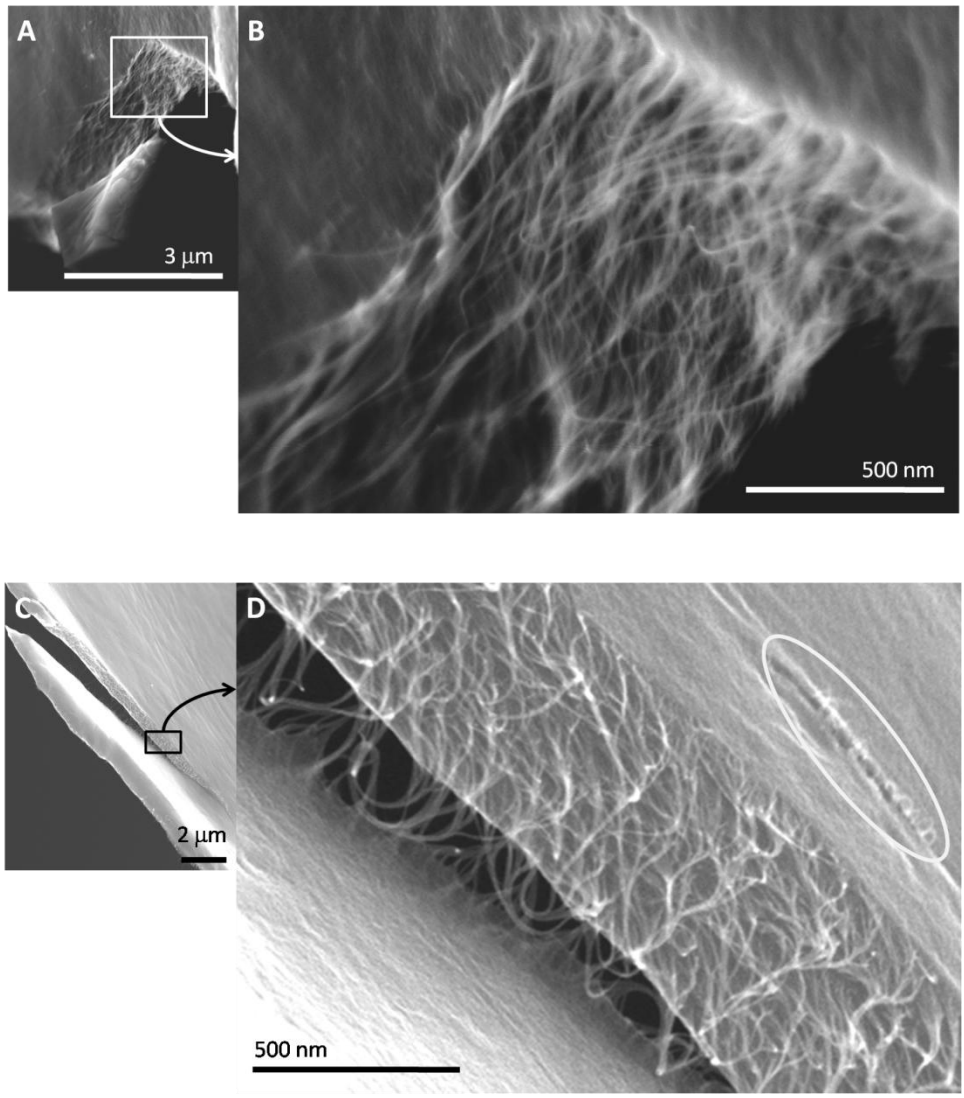

Figure 8 SEM images of torn surfaces of (A, B) a [PVA/SWNT$_{\text{-COOH}}$(7.9) +PSS] LBL composite with GA cross-linking and (C, D) a [PVA/SWNT$_{\text{-COOH}}$(15.8) +PSS] LBL composite with heat cross-linking.

In contrast, a different type of fracture patterns was observed in the system with lower toughness, i.e. the [PVA/ SWNT$_{\text{-COOH}}$(15.8) +PSS]$_{200}$ film with heat treatment. (Figure 8 CD) Unlike the tougher samples, the textile braking patterns are confined in shallow crack surfaces because of immature SWNT failures. The parallel cracks are

indicated by the circle in Figure 8D and are only present in limited range. However, this breaking pattern still provides useful information for improving our understanding of the reinforcing mechanism. First, there is dramatic roughening of the complementary surfaces by cracks that used to be in contact with each other. This roughened surface results in greater area of cracks, and hence requires much greater stress than those of clear-cut surfaces. This might be similar to the toughening mechanism of human cortical bone in transverse breaking.[81] Second, the sample breaks with multiple micro-crazing, which can share the stress so that it significantly increases the total capacity of transferred energy as well as the strain. A similar reinforcing mechanism was suggested in electro-spun SWNT nanofibers previously.[41] Third, exfoliated SWNTs having plastic inward deformation are well matched to the strain of PVA; however, this is not the case for MWNTs.[3] Thus, one can deduce that cross-linking further improves the strain transfer to these stretchable SWNTs, whereas the polymer matrix bound to the rigid fillers becomes more rigid as a consequence of strong interfacial interaction with the nanomaterials.[6] This strain transfer to stretchable fillers were also suggested as a possible toughening mechanism by Gojny et al.[82]

6. Conclusions

In this chapter, through systematic variation of quantifiable LBL fabrication conditions, we showed that the degree of SWNT oxidation and methods of cross-linking are the primary factors determining the mechanical properties of LBL composites. By judiciously tuning of the material structure and the interface bonding, we fabricated a composite material that produced record high mechanical properties not only among non-fibrous composites, but also surpassing most fibers drawn from SWNTs and MWNTs. Further improvements of the mechanical properties are certainly possible, and the capabilities of this organic-inorganic hybrid system can be greatly expanded. Future directions should include detailed computer simulations of this system to gain fundamental understanding in mechanisms such as the unusual effect of simultaneously increased strain and toughness upon cross-linking and potentially other nanometer-scale mechanics phenomena.

Reference

1. Baughman, R. H.; Zakhidov, A. A.; de Heer, W. A., Carbon nanotubes-the route toward applications. *Science* **2002,** 297, (5582), 787-792.
2. Yu, M. F.; Lourie, O.; Dyer, M. J.; Moloni, K.; Kelly, T. F.; Ruoff, R. S., Strength and breaking mechanism of multiwalled carbon nanotubes under tensile load. *Science* **2000,** 287, (5453), 637-640.
3. Calvert, P., Nanotube composites: A recipe for strength. *Nature* **1999,** 399, (6733), 210-211.
4. Shim, B. S.; Kotov, N. A., Single-Walled Carbon Nanotube Combing during Layer-by-Layer Assembly: From Random Adsorption to Aligned Composites. *Langmuir* **2005,** 21, (21), 9381-9385.
5. Shim, B. S.; Podsiadlo, P.; Lilly, D. G.; Agarwal, A.; Lee, J.; Tang, Z.; Ho, S.; Ingle, P.; Paterson, D.; Lu, W.; Kotov, N. A., Nanostructured Thin Films Made by Dewetting Method of Layer-By-Layer Assembly. *Nano Lett.* **2007,** 7, (11), 3266-3273.
6. Podsiadlo, P.; Kaushik, A. K.; Arruda, E. M.; Waas, A. M.; Shim, B. S.; Xu, J.; Nandivada, H.; Pumplin, B. G.; Lahann, J.; Ramamoorthy, A.; Kotov, N. A., Ultrastrong and Stiff Layered Polymer Nanocomposites. *Science* **2007,** 318, (5847), 80-83.
7. Coleman, J. N.; Khan, U.; Gun'ko, Y. K., Mechanical reinforcement of polymers using carbon nanotubes. *Advanced Materials* **2006,** 18, (6), 689-706.
8. Coleman, J. N.; Khan, U.; Blau, W. J.; Gun'ko, Y. K., Small but strong: A review of the mechanical properties of carbon nanotube-polymer composites. *Carbon* **2006,** 44, (9), 1624-1652.
9. Moniruzzaman, M.; Winey, K. I., Polymer nanocomposites containing carbon nanotubes. *Macromolecules* **2006,** 39, (16), 5194-5205.
10. Steele, B. C. H.; Heinzel, A., Materials for fuel-cell technologies. *Nature* **2001,** 414, (6861), 345-352.
11. Shiflet, G., Materials science: The more elements, the merrier. *Science* **2003,** 300, (5618), 443-444.
12. Jones, R., New materials, old challenges. *Nat.Nanotechnol.* **2007,** 2, (8), 453-454.
13. Wichmann, M. H. G.; Schulte, K.; Wagner, H. D., On nanocomposite toughness. *Composites Science and Technology* **2008,** 68, (1), 329-331.
14. Hersam, M. C., Progress towards monodisperse single-walled carbon nanotubes. *Nature Nanotechnology* **2008,** 3, (7), 387-394.
15. Chae, H. G.; Sreekumar, T. V.; Uchida, T.; Kumar, S., A comparison of reinforcement efficiency of various types of carbon nanotubes in polyacrylonitrile fiber. *Polymer* **2005,** 46, (24), 10925-10935.
16. Ericson, L. M.; Fan, H.; Peng, H.; Davis, V. A.; Zhou, W.; Sulpizio, J.; Wang, Y.; Booker, R.; Vavro, J.; Guthy, C.; Parra-Vasquez, A. N.; Kim, M. J.; Ramesh, S.; Saini, R. K.; Kittrell, C.; Lavin, G.; Schmidt, H.; Adams, W. W.; Billups, W. E.; Pasquali, M.; Hwang, W. F.; Hauge, R. H.; Fischer, J. E.; Smalley, R. E., Macroscopic, Neat, Single-Walled Carbon Nanotube Fibers. *Science* **2004,** 305, (5689), 1447-1450.

17. Zhang, X.; Liu, T.; Sreekumar, T. V.; Kumar, S.; Moore, V. C.; Hauge, R. H.; Smalley, R. E., Polyvinyl alcohol/SWNT composite film. *Nano Letters* **2003,** 3, (9), 1285-1288.
18. Heller, D. A.; Barone, P. W.; Swanson, J. P.; Mayrhofer, R. M.; Strano, M. S., Using Raman Spectroscopy to Elucidate the Aggregation State of Single-Walled Carbon Nanotubes. *Journal of Physical Chemistry B* **2004,** 108, (22), 6905-6909.
19. Graff, R. A.; Swanson, J. P.; Barone, P. W.; Baik, S.; Heller, D. A.; Strano, M. S., Achieving individual-nanotube dispersion at high loading in single-walled carbon nanotube composites. *Advanced Materials* **2005,** 17, (8), 980-984.
20. Vigolo, B.; Penicaud, A.; Coulon, C.; Sauder, C.; Pailler, R.; Journet, C.; Bernier, P.; Poulin, P., Macroscopic fibers and ribbons of oriented carbon nanotubes. *Science* **2000,** 290, (5495), 1331-1334.
21. Dalton, A. B.; Collins, S.; Munoz, E.; Razal, J. M.; Ebron, V. H.; Ferraris, J. P.; Coleman, J. N.; Kim, B. G.; Baughman, R. H., Super-tough carbon-nanotube fibres. *Nature* **2003,** 423, (6941), 703.
22. Dalton, A. B.; Collins, S.; Razal, J.; Munoz, E.; Ebron, V. H.; Kim, B. G.; Coleman, J. N.; Ferraris, J. P.; Baughman, R. H., Continuous carbon nanotube composite fibers: properties, potential applications, and problems. *J.Mater.Chem.* **2004,** 14, (1), 1-3.
23. Miaudet, P.; Badaire, S.; Maugey, M.; Derre, A.; Pichot, V.; Launois, P.; Poulin, P.; Zakri, C., Hot-drawing of single and multiwall carbon nanotube fibers for high toughness and alignment. *Nano Letters* **2005,** 5, (11), 2212-2215.
24. Pichot, V.; Badaire, S.; Albouy, P. A.; Zakri, C.; Poulin, P.; Launois, P., Structural and mechanical properties of single-wall carbon nanotube fibers. *Physical Review B: Condensed Matter and Materials Physics* **2006,** 74, (24), 245416/1-245416/8.
25. Sreekumar, T. V.; Liu, T.; Min, B. G.; Guo, H.; Kumar, S.; Hauge, R. H.; Smalley, R. E., Polyacrylonitrile single-walled carbon nanotube composite fibers. *Advanced Materials* **2004,** 16, (1), 58-61.
26. Chae, H. G.; Minus, M. L.; Kumar, S., Oriented and exfoliated single wall carbon nanotubes in polyacrylonitrile. *Polymer* **2006,** 47, (10), 3494-3504.
27. Zhang, X.; Liu, T.; Sreekumar, T. V.; Kumar, S.; Hu, X.; Smith, K., Gel spinning of PVA/SWNT composite fiber. *Polymer* **2004,** 45, (26), 8801-8807.
28. Kumar, S.; Dang, T. D.; Arnold, F. E.; Bhattacharyya, A. R.; Min, B. G.; Zhang, X.; Vaia, R. A.; Park, C.; Adams, W. W.; Hauge, R. H.; Smalley, R. E.; Ramesh, S.; Willis, P. A., Synthesis, Structure, and Properties of PBO/SWNT Composites. *Macromolecules* **2002,** 35, (24), 9039-9043.
29. Zhu, H. W.; Xu, C. L.; Wu, D. H.; Wei, B. Q.; Vajtai, R.; Ajayan, P. M., Direct synthesis of long single-walled carbon nanotube strands. *Science* **2002,** 296, (5569), 884-886.
30. Jiang, K.; Li, Q.; Fan, S., Spinning continuous carbon nanotube yarns. *Nature* **2002,** 419, (6909), 801.
31. Zhang, M.; Atkinson, K. R.; Baughman, R. H., Multifunctional Carbon Nanotube Yarns by Downsizing an Ancient Technology. *Science* **2004,** 306, (5700), 1358-1361.

32. Zhang, X.; Jiang, K.; Feng, C.; Liu, P.; Zhang, L.; Kong, J.; Zhang, T.; Li, Q.; Fan, S., Spinning and processing continuous yarns from 4-inch wafer scale super-aligned carbon nanotube arrays. *Advanced Materials* **2006,** 18, (12), 1505-1510.
33. Li, Y. L.; Kinloch, I. A.; Windle, A. H., Direct Spinning of Carbon Nanotube Fibers from Chemical Vapor Deposition Synthesis. *Science* **2004,** 304, (5668), 276-278.
34. Koziol, K.; Vilatela, J.; Moisala, A.; Motta, M.; Cunniff, P.; Sennett, M.; Windle, A., High-Performance Carbon Nanotube Fiber. *Science* **2007,** 318, 1892-1895.
35. Zhang, X.; Li, Q.; Holesinger, T. G.; Arendt, P. N.; Huang, J.; Kirven, D.; Clapp, T. G.; DePaula, R. F.; Liao, X.; Zhao, Y.; Zheng, L.; Peterson, D. E.; Zhu, Y., Ultrastrong, Stiff, and Lightweight Carbon-Nanotube Fibers. *Adv.Mater.* **2007,** 19, 4198-4201.
36. Zhang, M.; Fang, S.; Zakhidov, A. A.; Lee, S. B.; Aliev, A. E.; Williams, C. D.; Atkinson, K. R.; Baughman, R. H., Strong, Transparent, Multifunctional, Carbon Nanotube Sheets. *Science* **2005,** 309, (5738), 1215-1219.
37. Veedu, V. P.; Cao, A.; Li, X.; Ma, K.; Soldano, C.; Kar, S.; Ajayan, P. M.; Ghasemi-Nejhad, M. N., Multifunctional composites using reinforced laminae with carbon-nanotube forests. *Nature Materials* **2006,** 5, (6), 457-462.
38. Sen, R.; Zhao, B.; Perea, D.; Itkis, M. E.; Hu, H.; Love, J.; Bekyarova, E.; Haddon, R. C., Preparation of Single-Walled Carbon Nanotube Reinforced Polystyrene and Polyurethane Nanofibers and Membranes by Electrospinning. *Nano Letters* **2004,** 4, (3), 459-464.
39. Jose, M. V.; Steinert, B. W.; Thomas, V.; Dean, D. R.; Abdalla, M. A.; Price, G.; Janowski, G. M., Morphology and mechanical properties of Nylon 6/MWNT nanofibers. *Polymer* **2007,** 48, (4), 1096-1104.
40. Blond, D.; Walshe, W.; Young, K.; Blighe, F. M.; Khan, U.; Almecija, D.; Carpenter, L.; McCauley, J.; Blau, W. J.; Coleman, J. N., Strong, tough, electrospun polymer-nanotube composite membranes with extremely low density. *Advanced Functional Materials* **2008,** 18, (17), 2618-2624.
41. Ye, H.; Lam, H.; Titchenal, N.; Gogotsi, Y.; Ko, F., Reinforcement and rupture behavior of carbon nanotubes-polymer nanofibers. *Applied Physics Letters* **2004,** 85, (10), 1775-1777.
42. Ge, J. J.; Hou, H.; Li, Q.; Graham, M. J.; Greiner, A.; Reneker, D. H.; Harris, F. W.; Cheng, S. Z. D., Assembly of Well-Aligned Multiwalled Carbon Nanotubes in Confined Polyacrylonitrile Environments: Electrospun Composite Nanofiber Sheets. *J.Am.Chem.Soc.* **2004,** 126, (48), 15754-15761.
43. Hou, H.; Ge, J. J.; Zeng, J.; Li, Q.; Reneker, D. H.; Greiner, A.; Cheng, S. Z. D., Electrospun Polyacrylonitrile Nanofibers Containing a High Concentration of Well-Aligned Multiwall Carbon Nanotubes. *Chemistry of Materials* **2005,** 17, (5), 967-973.
44. Gao, J.; Itkis, M. E.; Yu, A.; Bekyarova, E.; Zhao, B.; Haddon, R. C., Continuous Spinning of a Single-Walled Carbon Nanotube-Nylon Composite Fiber. *Journal of the American Chemical Society* **2005,** 127, (11), 3847-3854.
45. Dyke, C. A.; Tour, J. M., Covalent Functionalization of Single-Walled Carbon Nanotubes for Materials Applications. *Journal of Physical Chemistry A* **2004,** 108, (51), 11151-11159.

46. Frankland, S. J. V.; Caglar, A.; Brenner, D. W.; Griebel, M., Molecular Simulation of the Influence of Chemical Cross-Links on the Shear Strength of Carbon Nanotube-Polymer Interfaces. *Journal of Physical Chemistry B* **2002,** 106, (12), 3046-3048.
47. Garg, A.; Sinnott, S. B., Effect of chemical functionalization on the mechanical properties of carbon nanotubes. *Chemical Physics Letters* **1998,** 295, (4), 273-278.
48. Gustavsson, S.; Rosen, A.; Grennberg, H.; Bolton, K., Computational studies of carbon nanotube-hydrocarbon bond strengths at nanotube ends: Effect of link heteroatom and hydrocarbon structure. *Chemistry--A European Journal* **2004,** 10, (9), 2223-2227.
49. Moniruzzaman, M.; Chattopadhyay, J.; Billups, W. E.; Winey, K. I., Tuning the Mechanical Properties of SWNT/Nylon 6,10 Composites with Flexible Spacers at the Interface. *Nano Letters* **2007,** 7, (5), 1178-1185.
50. Frankland, S. J. V.; Harik, V. M., Analysis of carbon nanotube pull-out from a polymer matrix. *Surface Science* **2003,** 525, (1-3), L103-L108.
51. Barber, A. H.; Cohen, S. R.; Wagner, H. D., Static and Dynamic Wetting Measurements of Single Carbon Nanotubes. *Physical Review Letters* **2004,** 92, (18), 186103/1-186103/4.
52. Barber, A. H.; Cohen, S. R.; Wagner, H. D., Measurement of carbon nanotube-polymer interfacial strength. *Applied Physics Letters* **2003,** 82, (23), 4140-4142.
53. Gao, J.; Zhao, B.; Itkis, M. E.; Bekyarova, E.; Hu, H.; Kranak, V.; Yu, A.; Haddon, R. C., Chemical engineering of the single-walled carbon nanotube-nylon 6 interface. *Journal of the American Chemical Society* **2006,** 128, (23), 7492-7496.
54. Xia, H.; Song, M., Preparation and characterisation of polyurethane grafted single-walled carbon nanotubes and derived polyurethane nanocomposites. *Journal of Materials Chemistry* **2006,** 16, (19), 1843-1851.
55. Zhang, W. D.; Shen, L.; Phang, I. Y.; Liu, T., Carbon Nanotubes Reinforced Nylon-6 Composite Prepared by Simple Melt-Compounding. *Macromolecules* **2004,** 37, (2), 256-259.
56. Blake, R.; Gun'ko, Y. K.; Coleman, J.; Cadek, M.; Fonseca, A.; Nagy, J. B.; Blau, W. J., A Generic Organometallic Approach toward Ultra-Strong Carbon Nanotube Polymer Composites. *Journal of the American Chemical Society* **2004,** 126, (33), 10226-10227.
57. Zhu, J.; Peng, H.; Rodriguez-Macias, F.; Margrave, J. L.; Khabashesku, V. N.; Imam, A. M.; Lozano, K.; Barrera, E. V., Reinforcing epoxy polymer composites through covalent integration of functionalized nanotubes. *Advanced Functional Materials* **2004,** 14, (7), 643-648.
58. Friddle, R. W.; Lemieux, M. C.; Cicero, G.; Artyukhin, A. B.; Tsukruk, V. V.; Grossman, J. C.; Galli, G.; Noy, A., Single functional group interactions with individual carbon nanotubes. *Nature Nanotechnology* **2007,** 2, (11), 692-697.
59. McQuade, D. T.; Pullen, A. E.; Swager, T. M., Conjugated polymer-based chemical sensors. *Chem.Rev.* **2000,** 100, (7), 2537-2574.
60. Westenhoff, S.; Kotov, N. A., Quantum Dot on a Rope. *J.Am.Chem.Soc.* **2002,** 124, (11), 2448-2449.

61. Chen, J.; Ramasubramaniam, R.; Xue, C.; Liu, H., A versatile, molecular engineering approach to simultaneously enhanced, multifunctional carbon nanotube-polymer composites. *Advanced Functional Materials* **2006,** 16, (1), 114-119.
62. Coleman, J. N.; Cadek, M.; Blake, R.; Nicolosi, V.; Ryan, K. P.; Belton, C.; Fonseca, A.; Nagy, J. B.; Gun'ko, Y. K.; Blau, W. J., High-performance nanotube-reinforced plastics: Understanding the mechanism of strength increase. *Advanced Functional Materials* **2004,** 14, (8), 791-798.
63. Coleman, J. N.; Cadek, M.; Ryan, K. P.; Fonseca, A.; Nagy, J. B.; Blau, W. J.; Ferreira, M. S., Reinforcement of polymers with carbon nanotubes. The role of an ordered polymer interfacial region. Experiment and modeling. *Polymer* **2006,** 47, (26), 8556-8561.
64. Ryan, K. P.; Cadek, M.; Nicolosi, V.; Blond, D.; Ruether, M.; Armstrong, G.; Swan, H.; Fonseca, A.; Nagy, J. B.; Maser, W. K.; Blau, W. J.; Coleman, J. N., Carbon nanotubes for reinforcement of plastics? A case study with poly(vinyl alcohol). *Composites Science and Technology* **2007,** 67, (7-8), 1640-1649.
65. Mamedov, A. A.; Kotov, N. A.; Prato, M.; Guldi, D. M.; Wicksted, J. P.; Hirsch, A., Molecular design of strong single-wall carbon nanotube/polyelectrolyte multilayer composites. *Nature Materials* **2002,** 1, (3), 190-194.
66. Olek, M.; Ostrander, J.; Jurga, S.; Moehwald, H.; Kotov, N.; Kempa, K.; Giersig, M., Layer-by-Layer Assembled Composites from Multiwall Carbon Nanotubes with Different Morphologies. *Nano Letters* **2004,** 4, (10), 1889-1895.
67. O'Connell, M. J.; Boul, P.; Ericson, L. M.; Huffman, C.; Wang, Y.; Haroz, E.; Kuper, C.; Tour, J.; Ausman, K. D.; Smalley, R. E., Reversible water-solubilization of single-walled carbon nanotubes by polymer wrapping. *Chemical Physics Letters* **2001,** 342, (3,4), 265-271.
68. Shim, B. S.; Tang, Z.; Morabito, M. P.; Agarwal, A.; Hong, H.; Kotov, N. A., Integration of Conductivity, Transparency, and Mechanical Strength into Highly Homogeneous Layer-by-Layer Composites of Single-Walled Carbon Nanotubes for Optoelectronics. *Chem.Mater.* **2007,** 19, (23), 5467-5474.
69. Kotov, N. A., Layer-by-layer self-assembly: The contribution of hydrophobic interactions. *Nanostructured Materials* **1999,** 12, 789-796.
70. Malikova, N.; Pastoriza-Santos, I.; Schierhorn, M.; Kotov, N. A.; Liz-Marzan, L. M., Layer-by-Layer Assembled Mixed Spherical and Planar Gold Nanoparticles: Control of Interparticle Interactions. *Langmuir* **2002,** 18, (9), 3694-3697.
71. Vollrath, F.; Knight, D. P., Liquid crystalline spinning of spider silk. *Nature* **2001,** 410, (6828), 541-548.
72. Chen, W.; Tao, X. M.; Xue, P.; Cheng, X. Y., Enhanced mechanical properties and morphological characterizations of poly(vinyl alcohol)-carbon nanotube composite films. *Applied Surface Science* **2005,** 252, (5), 1404-1409.
73. Bhattacharyya, S.; Salvetat, J. P.; Saboungi, M. L., Reinforcement of semicrystalline polymers with collagen-modified single walled carbon nanotubes. *Applied Physics Letters* **2006,** 88, (23), 3.

74. Shi, J. H.; Yang, B. X.; Pramoda, K. P.; Goh, S. H., Enhancement of the mechanical performance of poly(vinyl chloride) using poly(n-butyl methacrylate)-grafted multi-walled carbon nanotubes. *Nanotechnology* **2007,** 18, (37), 8.
75. Yang, B. X.; Shi, J. H.; Pramoda, K. P.; Goh, S. H., Enhancement of stiffness, strength, ductility and toughness of poly(ethylene oxide) using phenoxy-grafted multiwalled carbon nanotubes. *Nanotechnology* **2007,** 18, (12).
76. Wang, M.; Pramoda, K. P.; Goh, S. H., Enhancement of the mechanical properties of poly (styrene-co-acrylonitrile) with poly(methyl methacrylate)-grafted multiwalled carbon nanotubes. *Polymer* **2005,** 46, (25), 11510-11516.
77. Wang, T.; Dalton, A. B.; Keddie, J. L., Importance of Molecular Friction in a Soft Polymer-Nanotube Nanocomposite. *Macromolecules* **2008,** 41, (20), 7656-7661.
78. Kumeta, K.; Nagashima, I.; Matsui, S.; Mizoguchi, K., Crosslinking reaction of poly(vinyl alcohol) with poly(acrylic acid) (PAA) by heat treatment: Effect of neutralization of PAA. *J.Appl.Polym.Sci.* **2003,** 90, (9), 2420-2427.
79. Mansur, H. S.; Orefice, R. L.; Mansur, A. A. P., Characterization of poly(vinyl alcohol)/poly(ethylene glycol) hydrogels and PVA-derived hybrids by small-angle X-ray scattering and FTIR spectroscopy. *Polymer* **2004,** 45, (21), 7193-7202.
80. Liu, L.; Barber, A. H.; Nuriel, S.; Wagner, H. D., Mechanical properties of functionalized single-walled carbon-nanotube/poly(vinyl alcohol) nanocomposites. *Advanced Functional Materials* **2005,** 15, (6), 975-980.
81. Koester, K. J.; Ager, J. W.; Ritchie, R. O., The true toughness of human cortical bone measured with realistically short cracks. *Nature Materials* **2008,** 7, (8), 672-677.
82. Gojny, F. H.; Wichmann, M. H. G.; Fiedler, B.; Schulte, K., Influence of different carbon nanotubes on the mechanical properties of epoxy matrix composites - A comparative study. *Composites Science and Technology* **2005,** 65, (15-16), 2300-2313.

Chapter III

Electrical Properties of CNT LBL Composites

A. Motivation of Transparent, Flexible, Electronic Materials Research

Transparent conductors (TCs) have been essential electronic materials since 1907 when cadmium oxide was initially introduced.[1] Currently, rigid semiconducting oxide, such as indium tin oxide (ITO) are the TC material of choice in applications like flat-panel display.[2] However, rigorous research demand exists from the industry for current ITO replacements because of (1) economic factors including fast price increase of rare indium and expensive semiconductor thin film coating process and (2) material performance factors including mechanical flexibility, environmental stability, and smart functionality.[3] In addition, stretchable, foldable, and compressible electronic material systems are now emerging with noble application principles such as hemispherical eye cameras[4] and integrated circuits.[5, 6] Furthermore, wearable and smart electronic textiles[7] should be further developed to meet the many suggested applications.[8] There is rapid growth potential for these next generation electronic materials. However, the complex material requirements like optical-mechanical-electrical, mechanical-electrical, and chemical-electrical properties for those applications cannot be easily satisfied by conventional metals, semiconductors, and their oxides.

SWNT coatings have been introduced to fill the technological gaps and curb the cost of conventional TCs.[9, 10] Superior physicochemical properties of individual SWNTs, and, particularly, high electrical conductivity estimated at 10^4~10^6 S/cm[11-13], make them promising candidate for TCs. For comparison, the electrical conductivity of the state of the art ITO is around 9×10^3 S/cm.[14] The challenge of using carbon nanotubes in TC applications, however, is strong light absorption in, and thus, transparency of the coatings is achieved by nano-scale thickness of the coating. Such coatings can be described as 2D networks of SWNTs which provide both electrical charge carriers and electrically percolating conduction routes.[15, 16] Due to thinness of the SWNT films necessary for TC, the processing methods with nano-scale structure control of the coating are exceptionally important. They determine, to a large extent, the degree of nanotubes exfoliation and connectedness affecting the heights of tunneling barriers between the individual tubes. These methods also control the presence of poorly performing components of the nanotubes dispersion interrupting SWNT networks.[17] All of these structural parameters affect both electrical conductivity (σ) and optical absorbance (α). Efforts have been directed on forming SWNT-only-structures mostly by solution processing techniques such as spraying,[18, 19] spin-coating,[20] electrophoretic deposition,[21] and filtration.[9, 22] Direct synthesis of SWNTs for transparent electronics[23, 24] and dry spinning transparent sheet from multi-walled carbon nanotube (MWNTs) forests[25] were also demonstrated as non-solvent techniques.

Thinness of the coatings also puts very significant requirements on their mechanical properties. In fact, these properties have not been given sufficient attention

yet. The individual SWNTs do possess exceptional mechanical properties; $\boldsymbol{E}$ ~1 TPa and $\boldsymbol{\sigma}_{ult}$ ~ 63 GPa.[26] They also have ability for very high plastic deformation under stress.[27] However, translation of these properties observed for individual nanotube to macroscopic TCs should not be automatically assumed. In fact most of the TCs from SWNTs described above are easily destroyed or their conductivity is drastically reduced after elementary wear. As such, the strength of bucky papers, the most common filtrated SWNT-only-sheets structurally very similar to many TC coatings made from nanotubes, is truly disappointing displaying $\boldsymbol{\sigma}_{ult}$ ~ 10~74 MPa. Also important is that traditional networks of SWNTs are brittle rather than flexible displaying values of strain to failure not exceeding 0.5~5%.[28, 29] Finding the method of preparation of SWNT that could display simultaneously high TC performance, strength, resistance to wear, and flexibility is critical for practical realization of roll-out solar cells and flexible electronics for which SWNT TCs are projected for.

The art of combining the mechanical, optical and electrical properties lies in the accurate control of the nanoscale structure of the coatings. Improvement of the mechanical properties requires inclusion of adhesive polymer in the structure of the film. However, this can always jeopardize high σ values, which even further accentuates the importance of fine structural tuning. For examples, the degrees of nanotubes exfoliation and connectivity affect the levels of tunneling barriers between the individual tubes. Accordingly, developments of electronic properties controlled by molecular hierarchical structures as well as multi-functional properties added by matrix components in a SWNT nanocomposite without losing electrical conductivity are highly desirable.

We present layer-by-layer assembly (LBL) of SWNT as a method for TC applications with integrated strength and conductivities. LBL is one of the few thin film deposition techniques that allows one to control the structure of the coatings with actual nanometer scale precision, which includes both normal[30] and lateral[31]packing of the nanoscale building blocks in the coatings.

Indeed, these optically transparent and flexible (or stretchable) SWNT nanocomposite materials have many applications. Examples are the bio-medical wearable devices, bionic contact lenses, smart surgical gloves, rolled-up electronics, artificial skins, and electronic papers.[32] Overall, the principles for the next generation electronic materials will be further expanded to many other material applications such as smart windows, photovoltaic cells, and intelligent electronic textiles as well as replacements for conventional TCs.

B. Electrically Conductive LBL Composites of SWNT

1. Summary

Conductive organic and composite films represent the critical component of many areas of technology. This chapter demonstrates that highly conductive coatings can be made by layer-by-layer (LBL) assembly of single-walled carbon nanotubes (SWNTs). These films reveal electrical conductivities of 10^2 to ~10^3 S/m at room temperature without doping with nanotube loading as low as ~10%. This is indicative of efficient utilization of SWNT in percolation pathways. Low SWNT loading also makes the

coatings quite transparent with transmission as high as 97% for visible light. Thicker delaminated LBL films displayed conductivities of 4.15×10^4 S/m. The free-standing films were highly flexible and possessed 160 MPa of tensile strength, which makes them the strongest organic conductor. The high strength and conductivities are attributed to the unique homogeneity of the LBL assembled composites, which opens the way to future optimization of electrical, mechanical, and optical properties and to fit the needs of specific applications, which may be exemplified by transparent flexible electronics, light emitting diodes, smart windows, solar cells, sensors, structural materials, and biomedical devices.

2. Experimental Procedure

Materials: Poly(vinyl alcohol) (PVA; MW, 70 000 to _100 000) and poly(sodium 4-styrene-sulfonate), (PSS; MW, 1 000 000) were purchased from Sigma-Aldrich Co. The purified HiPco SWNTs were purchased from Carbon Nanotechnologies Incorporated (CNI).

LBL Assembly: Purified HiPco SWNTs were dispersed in 0.2 wt % PSS solution with 2 days of mild sonication in a VWR model 150HT ultrasonic cleaner.[33] The dispersion with 1 mg/ml of SWNTs was centrifuged at 5000 rpm, and then the supernatant was collected, which became one LBL component. PVA solution (1 wt %) was prepared for another LBL partner. By charge-transfer interaction between PSS which are wrapping SWNTs and PVA, or by hydrogen bonding between possible COOH groups

in SWNTs and OH in PVA, they formed LBL assemblies on a charged substrate (glass or Si). Each LBL layering process consists of 10 min of dipping in the PVA or in the SWNT solution, rinsing in deionized water, and drying. To denote LBL assemblies, $[PVA/SWNT + PSS]_n$ was used in which *n* represents the number of repeated dipping processes in PVA and SWNT solutions.

Instrumental Analysis: Scanning electron microscopy images were taken with a Philips XL30 field emission gun scanning electron microscope and an FEI Nova Nanolab dual-beam FIB and scanning electron microscope. Atomic force microscopy imaging was performed with a Nanoscope III (Digital Instruments/Veeco Metrology Group). UV-vis absorption measurements were taken using an Agilent 8453E UV-vis spectrophotometer. An Agilent 34401A multimeter was used for electrical measurements. Mechanical tests were done by a Q systems model 100 (Test Resources). Thermogravimetric analysis was performed by a Perkin-Elmer Pyris 1 TGA. Ellipsometric measurements were done by an M-44 IR spectroscopic ellipsometer (J. A. Woollam Co., Inc.).

3. Film Preparation and Structural Characteristics

Fabrication of a homogeneous SWNT-polymer LBL composite starts from preparation of well-dispersed SWNT solution. The quality of nanocolloids, as it relates to the degree of dispersion, can be preserved in the resulting material because micrometer-scale reorganization of the LBL multilayers is prevented due to the restricted mobility of the long SWNT fibers. The complete exfoliation can be achieved by wrapping the

nanotubes with charged aromatic polymers such as poly(sodium 4-styrene-sulfonate) (PSS) owing to π-π and hydrophobic interactions.[33-35] This stabilization also avoids an oxidation step for SWNTs used in older schemes so that prevents deterioration of electrical properties of SWNTs. At the same time it introduces a dielectric shell around the nanotubes. The bottleneck of the conductivity in both wrapped and oxidized nanotubes may not be the defects in the individual nanotubes but rather their spatial distribution and the probability of charge hopping from one SWNT to another.[36-38] Proper balance between dispersion methods and electrical conductivity is still to be found. It will require computer modeling of charge transport in a percolation network and establishing the charge tunneling parameters of SWNT-SWNT contacts.

We hypothesized that better transport properties are more likely to be found when nanotubes are intact. So, we took advantage of the methods of tuning of the molecular structure of the LBL stacks available to us. The LBL assembly was realized with a stable 0.1% SWNT dispersion in 0.2% PSS as component no. 1 and a 1% solution of poly(vinyl alcohol) (PVA) as component no. 2. The substrates were alternatively dipped in these solutions, producing stacks with cumulative structures $[PVA/(SWNT + PSS)]_n$, where n is the number of deposition cycles. Interestingly, the SWNT/PSS dispersion is attracted to PVA strongly enough to form an LBL assembly, whereas PVA is neutral. The alternate adsorption occurs predominantly due to hydrogen bonds, van der Waals, and to a lesser extent electrostatic interactions.

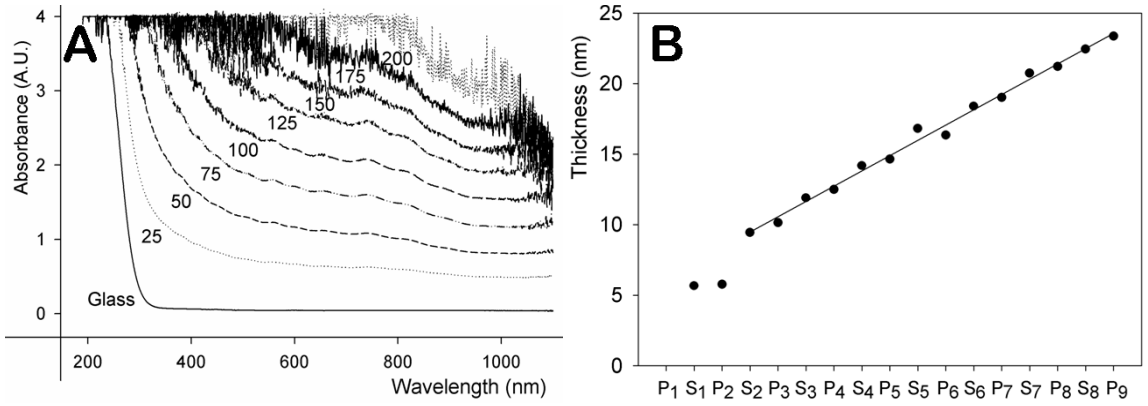

Figure 9 (A) UV-vis absorbance spectra measured every 25th bilayer of [PVA/(SWNT + PSS)]$_n$ LBL assemblies. The multilayers were formed on both sides of a glass substrate. The numbers by the curve indicate *n*. (B) Dependence of the thickness of the [PVA/(SWNT + PSS)]$_n$ film on the number of deposition cycles. PVA (P_n) and SWNT (S_n) layers with the same *n* correspond to one deposition cycle. Thickness changes were measured by ellipsometry as the LBL film was formed on a Si wafer. The displayed thickness points of each component layer are averages of three ellipsometric measurements.

PVA was chosen over a positively charged polyelectrolyte because this polymer has specific affinity to nanotubes producing high-strength materials.[39-41] Regardless of the absence of a traditional ± attractive electrostatic component in the interactions of PVA and PSS or SWNTs, UV-vis monitoring of the dependence on *n* demonstrated a linear increment in [PVA/SWNT + PSS]$_n$ thickness and light absorbance (Figure 9 A, B).

As is often the case with LBL films, there is an initial lag in the accumulation of LBL multilayers on the substrate manifesting in smaller thickness increments (Figure 9 B). After $n = 2$, the ellipsometry readings follow a straight line; the average thickness increments of SWNT layers and PVA layers in initial LBL assembly stages were calculated to 1.77 and 0.47 nm, respectively. Looking at the UV-vis spectra, one should

also point out the prominent van Hove singularity peaks. Their presence is a strong evidence of homogeneous dispersion of exfoliated SWNTs in the polymer matrix at the level of individual tubes (Figure 9 A). There are only few reported data for *solid* composites which display the same level of spectral resolution of the van Hove singularities.[42, 43] PVA and PSS are expected to wrap SWNTs in the layers in the same way as they might do this in solution. In addition to the exfoliation of nanotubes into single strands, high-performance electrical composites require homogeneity of their distribution. This should translate into high probability of their intersection and, consequently, into the formation of an extensive network of conductive pathways. It is the interdigitation of the multilayers that leads to uniform distribution of the nanotubes in the matrix and formation of an extensive 3D network. This feature is a great advantage of LBL composites for charge transport because it increases the probability of formation of multiple contacts with other SWNTs and formation of an efficient charge-transfer pathway.

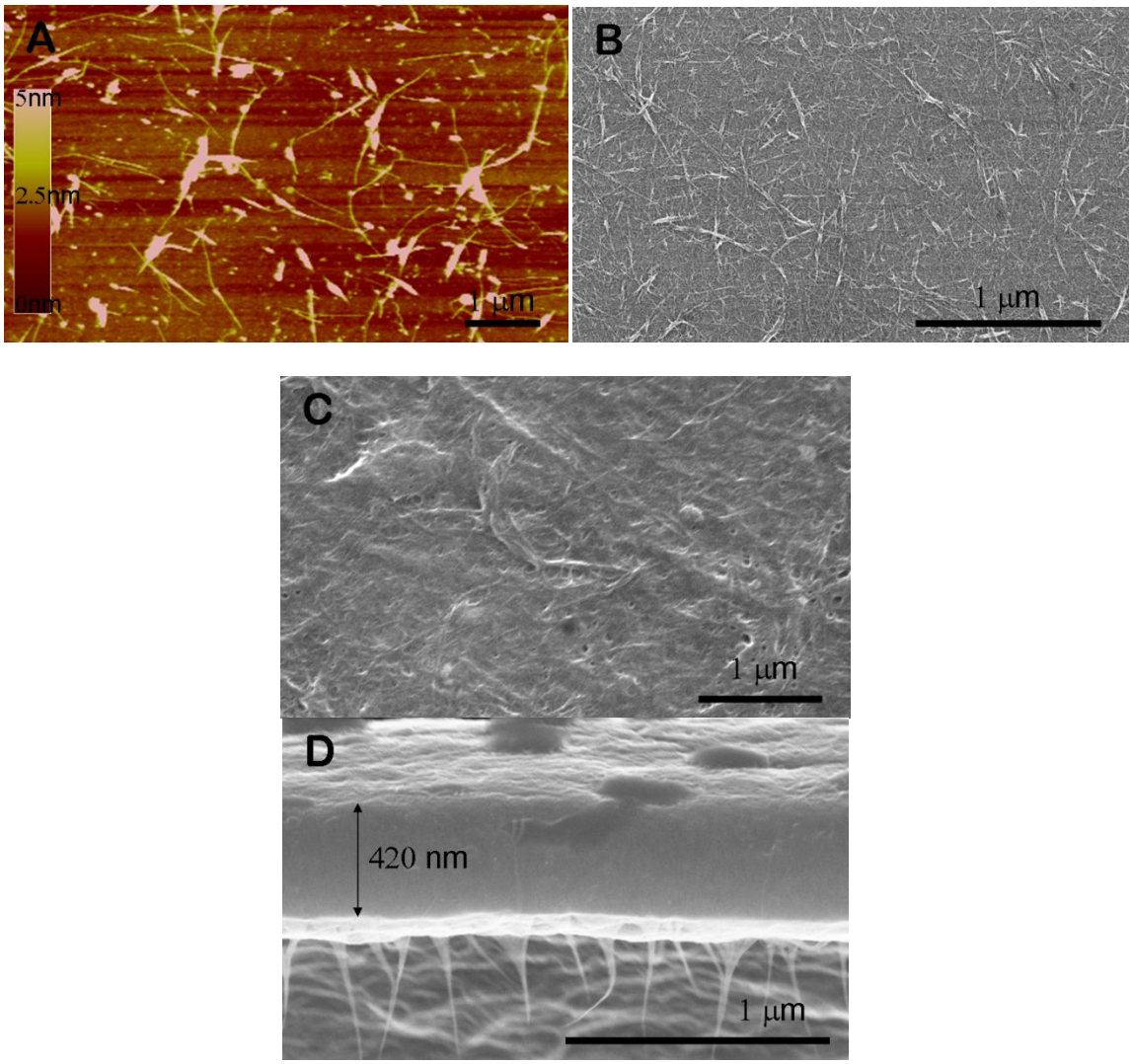

Figure 10 (A) AFM image of $[PVA/(SWNT + PSS)]_1$ and (B-D) SEM images of $[PVA/(SWNT + PSS)]_3$ (top view, B), $[PVA/(SWNT + PSS)]_{200}$ (top view, C), and $[PVA/(SWNT + PSS)]_{200}$ (cross section, D).

The state of high degree of debundling of the nanotubes in the films can also be confirmed by atomic force microscopy (AFM), scanning electron microscopy (SEM), and transmission electron microscopy (TEM) studies. The first layer indeed revealed a limited amount of SWNT adsorbed (Figure 10A) as expected from the ellipsometric

measurements (Figure 9B). Apparent heights of the SWNT strands visible in Figure 10 A are 1 to ~3 nm, which matches well with the known information about SWNT diameters, mostly 1 to ~2 nm and occasionally reaching as low as 0.4 nm and as high as 4 nm.[44] Thicker (bright in AFM) spots in the midsections of some strands could be due to spontaneous accumulation of underlying polymers (both PVA and PSS) after adsorption (macromolecular crawling) rather than SWNT bundles previously observed in nanoparticle multilayers.[45] The exfoliation of SWNTs in an LBL film was corroborated by TEM images of $[PVA/(SWNT + PSS)]_2$ (Figure 11) and X-ray diffraction data (Figure 12). The contrast of the TEM images is low because of the thinness of SWNTs which can be identified as long straight strands crossing the image in all directions. The low contrast of the images is informative in its own sense. It is indicative of the absence of SWNT bunching into much thicker aggregates and size separation of nanotube and polymer. The lack of the peak corresponding to SWNT bundles in small-angle X-ray scattering (SAXS) and wide-angle X-ray scattering (WAXS) spectra agrees well with the minimal degree of nanotube bundling in the films.

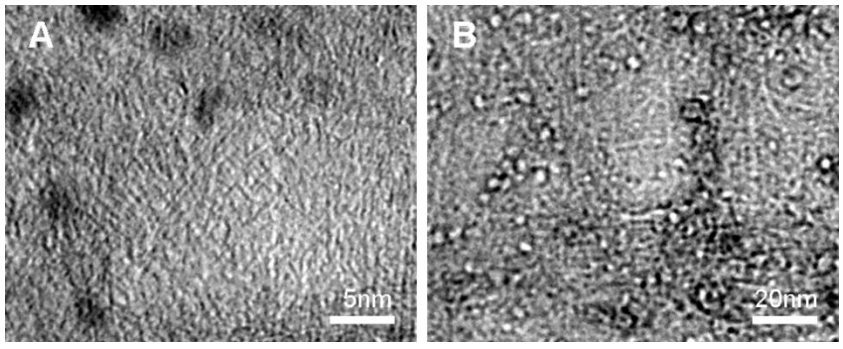

Figure 11 (A, B) TEM images of $[PVA/(SWNT + PSS)]_2$ over a thin PVA film.

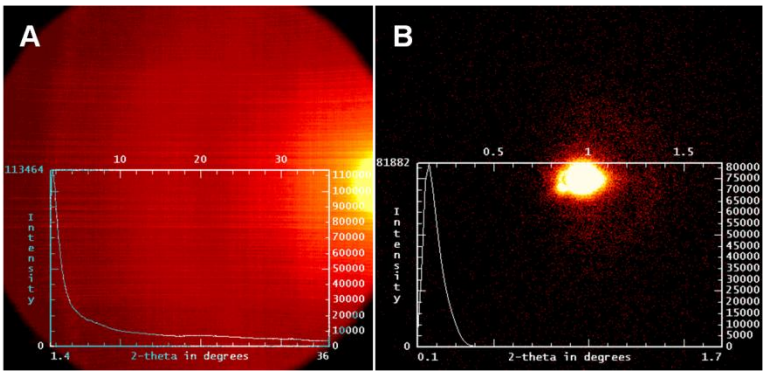

Figure 12 (A) WXRD, (B) SXRD scanning of a $[PVA/SWNT+PSS]_{200}$ LBL film

The surface roughness of LBL films measured from AFM and SEM images was ~2.2 nm (Figure 10 A, B), which is similar to the ellipsometric thickness of an individual SWNT + PSS multilayer. One can also contemplate that each PVA sublayer is infiltrating the initial nanoscale nooks and crevices that random absorption of SWNTs creates. We previously saw a similar process for LBL multilayers made from carbon fibers, which have much bigger diameter, i.e., 50-100 nm.[46] When crevices are filled, SWNTs are not only well-dispersed but also well-packed in the composite, which can be observed in a cross-sectional image of a 200-layer free-standing film, $[PVA/(SWNT +PSS)]_{200}$ (Figure 10 D). The thickness of the LBL film was found to be 420 nm, which gives an average of 2.1 nm film increment per bi-layer. This corresponds very well with the average thickness increment of 2.24 nm calculated from the ellipsometry measurements (Figure 9 B).

Substantial accumulation of polymers between the SWNT strands can also be inferred from thermogravimetric analysis (TGA) which used to estimate the nanotube contents of polymer composites. However, the TGA data often display the overlap of

decomposition curves characteristic for several components. In the case of LBL assembly, one also needs to remember that the multilayer structure of the LBL composites where the inorganic phase sandwiches can significantly modify (increase) their characteristic decomposition temperature. To combat the overlap and related experimental errors, we analyzed TGA curves obtained in N_2 gas and in air. The gaps between the data in N_2 and in air were plotted. After that, one can clearly observe the characteristic peaks of each component; PVA 330 ^oC, SWNT ~550 ^oC, and PSS ~650 ^oC (Figure 12 A-C). These component peaks are also shown in the N_2-air residual gap analysis of the LBL film (Figure 13 D). One can calculate the weight fraction of SWNTs as ~10% of the peaks by comparing the ratio of SWNT peaks in N_2-air residual gap curves. This analysis is a more robust and reproducible tool for estimating the SWNT weight loading ratio in LBL films than classical TGA curves. Knowing the densities of PVA and SWNTs, i.e., 1.27 to ~1.31[47] and 1.11 to ~1.3,[48] respectively, the volume fraction of SWNTs can be determined as ~10%. Although higher loadings of SWNTs might be beneficial, at least in some cases, for conductance in the composites, structural optimization of the SWNT-polymer system including preservation of its electronic structure has actually a much greater effect than the mass contents.

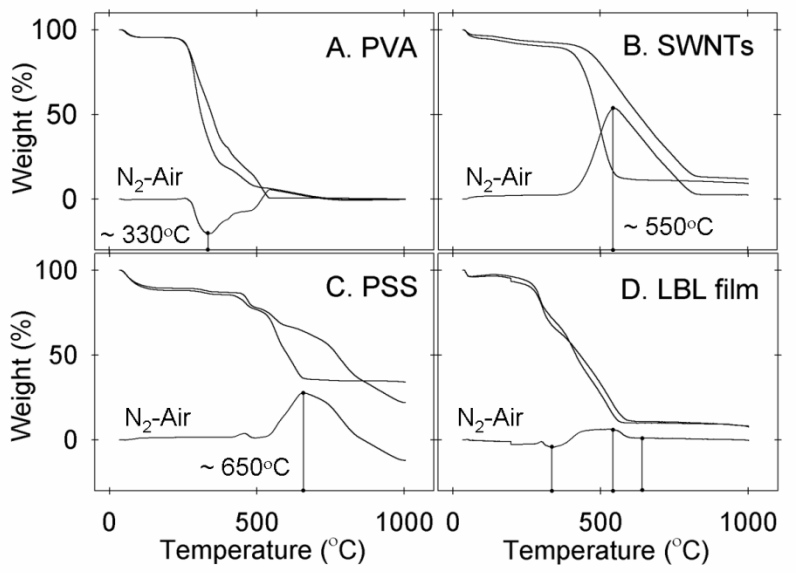

Figure 13 Thermogravimetric analysis of (A) PVA, (B) SWNTs, (C) PSS, and (D) $[PVA/(SWNT + PSS)]_{200}$ LBL film. Each sample was analyzed both in N_2 gas and air environment. The N_2-air curve at the bottom indicates the N_2-air residual gap which contains the LBL components' characteristic peaks.

4. Electrical Properties of SWNT LBL Films

Electrical conductivities in a SWNT-polymer composite are based on charge percolation, which is the spontaneous formation of electrically conductive routes through an insulating matrix by randomly distributed conducting fillers. Normally, there is a dramatic conductivity change at the percolation threshold concentration of the filler. In addition, if the density of intersecting pathways above the percolation threshold is increasing, which happens when both the homogeneity and the volumetric ratio of SWNT distribution in the matrix are improved, then electrical conductivities still increase significantly.[49, 50] As a matter of fact, the same effect can be achieved by increasing the specific spot attraction of SWNTs, i.e., by realization of the so-called "sticky contacts",[36]

which might be achieved by biological conjugation,[51] but this property has to be carefully balanced with maintaining the uniform distribution of SWNTs.

Electrical measurements were carried out by the van der Pauw method assuming two-dimensionally isotropic conductivities and by the formation of electrical contacts between the sample and silver wires with conductive silver pastes (Figure 13 A inset). For $[PVA/(SWNT + PSS)]_n$ LBL assemblies, the thicknesses of thin (n = 1-7) and thick (n = 200) films were estimated by ellipsometry (Figure 9B) and direct measurements of cross-sectional thickness (Figure 10D). Even the very thin layered films (n = 1-2) clearly indicated the conductivities much above the percolation threshold, 10^2 S/m. As more LBL layers were added (n = 3-7, 200), the conductivities increase to 2 to ~5×10^3 S/m. (Figure 14A) A reasonable explanation to the gradual increase of the overall conductivity as the number of LBL layers increases is that SWNTs are adsorbed predominantly parallel to the substrate. The molecularly parallel layered adsorptions are intrinsic features of LBL assemblies, and high aspect ratio SWNTs naturally lie down on the surface rather than stand up. Thus, SWNTs in the film have two-dimensionally aligned structures even in a thick LBL film.

The controllability of the thickness with an increment of 2-3 nm implies precise tuning of the light transmission, which is important for a variety of optoelectronic devices as a replacement of ITO coating necessary to combat the shortage of indium. Light transmittance as high as 97% at 600 nm can be achieved for 5 nm films with conductivity in the range of 10^2 S/m made after one deposition cycle. Notably, the actual transparency of single SWNT LBL coatings is even better than 97% because the light transmittance

measurements in Figure 14 B, C were performed with the samples in which both sides are coated on a glass substrate, not a single-side coating, whereas the conductivity is measured only on one side at a time.

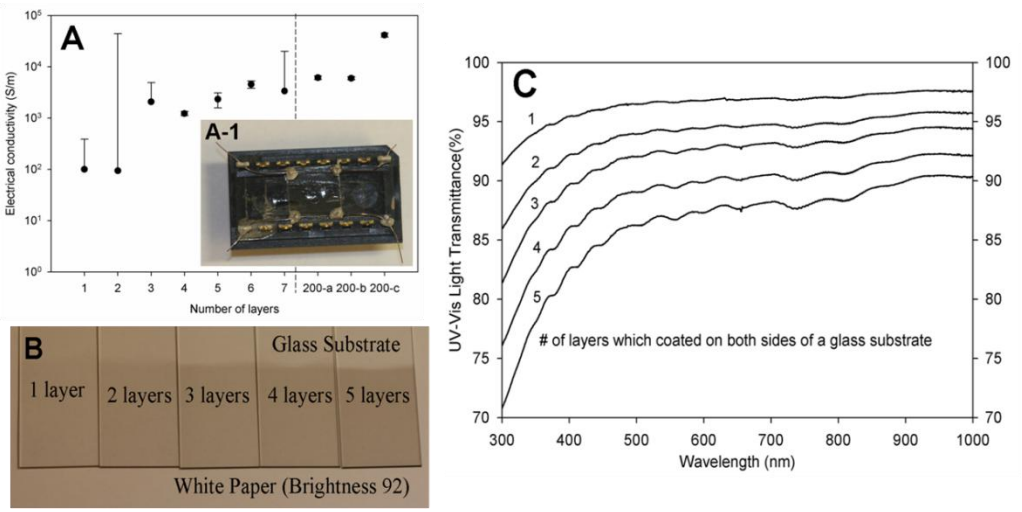

Figure 14 (A) Electrical conductivity measurements of $[PVA/SWNT + PSS]_n$ (n=1-7, 200); 200-a, 200-b, and 200-c indicate as-prepared, 200 ^oC, and 300 ^oC treated films of 200 bilayers; LBL films with the van der Pauw measurement setup are shown in the inset. (B) Photograph and (C) UV-vis light transmittance of $[PVA/SWNT + PSS]_n$ (n=1-5) LBL coatings on both sides of a glass substrate.

One can obtain above 90% transmittance in the range of 400 to ~750 nm and conductivities of 10^2 to ~2 × 10^3 S/m. Even though SWNT thin film made by filtering techniques may have a maximum conductivity of 10^5 to ~10^6 S/m with moderate transparency, their electrical percolation routes deteriorate above 90% of light transmittance.[9, 15, 16, 29, 52] For that reason only extrapolations based on empirical data at lower transparencies are typically provided for these films rather than the actual measurements. When one looks at the combined structural, optical, and electrical data in

conjunction with each other, it can be concluded that the utilization of SWNTs in LBL films is exceptionally efficient due to high homogeneity and degree of dispersion of the nanotubes in them (Figure 9). Another noticeable distinction from SWNT mats is that LBL films can be directly coated on a variety of complex surfaces. Examples when this property may become very essential include optical fiber, microfluidic channels, and the porous surfaces of flexible moving structures.

LBL assemblies of SWNT-PVA can be expanded to fabricate a membrane-like flexible free-standing film detached from the substrates. The electrical conductivity of the as-prepared 200-layered film measured by the same van der Pauw technique was 6.1×10^3 S/m. Thermal treatment of the film at 200 ^{o}C makes little change in the conductivity, while increase of the annealing temperature to 300 ^{o}C boosts it further to 4.15×10^4 S/m. After the creation of the percolation network, the improvement of the quality of SWNT-SWNT contacts is one of the most important requirements to the design of electrically conductive SWNT composites, because the efficiency of electron tunneling through the gap is exponentially dependent on the SWNT-SWNT distance. So, the effect of heat treatments can be understood as a gradual closing of intrinsic nano- and angstrom-scale voids/pores and relaxation of the polymer conformation to the one that adheres to nanotubes better. Altogether, this makes better contact between individual SWNTs in the network. The temperature threshold of conductivity improvement, i.e., 200-300 ^{o}C, corresponds very well with the expected melting temperature of PVA in the LBL films. Although heat treatment effects onto nanostructures of our SWNT LBL composite were

not simple, thickness changes of the film were 5% and 10% reduction with 200 ^{o}C and 300 ^{o}C treatments.

5. SWNT Tightening by Thermal Annealing

After the creation of percolation network, the improvement of the quality of SWNT-SWNT contacts is one of the most important requirements to the design of electrically conductive SWNT composites, because the efficiency of electron tunneling gap is exponentially dependent on the SWNT-SWNT distance. Therefore we tried molecular tightening by thermal annealing above polymer's glass transition temperature, even though high temperature treatments have negative impacts on the conductivity of polymeric LBL films because of reducing volatile admixture and ion doping effects and density increasing micro-Brownian motion.[53] After a simple thermal annealing, the 200 layered sample showed significant improvements in its conductivity reaching $6.3\pm0.3\times10^{3}$ S/m, which can be attributed to annealing of structural imperfections due to slightly increased molecular mobility. We further investigated the heat treatment effects by monitoring the electrical properties of $[PVA/(SWNT+PSS)]_{200}$ while gradually varying temperature in two cycles from 40^{o}C to 200^{o}C (Figure 14). In addition to potential enhancement of charge transport, these data will also provide information on thermal stability of the electrical properties. The electrical conductivity of $[PVA/(SWNT+PSS)]_{200}$ was initially 3×10^{3} S/m at 40^{o}C and increased to 4.15×10^{4} S/m at 300^{o}C. However, the electrical conductivity increase is reversed if the heat treatments

at 200°C are prolonged or repeated. Here, we noticed that the sharp conductivity increase at 300°C might be associated with not only chemical/physical relaxation of the composite but also with irreversible structural rearrangement of SWNTs because the annealing process caused permanent changes in electrical properties. This is consistent with strengthening of van-der-Waals bonds with temperature, which is typically irreversible.

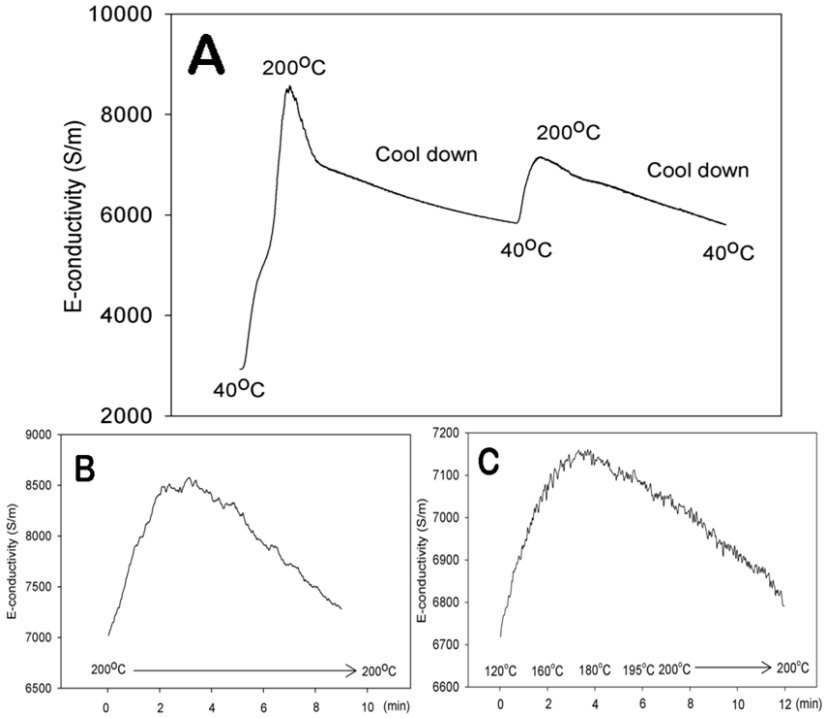

Figure 15 (A)-(C) In-situ electrical conductivity changes during heat treatment of the $[PVA/(SWNT+PSS)]_{200}$ film. (A) Electrical conductivity dramatically increases when temperature goes to 200°C decreasing slowly afterwards. (B) Electrical conductivity changes for the first treatment at 200°C, the first peak in (A) as forming sticky contacts and then aggregates. (C) Electrical conductivity changes for the second treatment at 200°C, the second peak in (A).

Considering the nature of the temperature effects on the composite structure, one can investigate the changes of van Hove singularity peaks in UV-vis spectroscopy before

and after thermal treatments. Spectral positioning of van Hove singularities depends on SWNT diameters and specific chiral structures.[54] So, if SWNTs are fully exfoliated as a single strand, absorption spectra of the SWNT mixture have discrete peaks corresponding to electronic excitation energy, e.g., $E_{11(S)}$, $E_{22(S)}$, $E_{11(M)}$ etc. Also, both $E_{11(S)}$ and $E_{22(S)}$ peaks of semiconducting SWNTs can provide useful information about inner organization of the composites. As such, $E_{22(S)}$ peaks or peaks in the visible light range are less sensitive to chemical doping changes around SWNTs than $E_{11(S)}$ peaks.[55, 56] Therefore, only $E_{22(S)}$ or higher energy peaks were examined for the transparent 8, 12, and 16 layered films of [PVA/(SWNT+PSS)]. Existence of these van Hove singularity peaks is a distinct criterion of the "goodness" of the SWNT solvent as well as the quality of the SWNT dispersions.[57] If these SWNTs are bundled, then down shifting and broadening of the peaks can be expected due to band gap lowering inter-tube interactions.[58] In the solid composite system these peak shifting and broadening effects become a prominent evidence of molecularly controlled SWNT rearrangements (Figure 16) leading to tighter connection between SWNTs. Also, thermal annealing does not produce any change in macro-appearances at all, but these are only monitored by the shape and shift of the van Hove transition peaks.

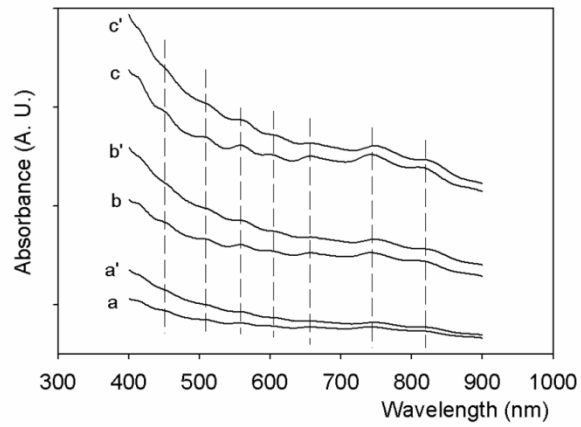

Figure 16 UV-vis spectroscopy of (a) 8 layered, (b), 12 layered, and (c) 16 layered LBL film of [PVA/(SWNT+PSS)]. (a', b', c') The same measurements of the samples were compared after 300^{o}C thermal annealing treatments. Conspicuous van Hove singularity peaks in the original films were broadened and red-shifted which was a good indication of permanent molecular structure rearrangement of SWNTs from extreme dispersion to tightly connected state.

6. SWNT Concentration Effect during LBL Assemblies

The solution quality of LBL assemblies affects the layered structure. For example, if the concentration of a SWNTs dispersion solution is diluted, then the adsorbed amount of SWNT in a given amount of time dipping decreases and the material properties of the resulting composite changes. Here, we compared the optical properties of LBL assemblies with varied SWNT concentration solutions and the electrical properties of the resulting 10 layered films before and after heat treatment at 300^{o}C for 10 min. (Figure 17)

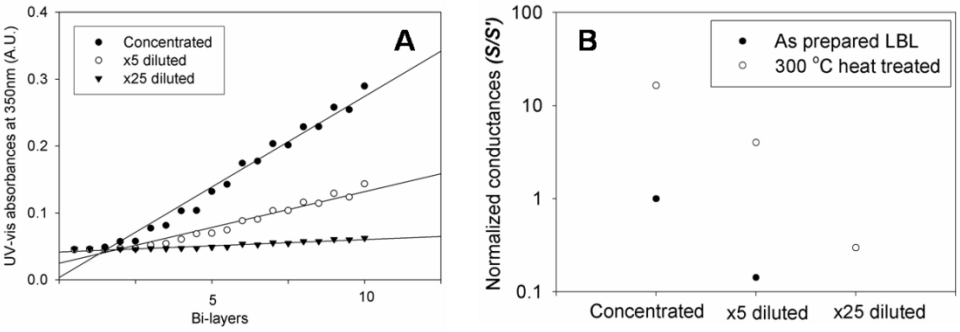

Figure 17 SWNT concentration effect during LBL assemblies (A) UV-vis spectroscopy of [PVA/diluted (SWNT+PSS)]$_n$ LBL assemblies with concentrated, x5 diluted, x25 diluted SWNT solution. (B) Normalized conductance (***S/S'***) of the resulting 10 layered LBL film with and without heat treatment. S' indicated the conductance of as-prepared [PVA/concentrated (SWNT+PSS)]$_{10}$ LBL film.

7. Mechanical Properties of a Conductive LBL Film

The strength of the transparent thin films is also an important parameter when it comes to device manufacturing. Although the strength of very thin films cannot be directly quantified, the integrity of the films was not affected at all when we rubbed the surface and cut it into a small square (4 mm × 4 mm) to fit our van der Pauw measurement setups. To quantify these empirical observations, mechanical properties of fairly thick [PVA/SWNT + PSS]$_{200}$ films were measured. The mechanical strength of the thick LBL film was estimated before and after 200 ^{o}C heat treatment by direct sample stretching tests (ASTM D 3039). Tensile strengths/strains of the sample were 150 ± 18 MPa/6% before and 159 ± 21MPa/5% after the heat treatment, respectively (Figure 18 A, B). It makes the LBL films around 2 to ~10 times stronger than the bucky papers.[28, 29] They are also exceptionally flexible (Figure 18 C, D), which cannot be attributed to SWNT mats without the polymer impregnation.

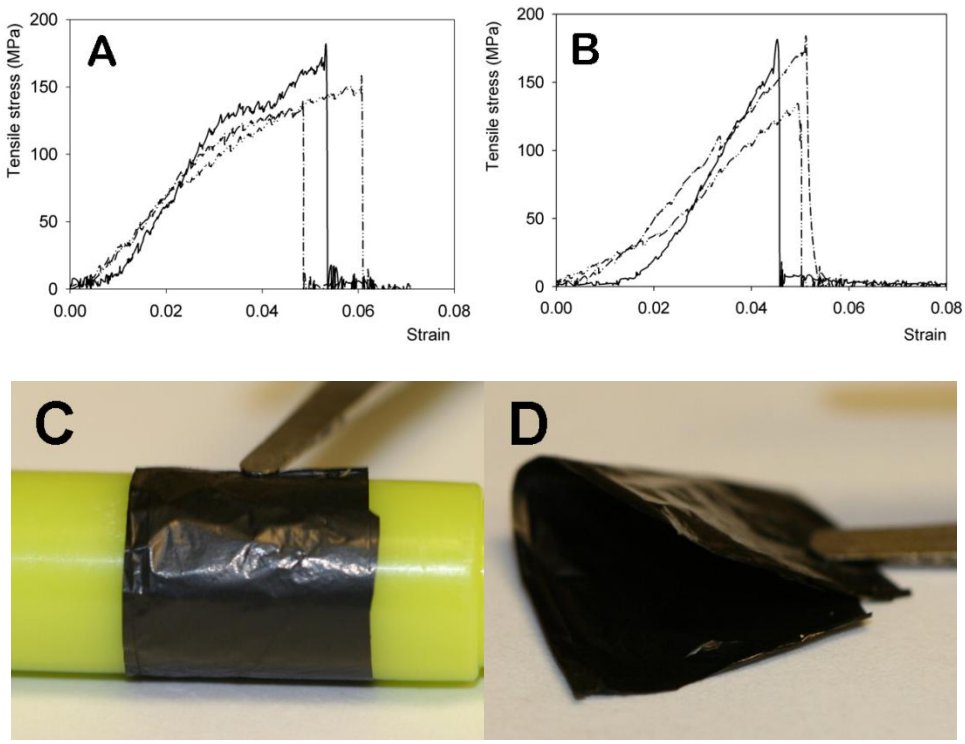

Figure 18 Mechanical stretching test results of the $[PVA/(SWNT+PSS)]_{200}$ LBL film (A) before and (B) after 200°C heat treatment. (C, D) Demonstration of the flexibility of a LBL composite film which is contrasted with rigid SWNT only mats.

8. Phenomenological Analysis of Conductivity in LBL Films

One of the advantages of LBL films is that one can engineer their nanoscale and molecular structure to obtain desirable properties. In this respect, we need to map out potential directions for further improvement of their electrical characteristics. In order to do that let's consider the linear reversible electrical conductivity decrease with temperature increase in the set composite leading to more fundamental understanding of electrical transport in LBL structures. It can be explained by taking into account (1) semiconducting characteristics of SWNTs and (2) Schottky barriers or structural

mismatch in metallic and semicoducting SWNT junctions.[59] The electrical resistance ($R_{composite}$) of a SWNT-polymer composite is associated with intrinsic semiconducting or metallic SWNT resistances (R_{SWNTs}) and SWNT-SWNT contact resistances ($R_{contact}$) between the nanotubes because polymer matrix in this system is an electrical insulator.[60] Despite significant improvement of electrical parameters, the electrical conductivities of a composite are below the axial direction measured conductivities of individual SWNTs, $1\sim3\times10^6$ S/m. This leads to the conclusion that the SWNT-SWNT contact resistances in a composite dominate the total resistance of a composite ($R_{contact} >> R_{SWNTs}$). The SWNT-SWNT contact resistance ($R_{contact}$) is further factorized into SWNT junction resistances including semiconducting-semiconducting (R_{SS}), semiconducting-metallic (R_{SM}), and metallic-metallic (R_{MM}) which are much different in their magnitude ($R_{SM} >> R_{SS} > R_{MM}$). However, SWNT junctions in a well dispersed SWNT-polymer composite are not simply formed as physically perfect contacts. Instead, very thin polymeric layers, which are essential in an LBL system, are likely to be often sandwiched between the tubes preventing the pure ohmic contact. Note that the polymer is a necessary part of the SWNT –based material which allows one to make macroscopic objects. Since the polymers used here are insulating, one can safely assume that $R_{polymer} >> R_{SM}$. Therefore, $R_{contact}$ can be substituted with one of R_{SS}, R_{SM}, R_{MM}, and $R_{polymer}$. Taking a single electrical conductive route, one can represent it as a series of SWNT-SWNT contacts, whose electrical resistance is simply a sum of all these resistances.

$$R_1 = x \cdot \left[R_{SWNTs} + R_{contact}\right] = x \cdot R_{SWNTs} + x_1 \cdot R_{SS} + x_2 \cdot R_{MS} + x_3 \cdot R_{MM} + x_4 \cdot R_{polymer} \quad (1)$$

where, $x = x_1 + x_2 + x_3 + x_4$

If a composite has anisotropic molecular structures such as SWNT alignments, the magnitude of x significantly decreases. Numerous electrical conductive routes exist which are considered as parallel circuits in a SWNT-polymer composite. Therefore, the reciprocal of total resistance ($1/R_{tot}$), conductance (G_{tot}), of a composite can be calculated as a sum of the reciprocals of electrical resistances from possible conductive routes.

$$1/R_{tot} = 1/R_1 + 1/R_2 + \cdots + 1/R_y = G_{tot} \quad (2)$$

From this analysis, we can set the priority of optimization process for improving electrical conductivity because the largest resistance term dominates the total resistance of a composite. The first stage of the optimization is to minimize the term, $x_4 \cdot R_{polymer}$, which was achieved here by thermal treatment tightening, because it apparently reduced the gap between the nanotubes. The second stage should be modification of R_{SM} to R_{SS} or R_{MM} because R_{SM} is much larger than R_{SS} or R_{MM} and x_1, x_2, and x_3 are all same orders of magnitude. However, current technology can produce only SWNTs mixtures, so that the semiconducting-metallic Schottky junctions will remain the main contributors to the remaining electrical resistance until the SWNT separation problem is solved. At last, the third stage is to minimize the magnitude of x, the number of SWNT contacts, and more specifically, hopping chances of a charge carrier. Creating anisotropic nanoscale structures such as SWNT's layered structures or alignments or using longer conducting fillers could be options to reduce x. In the other respect, bundling of SWNTs may dramatically limit the number of percolation routes, the magnitude of y, # of effective

conductive routes, although SWNT ropes may generate reduced *x* and, sometimes, the composite to be metallic. The reduction of effective conductive routes is a critical issue because of structural mismatch of SWNTs which implies that not every SWNT junction is effective site for charge carrier hopping.[59] Therefore, exfoliation in single stranded SWNT indeed improves so much the electrical conductivities by increasing the total numbers of conductive routes with the same SWNT filling ratio.

Using the language of this analysis, one can say that the heat treatment improves the quality of SWNT-SWNT contacts by partially removing polymer sandwiched between them. SWNT LBL composites have much bigger *y* than bucky paper because bundled SWNTs of a bucky paper critically decrease the possible number of conductive routes, *y*. Hence, SWNT LBL composite with an order of magnitude lower SWNT contents could demonstrate the level of electrical conductivities not too far from some SWNT-only bucky papers.

9. Conclusion

In this section, we introduced a pristine SWNT – polymer LBL composite and demonstrated effective reinforcement, unique optical transparencies including super clearness and useful electrical conductivities with small SWNT contents. The described SWNT-polymer LBL composites created effective SWNT-SWNT contacts due to a high degree of exfoliation, high homogeneity, and a thermal tightening of gaps between them. The electrical conductivities which we measured in the LBL films were substantially

higher than most of other PVA-SWNT or insulating polymer-SWNT composites which have conductivities of 10^{-2}-10^{4} S/m. Compared to the conductivites of SWNT mats made of pure nanotubes (10^{4}~10^{6} S/m), the conductivities here are lower. Although not exceeding the 10^{6} S/m record, the current achievement definitely fills the functional property gap between pure SWNT films and SWNT-polymer composite system. We should make three points about the LBL structures as it relates to the conductivities: (1) the SWNT loading is more than an order of magnitude smaller than in other thin films; (2) the SWNTs were not doped; and (3) polymers we used are insulators. The conductivities of the composite can potentially be improved several orders of magnitude by addressing these aspects in the future structures, but even with current electrical and mechanical data this study is a demonstration of effective transfer of SWNT properties in organic thin films, which could be applied in numerous fields, from solution processed transparent flexible organic electronics to physicochemical sensors in biomedical, space and civil engineering.

C. SWNT LBL Composites for Flexible Transparent Conductor Applications

1. Summary

Transparent conductors (TCs) have been actively searched for a century because of continuous expansion for the applications starting from sensors, solar cells, and displays and continuing to smart windows, and next generation flexible electronics. Rigid semiconducting oxides weredominant material options for years. However, technical requirements of TCs not only include electrical conductivity and transparency but also demanding mechanical properties and environmental resistance which become particularly critical for flexible electronics and solar cells. Traditional single-walled carbon nanotube (SWNT) coatings have been suggested as alternative TC materials but typically lack mechanical properties. Balancing conductance and strength is regarded as a formidable fundamental and practical challenge. As a result of fine tuning of nanometer scale structure, SWNT layer-by-layer (LBL) polymeric nanocomposites can (1) integrate mechanical strength and fast charge transport; (2) produce TC films with 86±1 Ω/sq above 80.2±0.1 % transmittance, which is highly comparable with traditional indium-tin oxide ITO parameters, and (3) produce sophisticated easy-to-scale-up properties on any flexible/complex surfaces. These technical parameters make LBL SWNT coatings suitable for a variety of electronics and energy applications.

2. Experimental Procedure

Materials: Poly(vinyl alcohol) (PVA, MW: 9,000, 70,000, and 196,000), poly(sodium 4-styrene-sulfonate), (PSS, MW: 200,000, PSS(200K) and 1,000,000, PSS(1M)) and sodium dodecyl sulfate (SDS) were purchased from Sigma-Aldrich Co. SWNTs were purchased from Carbon Nanotechnologies Incorporated (purified HiPco SWNTs. Now the company merged with Unidym) (CNI SWNTs) and Carbon Solution Co. (P-2, SWNTs) (C-Sol SWNTs).

LBL assembly: Purified SWNTs were dispersed in water with helps of negatively charged stabilizers such as PSS and SDS. Various molecular weights of PVA solutions were prepared. By charge transfer interaction between SWNTs and PVA, or by hydrogen binding between possible COOH groups in SWNTs and OH in PVA, they formed LBL assemblies on a charged substrate (glass or Si). Each LBL layering process consists of dipping in the PVA or the SWNT solution, water rinsing, and drying. To denote LBL assemblies, [PVA / SWNT (CNI or C-Sol) + stabilizer (PSS or SDS)]$_n$ was used in which *n* represents the number of repeated dipping processes in PVA and SWNT solutions.

Instrumental analysis: Scanning electron microscopy (SEM) images were taken with a Philips XL30 field emission gun scanning electron microscope and an FEI Nova Nanolab dualbeam FIB and scanning electron microscope. Atomic force microscopy (AFM) imaging was performed with Nanoscope III (Digital Instruments/Veeco Metrology Group). UV-vis absorption measurements were taken using an Agilent 8453E UV-visible spectroscopy. An Agilent 34401A multimeter was used for electrical

measurements. Mechanical tests were done by Q systems model 100 (Test Resources). Thermo gravimetric analysis (TGA) was performed by a PerkinElmer Pyris 1 TGA. Ellipsometric measurements were done by M-44 IR Spectroscopic Ellipsometer (J. A. Woollam Co., Inc.). X-ray photoelectron spectroscopy (XPS) was carried out using a Kratos Axis Ultra. A monochromated Al K alpha X-ray source was used to irradiate the sample using a power of 140 W (14 kV, 10 mA). A chamber pressure of better than 1 x 10^{-9} was maintained throughout the experiment. Survey scans were performed using a pass energy of 160 eV, a step size of 1 eV, and a dwell time of 200 ms. Detailed scans were acquired with a pass energy of 20 eV, a step size of 0.1 eV, and a dwell time of 200 ms. A flood gun was used for charge compensation.

3. Optical Properties by Bundling State of SWNTs

One of the apparent advantages of molecular LBL assemblies over conventional solution casting is a preservation of nanoscale building block dispersion quality from a solution to the solid state. As introduced in the previous section, exfoliated SWNTs dispersed in a PSS solution were maintained in a thin film composite by a direct adsorption layering and a molecular thin sandwiched LBL structures.[17] The role of stabilizers such as polyelectrolytes and surfactants is to increase SWNT's solvation in water by shielding hydrophobic sidewalls of SWNTs. In SWNT TC applications, stabilizers are considered to be impurities hampering free movement of charge carriers in percolation type conduction routes. Thus, efforts have been focused on removing residual stabilizers in SWNT networks by rinsing[9], burning[9, 61], and chemical treatment[18, 62].

These stages actually negated some of the conceptual advantages of the TCs from SWNTs, such as low temperature processing. If we change the perspectives and consider the benefits of a suitable stabilizer for TC applications, they can (1) increase mechanically stability; (2) increase environmental stability in harsh environments, (3) serve as in-situ doping agent, and (4) of course, improve SWNT exfoliation.

PSS and SDS are two of most commonly used stabilizers of SWNT dispersions (Figure 19 A). UV-vis absorbance spectra display van Hove singularity peaks indicative of the high degree of nanotubes exfoliation, predominantly at the level of single stranded nanotubes. Comparing peaks' positions and shapes, SWNTs from CNI stabilized by PSS (SWNT/PSS) have slightly sharper shape and their positions are more shifted to the blue side of the spectrum than the sample dispersed with SDS (SWNT/SDS). Similarly, it is shown that high molecular PSS (1M) produced slightly better exfoliation than lower molecular PSS (200K). Thicker SWNT bundles are usually corresponded to broadened peak shape and red shifted peaks in the spectra. (Figure 19 B)

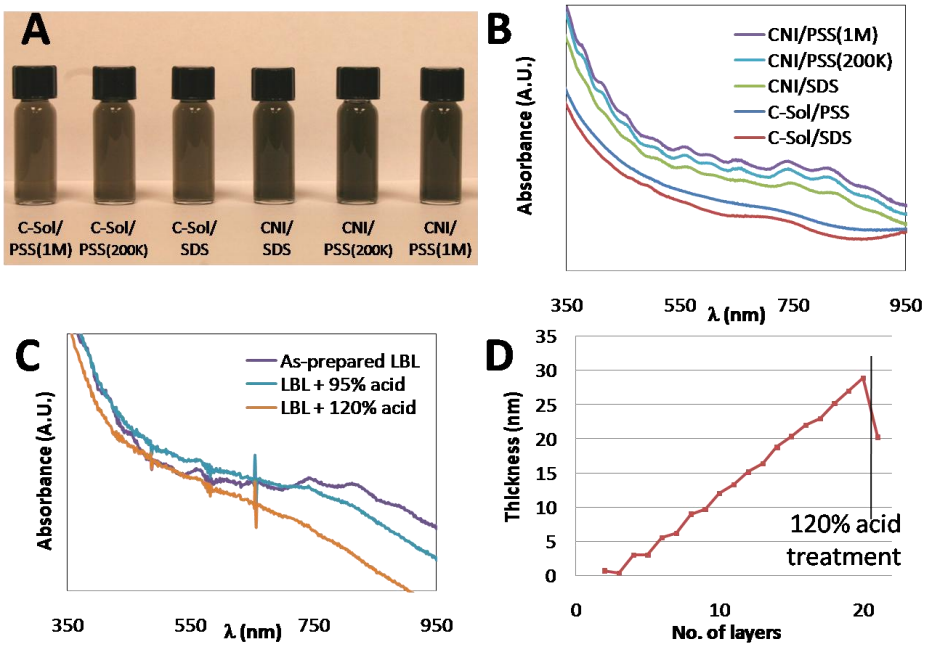

Figure 19 (A) Visibly black-colored homogenous dispersions of C-Sol and CNI SWNTs with PSS (1M , 200K) and SDS stabilization. (B, C) UV-spectroscopy of (B) solutions demonstrated in A and (C) [PVA / CNI SWNTs + PSS (1M)] LBL TC films before and after H_2SO_4 (95%, 120%) treatments. (D) Ellipsometry thickness measurements of [PVA / C-Sol SWNTs + PSS(1M)] LBL assembly.

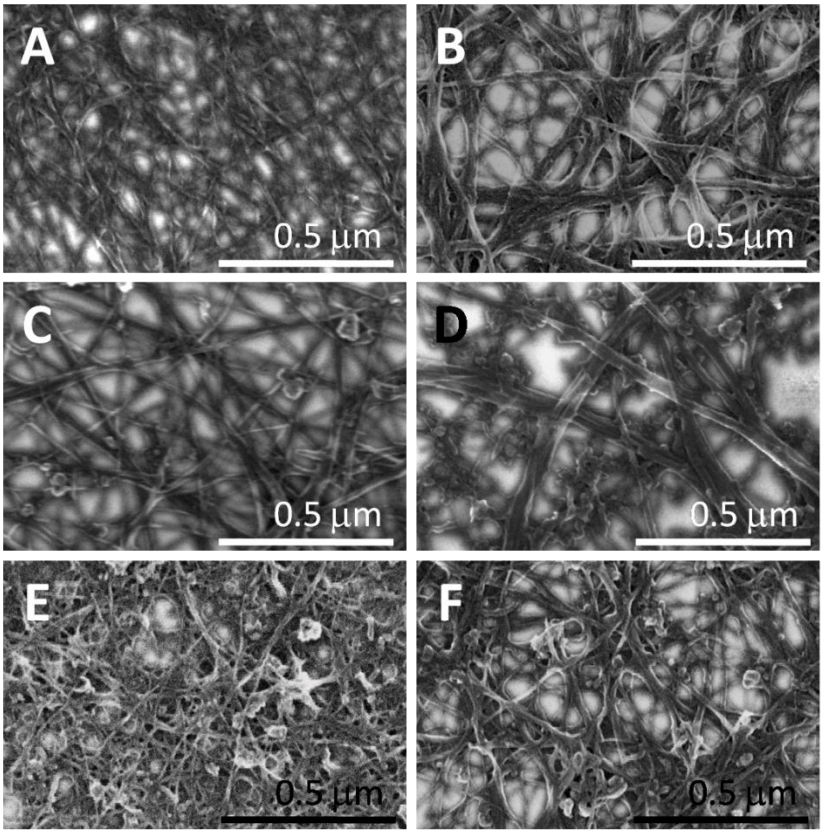

Figure 20 SEM images of (A) [PVA / CNI SWNT + PSS (1M)] (*T*=95%) after superacid treatment, (B) [PVA / CNI SWNT + SDS] (*T*=83%) after superacid treatment, (C) [PVA / C-Sol SWNT + PSS (1M)] (*T*=86%) after superacid treatment, and (D) [PVA / C-Sol SWNT + SDS] (*T*=82%) LBL films after superacid treatment. (E) [PVA/ C-Sol SWNT + PSS(1M)] LBL film without acid treatment. (F) $[PVA / C\text{-}Sol\ SWNT + PSS(1M)]_{200}$ free-standing LBL film with super-acid treatment.

The degree of exfoliation in the coating is expected to go in parallel with that in solution. Indeed, substantial difference in SWNT bundle sizes in LBL films for the two stabilizers was noticed. (Figure 20 AB) SWNT bundles made with SDS wrapping were 2~5 times thicker than those made by PSS stabilization although macroscale appearance was identical. The bundle size also significantly influenced the light transmittance (***T***) at λ=550nm ($\boldsymbol{T}/100 = 10^{-\alpha}$) of the LBL films measured after 10 deposition cycles: ***T*** =

95±0.5% for more exfoliated SWNT/PSS versus ***T*** = 83±0.5% for more bundled SWNT/SDS. This effect can be understood as the result of (1) greater incorporation of graphene-based compounds in the LBL films and (2) SWNT-SWNT electronic state coupling leading to stronger adsorption in the visible range[15-17] for dispersions and composites with greater degree of bundling.

Currently, the properties of nanotubes are critically dependent on a manufacturer. While the previous experiments were carried out with nanotubes from CNI made by high-pressure CO conversion (HiPCO), it was necessary to verify the observation for a different kind of SWNTs, such as C-Sol SWNTs, which were produced by electric arc discharge (EA). Commercially available P-2 SWNTs from C-Sol are known to longer and larger in diameter than those from CNI. Light absorbance spectra of C-Sol SWNT dispersions did not reveal van Hove singularities, which is indicative of more bundling (Figure 19 B). SEM observation of C-Sol SWNTs by PSS and SDS, however, showed the same trends of agglomeration state in LBL films as SWNTs from CNI. Although exfoliation of longer C-Sol SWNTs as not efficient as the shorter CNI ones, PSS still works better for debundling them. (Figure 20 CD) The light transmittances at λ=550 nm of LBL coatings made after 10 deposition cycles with PSS and SDS was found to be ***T*** = 86±0.5% and ***T*** = 82±0.5%, respectively.

4. TC Performance Change by Super-Acid Treatment

Here, we focus on the effect of chemical treatment in which we expect two effects: (1) annealing by removing loosely bound polymer, and (2) chemical doping. Previously, we demonstrated that tighter SWNT contacts formed by thermal annealing of CNI SWNT/PSS LBL thin films at 300^{o}C increase more than an order of magnitude of electrical conductivities. Analogously, acid treatments such as 70% HNO_3,[18, 28] and 97% $SOCl_2$[62, 63] were introduced to increase the TC performance. In order to maximize conductivity, extreme concentrations, 120 % of H_2SO_4 ('super-acid') were tested here.

For understanding the acid treatment effects on SWNT polymeric nanocomposites, light absorbance spectra (Figure 19 C) were useful. 95% H_2SO_4 causes significance absorbance drop at the S22 transition in the range of 700~900nm characteristic for semiconducting SWNTs as well as sweeping all the characteristic peaks. These changes are typical for *p*-type ion doping transitions[64, 65] caused by down-shifting of the Fermi level, E_F.[65] 120% H_2SO_4 increased the ion doping effects further. Although the analysis of doping effects of this polymeric nanocomposite system cannot be easily done, one can speculate based on the data for simpler systems that intercalated SO_3^- dopant increases the percentage of highly-doped metallic behaving SWNTs, unlike HNO_3 doping.[65, 66]

However, chemical doping effects are known to be weakened gradually in air environment. For preventing this weakening effect, PEDOT/PSS capping layers were employed and the doped SWNT films became quasi-stable in their conductivities for 2 weeks.[67] By utilizing the same principles, we doped our LBL film with super-acid every

5 layers, which covers SWNT doping of a SWNT LBL composite with successive polymer layers. Furthermore, in order to maximize TC performance, we tried C-Sol P-2 SWNTs in this work. Although C-Sol SWNTs have higher optical resistance as seen in the previous section, overall TC performance of C-Sol SWNTs are better than that of CNI SWNTs.

Figure 21 compares TC performances by three stabilizers - SDS, PSS (200K), and PSS (1M) - in the plots of electrical conductivity vs. optical transparency. Interestingly, TC performances of C-Sol SWNT LBL coatings with super-acid treatments ranked from higher molecular weight stabilizers, which contradict to our current knowledge on the roles of stabilizers. The optimally conditioned [PVA / C-Sol SWNT + PSS(1M)] LBL nanocomposite showed $\boldsymbol{R_s}$=86 Ω/sq with $\boldsymbol{T}$ (λ=550nm) = 80% which is the similar level of the best performance of all SWNT TC coatings.[18, 22, 68] Among these SWNT coatings, this SWNT LBL composite is differentiated as polymeric nanomoposites with strong binding interactions as shown in chapter 1. It might be useful to know the performance of SWNT LBL coatings with industrial specifications: $\boldsymbol{R_s}$ = 90 Ω/sq at $\boldsymbol{T}$ = 90%.

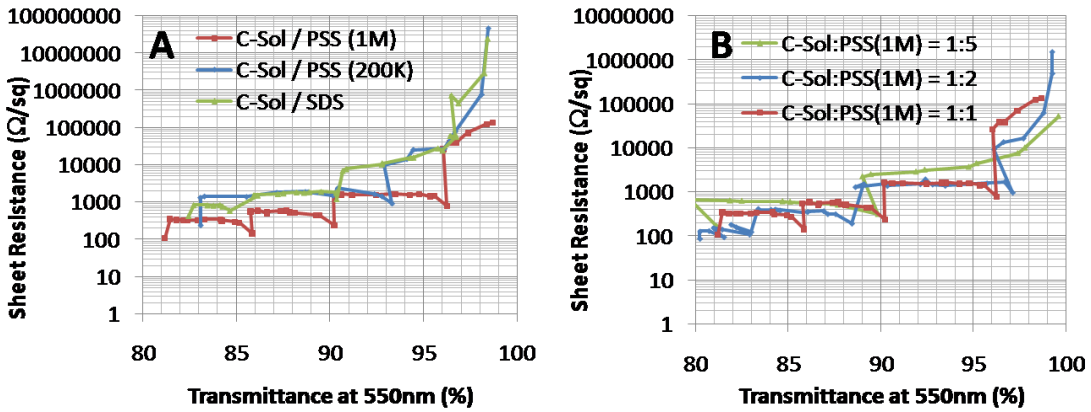

Figure 21 Comparisons of TC performances in (A) [PVA / C-Sol SWNT + PSS(1M)], [PVA / C-Sol SWNT + PSS(200K)], and [PVA / C-Sol SWNT + SDS] LBL films with super-acid treatment every 5 bi-layers, and (B) [PVA / C-Sol SWNT + PSS(1M)] LBL films with super-acid treatment every 5 bi-layers.

5. Mechanical Properties

It should be emphasized that after super-acid treatment the residual polymer binders, which are actually strongly interacting with SWNTs, contribute significantly to the mechanical properties of the coatings, which essential for TC applicatons. For accurate mechanical property measurements, we constructed a [PVA / C-Sol SWNT + PSS (1M)]$_{200}$ free-standing LBL film. After super-acid treatment, the free-standing LBL composite became 250nm in thickness. Tensile modulus, strength, and toughness of the free-standing film were estimated to be 12.3±3.4 GPa, 218±13 MPa, and 8±1.7 J/g, respectively. (Figure 22 A) These values are 2.5 times in modulus and 2.9 times in strength higher than the strongest bucky papers.[28] Finally, we demonstrated that the described films can be easily deposited on the large scale plastic samples. (Figure 22 B)

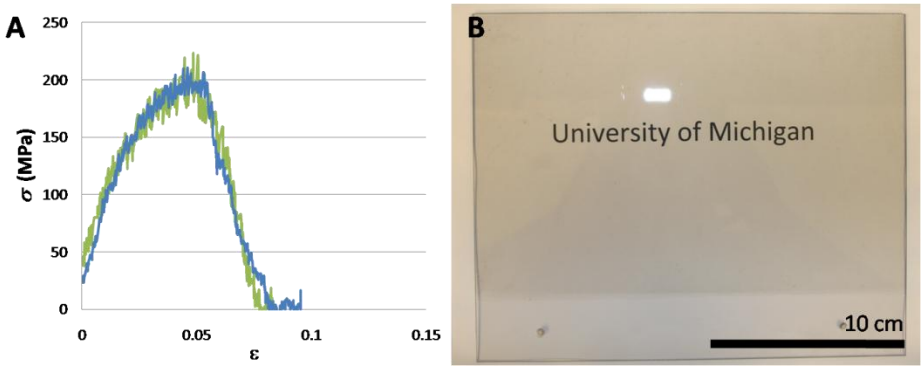

Figure 22 (A) Mechanical property measurement data by direct streteching test of [PVA / C-Sol SWNT + PSS (1M)]$_{200}$ free-stading LBL film with super-acid treatment. (B) Large-scale demonstration of SWNT LBL TC coating.

6. Conclusion

In this section, we demonstrate that inclusion of a non-conductive polymer in LBL SWNT composites that might be considered as a counter-intuitive decision for making TCs, can not only produce viable TC coatings but actually matches if not improves the best electrical parameters for analogous systems reported so far. Equally important, molecularly thin polymeric binders between SWNT layers significantly improve mechanical stability. Additionally, TC performance of the SWNT LBL film can be fine-tuned by 1% increments in transmittance. The dip-coating based LBL process can be easily scaled-up without dramatic cost or quality deterioration as the case for other processes of nanortube deposition. Although, more work still needed to exceed the performance of ITO and to establish compatibility with electronic and chemical properties of other materials, the current coatings can be used for ITO replacement in ionic reactive environments.

Reference

1. Baedeker, K., Electrical conductivity and thermoelectric power of some heavy metal compounds. *Annalen der Physik* **1907,** 22, 749-766.
2. Gordon, R. G., Criteria for choosing transparent conductors. *Mrs Bulletin* **2000,** 25, (8), 52-57.
3. Chipman, A., A commodity no more. *Nature* **2007,** 449, (7159), 131-131.
4. Ko, H. C.; Stoykovich, M. P.; Song, J. Z.; Malyarchuk, V.; Choi, W. M.; Yu, C. J.; Geddes, J. B.; Xiao, J. L.; Wang, S. D.; Huang, Y. G.; Rogers, J. A., A hemispherical electronic eye camera based on compressible silicon optoelectronics. *Nature* **2008,** 454, (7205), 748-753.
5. Kim, D. H.; Ahn, J. H.; Choi, W. M.; Kim, H. S.; Kim, T. H.; Song, J. Z.; Huang, Y. G. Y.; Liu, Z. J.; Lu, C.; Rogers, J. A., Stretchable and foldable silicon integrated circuits. *Science* **2008,** 320, (5875), 507-511.
6. Cao, Q.; Kim, H. S.; Pimparkar, N.; Kulkarni, J. P.; Wang, C. J.; Shim, M.; Roy, K.; Alam, M. A.; Rogers, J. A., Medium-scale carbon nanotube thin-film integrated circuits on flexible plastic substrates. *Nature* **2008,** 454, (7203), 495-U4.
7. Service, R. F., Technology: Electronic textiles charge ahead. *Science* **2003,** 301, (5635), 909-911.
8. Coyle, S.; Wu, Y.; Lau, K. T.; De Rossi, D.; Wallace, G.; Diamond, D., Smart nanotextiles: a review of materials and applications. *MRS Bull.* **2007,** 32, (5), 434-442.
9. Wu, Z.; Chen, Z.; Du, X.; Logan, J. M.; Sippel, J.; Nikolou, M.; Kamaras, K.; Reynolds, J. R.; Tanner, D. B.; Hebard, A. F.; Rinzler, A. G., Transparent, conductive carbon nanotube films. *Science* **2004,** 305, (5688), 1273-1277.
10. Gruner, G., Carbon nanotube films for transparent and plastic electronics. *Journal of Materials Chemistry* **2006,** 16, (35), 3533-3539.
11. Fischer, J. E.; Dai, H.; Thess, A.; Lee, R.; Hanjani, N. M.; Dehaas, D. L.; Smalley, R. E., Metallic resistivity in crystalline ropes of single-wall carbon nanotubes. *Physical Review B: Condensed Matter* **1997,** 55, (8), R4921-R4924.
12. Panhuis, M. I. H., Carbon nanotubes: enhancing the polymer building blocks for intelligent materials. *Journal of Materials Chemistry* **2006,** 16, (36), 3598-3605.
13. Mann, D.; Javey, A.; Kong, J.; Wang, Q.; Dai, H. J., Ballistic transport in metallic nanotubes with reliable Pd ohmic contacts. *Nano Letters* **2003,** 3, (11), 1541-1544.
14. Lewis, B. G.; Paine, D. C., Applications and processing of transparent conducting oxides. *Mrs Bulletin* **2000,** 25, (8), 22-27.
15. Hu, L.; Hecht, D. S.; Gruener, G., Percolation in Transparent and Conducting Carbon Nanotube Networks. *Nano Letters* **2004,** 4, (12), 2513-2517.
16. Unalan, H. E.; Fanchini, G.; Kanwal, A.; Du Pasquier, A.; Chhowalla, M., Design criteria for transparent single-wall carbon nanotube thin-film transistors. *Nano Letters* **2006,** 6, (4), 677-682.

17. Shim, B. S.; Tang, Z.; Morabito, M. P.; Agarwal, A.; Hong, H.; Kotov, N. A., Integration of Conductivity, Transparency, and Mechanical Strength into Highly Homogeneous Layer-by-Layer Composites of Single-Walled Carbon Nanotubes for Optoelectronics. *Chem.Mater.* **2007,** 19, (23), 5467-5474.
18. Geng, H. Z.; Kim, K. K.; So, K. P.; Lee, Y. S.; Chang, Y.; Lee, Y. H., Effect of Acid Treatment on Carbon Nanotube-Based Flexible Transparent Conducting Films. *J.Am.Chem.Soc.* **2007,** 129, (25), 7758-7759.
19. Barnes, T. M.; de Lagemaat, J. V.; Levi, D.; Rumbles, G.; Coutts, T. J.; Weeks, C. L.; Britz, D. A.; Levitsky, I.; Peltola, J.; Glatkowski, P., Optical characterization of highly conductive single-wall carbon-nanotube transparent electrodes. *Physical Review B* **2007,** 75, (23).
20. Meitl, M. A.; Zhou, Y. X.; Gaur, A.; Jeon, S.; Usrey, M. L.; Strano, M. S.; Rogers, J. A., Solution casting and transfer printing single-walled carbon nanotube films. *Nano Letters* **2004,** 4, (9), 1643-1647.
21. Lima, M. D.; de Andrade, M. J.; Bergmann, C. P.; Roth, S., Thin, conductive, carbon nanotube networks over transparent substrates by electrophoretic deposition. *Journal of Materials Chemistry* **2008,** 18, (7), 776-779.
22. Zhang, D.; Ryu, K.; Liu, X.; Polikarpov, E.; Ly, J.; Tompson, M. E.; Zhou, C., Transparent, Conductive, and Flexible Carbon Nanotube Films and Their Application in Organic Light-Emitting Diodes. *Nano Lett.* **2006,** 6, (9), 1880-1886.
23. Kang, S. J.; Kocabas, C.; Ozel, T.; Shim, M.; Pimparkar, N.; Alam, M. A.; Rotkin, S. V.; Rogers, J. A., High-performance electronics using dense, perfectly aligned arrays of single-walled carbon nanotubes. *Nature Nanotechnology* **2007,** 2, (4), 230-236.
24. Ma, W. J.; Song, L.; Yang, R.; Zhang, T. H.; Zhao, Y. C.; Sun, L. F.; Ren, Y.; Liu, D. F.; Liu, L. F.; Shen, J.; Zhang, Z. X.; Xiang, Y. J.; Zhou, W. Y.; Xie, S. S., Directly synthesized strong, highly conducting, transparent single-walled carbon nanotube films. *Nano Letters* **2007,** 7, (8), 2307-2311.
25. Zhang, M.; Fang, S.; Zakhidov, A. A.; Lee, S. B.; Aliev, A. E.; Williams, C. D.; Atkinson, K. R.; Baughman, R. H., Strong, Transparent, Multifunctional, Carbon Nanotube Sheets. *Science* **2005,** 309, (5738), 1215-1219.
26. Baughman, R. H.; Zakhidov, A. A.; de Heer, W. A., Carbon nanotubes-the route toward applications. *Science* **2002,** 297, (5582), 787-792.
27. Calvert, P., Nanotube composites: A recipe for strength. *Nature* **1999,** 399, (6733), 210-211.
28. Zhang, X.; Sreekumar, T. V.; Liu, T.; Kumar, S., Properties and Structure of Nitric Acid Oxidized Single Wall Carbon Nanotube Films. *Journal of Physical Chemistry B* **2004,** 108, (42), 16435-16440.
29. Sreekumar, T. V.; Liu, T.; Kumar, S.; Ericson, L. M.; Hauge, R. H.; Smalley, R. E., Single-wall carbon nanotube films. *Chemistry of Materials* **2003,** 15, (1), 175-178.
30. Mamedov, A. A.; Belov, A.; Giersig, M.; Mamedova, N. N.; Kotov, N. A., Nanorainbows: Graded semiconductor films from quantum dots. *Journal of the American Chemical Society* **2001,** 123, (31), 7738-7739.
31. Ostrander, J. W.; Mamedov, A. A.; Kotov, N. A., Two modes of linear layer-by-layer growth of nanoparticle-polylectrolyte multilayers and different interactions in the

layer-by-layer deposition. *Journal of the American Chemical Society* **2001,** 123, (6), 1101-1110.
32. Reuss, R. H.; Chalamala, B. R.; Moussessian, A.; Kane, M. G.; Kumar, A.; Zhang, D. C.; Rogers, J. A.; Hatalis, M.; Temple, D.; Moddel, G.; Eliasson, B. J.; Estes, M. J.; Kunze, J.; Handy, E. S.; Harmon, E. S.; Salzman, D. B.; Woodall, J. M.; Alam, M. A.; Murthy, J. Y.; Jacobsen, S. C.; Olivier, M.; Markus, D.; Campbell, P. M.; Snow, E., Macroelectronics: Perspectives on technology and applications. *Proceedings of the Ieee* **2005,** 93, (7), 1239-1256.
33. O'Connell, M. J.; Boul, P.; Ericson, L. M.; Huffman, C.; Wang, Y.; Haroz, E.; Kuper, C.; Tour, J.; Ausman, K. D.; Smalley, R. E., Reversible water-solubilization of single-walled carbon nanotubes by polymer wrapping. *Chemical Physics Letters* **2001,** 342, (3,4), 265-271.
34. Kim, B.; Park, H.; Sigmund, W. M., Electrostatic Interactions between Shortened Multiwall Carbon Nanotubes and Polyelectrolytes. *Langmuir* **2003,** 19, (6), 2525-2527.
35. Sinani, V. A.; Gheith, M. K.; Yaroslavov, A. A.; Rakhnyanskaya, A. A.; Sun, K.; Mamedov, A. A.; Wicksted, J. P.; Kotov, N. A., Aqueous dispersions of single-wall and multiwall carbon nanotubes with designed amphiphilic polycations. *Journal of the American Chemical Society* **2005,** 127, (10), 3463-3472.
36. Vigolo, B.; Coulon, C.; Maugey, M.; Zakri, C.; Poulin, P., An Experimental Approach to the Percolation of Sticky Nanotubes. *Science* **2005,** 309, (5736), 920-923.
37. Grunlan, J. C.; Mehrabi, A. R.; Bannon, M. V.; Bahr, J. L., Water-based single-walled-nanotube-filled polymer composite with an exceptionally low percolation threshold. *Advanced Materials* **2004,** 16, (2), 150-153.
38. Fuhrer, M. S.; Nygard, J.; Shih, L.; Forero, M.; Yoon, Y. G.; Mazzoni, M. S. C.; Choi, H. J.; Ihm, J.; Louie, S. G.; Zettl, A.; McEuen, P. L., Crossed nanotube junctions. *Science* **2000,** 288, (5465), 494-497.
39. Vigolo, B.; Penicaud, A.; Coulon, C.; Sauder, C.; Pailler, R.; Journet, C.; Bernier, P.; Poulin, P., Macroscopic fibers and ribbons of oriented carbon nanotubes. *Science* **2000,** 290, (5495), 1331-1334.
40. Dalton, A. B.; Collins, S.; Munoz, E.; Razal, J. M.; Ebron, V. H.; Ferraris, J. P.; Coleman, J. N.; Kim, B. G.; Baughman, R. H., Super-tough carbon-nanotube fibres. *Nature* **2003,** 423, (6941), 703.
41. Zhang, M.; Atkinson, K. R.; Baughman, R. H., Multifunctional Carbon Nanotube Yarns by Downsizing an Ancient Technology. *Science* **2004,** 306, (5700), 1358-1361.
42. Zhang, X.; Liu, T.; Sreekumar, T. V.; Kumar, S.; Moore, V. C.; Hauge, R. H.; Smalley, R. E., Polyvinyl alcohol/SWNT composite film. *Nano Letters* **2003,** 3, (9), 1285-1288.
43. Delozier, D. M.; Watson, K. A.; Smith, J. G.; Connell, J. W., Preparation and characterization of space durable polymer nanocomposite films. *Composites Science and Technology* **2005,** 65, (5), 749-755.
44. Dresselhaus, M. S.; Dresselhaus, G.; Jorio, A., Unusual properties and structure of carbon nanotubes. *Annual Review of Materials Research* **2004,** 34, 247-278.

45. Wang, Y.; Tang, Z.; Podsiadlo, P.; Elkasabi, Y.; Lahann, J.; Kotov, N. A., Mirror-like Photoconductive LBL Thin Films of Te Nanorods: The Fusion of Semiconductor, Metal and Insulator Properties. *Advanced Materials* **2006,** 18, (4), 518-522.
46. Shim, B. S.; Starkovich, J.; Kotov, N., Multilayer composites from vapor-grown carbon nano-fibers. *Composites Science and Technology* **2006,** 66, (9), 1174-1181.
47. Lewis, R. J., Sr., *Hawley's Condensed Chemical Dictionary*. John Wiley & Sons: 2002.
48. Arnold, M. S.; Stupp, S. I.; Hersam, M. C., Enrichment of single-walled carbon nanotubes by diameter in density gradients. *Nano Letters* **2005,** 5, (4), 713-718.
49. Shaffer, M. S. P.; Windle, A. H., Fabrication and characterization of carbon nanotube/poly(vinyl alcohol) composites. *Advanced Materials* **1999,** 11, (11), 937-941.
50. Yang, Y.; Gupta, M. C.; Dudley, K. L.; Lawrence, R. W., The fabrication and electrical properties of carbon nanofibre-polystyrene composites. *Nanotechnology* **2004,** 15, (11), 1545-1548.
51. Lee, J.; Shanbhag, S.; Kotov, N. A., Inverted colloidal crystals as three-dimensional microenvironments for cellular co-cultures. *Journal of Materials Chemistry* **2006,** 16, (35), 3558-3564.
52. Zhou, Y.; Hu, L.; Gruner, G., A method of printing carbon nanotube thin films. *Applied Physics Letters* **2006,** 88, (12), 123109/1-123109/3.
53. Yamagata, Y.; Shiratori, S., Evaluation of electrical characteristics of the layer-by-layer self-assembled films after the various annealing temperatures. *Thin Solid Films* **2003,** 438-439, 238-242.
54. Bachilo, S. M.; Strano, M. S.; Kittrell, C.; Hauge, R. H.; Smalley, R. E.; Weisman, R. B., Structure-Assigned Optical Spectra of Single-Walled Carbon Nanotubes. *Science* **2002,** 298, (5602), 2361-2366.
55. Ramesh, S.; Ericson, L. M.; Davis, V. A.; Saini, R. K.; Kittrell, C.; Pasquali, M.; Billups, W. E.; Adams, W. W.; Hauge, R. H.; Smalley, R. E., Dissolution of Pristine Single Walled Carbon Nanotubes in Superacids by Direct Protonation. *Journal of Physical Chemistry B* **2004,** 108, (26), 8794-8798.
56. Jacquemin, R.; Kazaoui, S.; Yu, D.; Hassanien, A.; Minami, N.; Kataura, H.; Achiba, Y., Doping mechanism in single-wall carbon nanotubes studied by optical absorption. *Synthetic Metals* **2000,** 115, (1-3), 283-287.
57. O'Connell, M. J.; Bachilo, S. M.; Huffman, C. B.; Moore, V. C.; Strano, M. S.; Haroz, E. H.; Rialon, K. L.; Boul, P. J.; Noon, W. H.; Kittrell, C.; Ma, J.; Hauge, R. H.; Weisman, R. B.; Smalley, R. E., Band gap fluorescence from individual single-walled carbon nanotubes. *Science* **2002,** 297, (5581), 593-596.
58. Reich, S.; Thomsen, C.; Ordejon, P., Electronic band structure of isolated and bundled carbon nanotubes. *Physical Review B: Condensed Matter and Materials Physics* **2002,** 65, (15), 155411/1-155411/11.
59. Avouris, P., Molecular Electronics with Carbon Nanotubes. *Accounts of Chemical Research* **2002,** 35, (12), 1026-1034.
60. Bae, D. J.; Kim, K. S.; Park, Y. S.; Suh, E. K.; An, K. H.; Moon, J. M.; Lim, S. C.; Park, S. H.; Jeong, Y. H.; Lee, Y. H., Transport phenomena in an anisotropically aligned

single-wall carbon nanotube film. *Physical Review B: Condensed Matter and Materials Physics* **2001,** 64, (23), 233401/1-233401/4.
61. Yim, J. H.; Kim, Y. S.; Koh, K. H.; Lee, S., Fabrication of transparent single wall carbon nanotube films with low sheet resistance. *Journal of Vacuum Science & Technology B* **2008,** 26, (2), 851-855.
62. Parekh, B. B.; Fanchini, G.; Eda, G.; Chhowalla, M., Improved conductivity of transparent single-wall carbon nanotube thin films via stable postdeposition functionalization. *Applied Physics Letters* **2007,** 90, (12).
63. Dettlaff-Weglikowska, U.; Skakalova, V.; Graupner, R.; Jhang, S. H.; Kim, B. H.; Lee, H. J.; Ley, L.; Park, Y. W.; Berber, S.; Tomanek, D.; Roth, S., Effect of SOCl2 treatment on electrical and mechanical properties of single-wall carbon nanotube networks. *Journal of the American Chemical Society* **2005,** 127, (14), 5125-5131.
64. Fischer, J. E., Chemical doping of single-wall carbon nanotubes. *Accounts of Chemical Research* **2002,** 35, (12), 1079-1086.
65. Zhou, W.; Vavro, J.; Nemes, N. M.; Fischer, J. E.; Borondics, F.; Kamaras, K.; Tanner, D. B., Charge transfer and Fermi level shift in p-doped single-walled carbon nanotubes. *Physical Review B* **2005,** 71, (20).
66. Graupner, R.; Abraham, J.; Vencelova, A.; Seyller, T.; Hennrich, F.; Kappes, M. M.; Hirsch, A.; Ley, L., Doping of single-walled carbon nanotube bundles by Bronsted acids. *Physical Chemistry Chemical Physics* **2003,** 5, (24), 5472-5476.
67. Jackson, R.; Domercq, B.; Jain, R.; Kippelen, B.; Graham, S., Stability of doped transparent carbon nanotube electrodes. *Advanced Functional Materials* **2008,** 18, (17), 2548-2554.
68. Saran, N.; Parikh, K.; Suh, D. S.; Munoz, E.; Kolla, H.; Manohar, S. K., Fabrication and characterization of thin films of single-walled carbon nanotube bundles on flexible plastic substrates. *Journal of the American Chemical Society* **2004,** 126, (14), 4462-4463.

Chapter IV

Advanced LBL Assemblies

A. SWNT Combing during LBL Assembly: from Random Adsorption to Aligned Composites

1. Summary

Oriented SWNTs in polymer composites have shown improvements in the physical properties of a composite due to the anisotropic shape and properties of SWNTs. Beside fundamental importance, controlled alignment of SWNTs during composite fabrication implies better material function performance in a variety applications including biomedical field. This chapter presents a new fabrication technique, where aligned SWNTs and robust SWNT-polymer composites can be made using a fusion method of SWNT combing and LBL assembly. As mentioned, LBL assembly demonstrated exceptional processing ability in constructing the uniform distribution of a SWNT-polymer composite. Combined with this uniformity, this SWNT combing technique endows controlled alignment of single stranded SWNTs in a SWNT-polymer composite system. SWNT combing employs air-water interfacial forces to change the molecular topography from random adsorption state to stretched alignment of SWNTs. More specifically, air-water interfacial forces are associated with an excess viscous drag

force and an intrinsic dewetting rate along SWNTs. Moreover, the alignment efficiency of SWNTs is high enough to construct a multilayered LBL film with horizontal-linear weaving structures. This simple method also can be applied for aligning other nanowire materials because it utilizes simple geometric features of SWNTs.

2. Introduction

Controlled alignment of anisotropic nanoscale building blocks such as nanotubes, nanorods, and nanowires is considered a critical factor for fabricating functional nanocomposites which have anisotropic physical properties with exceptionally high nanomaterial content.[1-3] For example, exceptional physical and chemical properties of SWNTs are closely related to their highly anisotropic geometrical structures; hollow tubular structures with a diameter of few nanometers and a length of a few micrometers.[4] Hence, the alignment of SWNT has been attempted utilizing various means of SWNT orientation such as gas flow,[5] liquid flow,[2, 6-8] magnetic,[9-11] and gas-liquid interfacial[7, 8, 12] fields. While substantial success had been achieved on obtaining coatings of independent SWNT with parallel orientation, the method of making bulk SWNT composites, still needs to be elaborated.[13, 14] Additionally, the magnetic field techniques applied to non-modified SWNTs can hardly be utilized in a common setting due to the high field strengths required.[9, 15] LBL assembly[16] has demonstrated exceptional uniformity and versatility for constructing a nanostructure composite with various nano-building blocks.[17, 18] In scientific context of organized SWNT composites, we introduce a new fusion method for aligning SWNTs during LBL assembly by air-water interfacial force, which can be termed as “SWNT combing”.[19] Pressurized air flow over a wet surface with

randomly adsorbed SWNTs, combs and stretches SWNTs so that the surface topography changes from random to a unidirectional orientation. A similar technique has been used for DNA stretching.[19-21] This simple method is not only efficient for aligning SWNTs but also robust enough to stack the multilayer through adoption of a high temperature annealing step for fixing aligned structures. Thus, multilayered LBL film combined with SWNT combing demonstrated a high density of SWNT loading with horizontal-linear alignment of single-stranded SWNTs. The oriented structure of a SWNT nanocomposite film will improve the functional performance of nanotube materials[22] in applications to biological tissue engineering, solar cell, artificial muscle, sensor, and a wide range of electronics. Furthermore, the methodological principle of a SWNT combing can be applied to other materials such as nanowires or nanorods because the alignment driving forces are associated with the geometrical anisotropic feature and the interfacial bonding between the nano-blocks and the substrate, instead of their intrinsic physical properties.[1]

3. Experimental Procedure

Materials: Poly(vinyl alcohol) (PVA, MW: 70,000 ~ 100,000) and Poly(sodium 4-styrene-sulfonate), (PSS, MW: 1,000,000) were purchased from Sigma-Aldrich Co. The purified HiPco single-wall carbon nanotubes (SWNTs) used for the experiment were purchased from Carbon Nanotechnologies Incorporated (CNI).

LBL assembly: Purified HiPco SWNTs were dispersed in 1 wt-% PSS solution with a 2 hr mild sonication in a VWR Model 150HT ultrasonic cleaner.[23] The dispersion

was centrifuged at 5000 rpm and then the supernatant was collected. 1 wt-% of PVA solution was prepared for another LBL partner. By charge transfer or hydrogen bonding interactions, PVA formed LBL assemblies with SWNTs or PSS which is wrapping SWNTs. Each LBL layering process consists of 10 min dipping in the PVA or the SWNT solution, water rinsing, and drying. For denoting LBL assemblies, $[PVA/SWNT]_n$ was used in which *n* represents the number of repeated dipping processes in PVA and SWNT solutions. SWNT combing is performed by 15 psig of an air flow during this interim drying step following a water rinsing step. For a multilayered film with aligned SWNTs, a high temperature annealing step, 150 ^{o}C for 10 min, is followed in order to fix the aligned structures.

Instrumental analysis: Scanning electron microscopy (SEM) images were taken with a Philips XL30 Field Emission Gun Scanning Electron Microscope and a FEI Nova Nanolab Dualbeam FIB and Scanning Electron Microscope. Atomic force microscopy (AFM) imaging was performed with Nanoscope III (Digital Instruments/Veeco Metrology Group). UV-vis absorption measurements were taken using an Agilent 8453E UV-visible spectroscopy and Newport PR-950 Broadband polarization rotator.

4. SWNT Combing during LBL Assembly

Although SWNT LBL composites have exceptional uniformity with virtually perfect single-stranded dispersion of SWNTs, it is perceived that the alignment of SWNTs in controlled directions while preserving a single-stranded dispersion quality of

SWNTs is difficult.[6, 11] In this respect, we want to point out that some degree of organization of SWNT, i.e. restriction on their special orientation, is introduced by LBL simply for the nature of the adsorption process.[24] SWNTs have inherently preferential in-plane orientation in LBL composites because nanotubes approaching the substrate surface in a perpendicular direction have obvious difficulty with adhering to the polymer layer. The orientation effects can be observed particularly well for flat nanocolloids, such as clay sheets.[25] In this work, purified HiPCO SWNTs, which has been purchased from Carbon Nanotechnologies, Inc., were dispersed in a poly(4-styrene sulfonate) (PSS) solution. Dispersed SWNTs wrapped by PSS become one LBL assembly component and poly(vinyl alcohol) becomes its LBL partner enabling sequential adsorption. On a charged substrate, these two components are assembled with dipping processes in each component followed by an interim rinsing step which removes excess non-adsorbed components from the surface and a drying step which stabilizes the newly formed molecular layer. The orientation of SWNT, i.e. nanotube combing, is carried out during these interim drying steps which follow the rinsing of excess SWNTs on the PVA surface. Pressurized air blowing at 1.5 psig makes the randomly oriented SWNTs stretched by air-water interfacial forces (for experimental schematics, see Figure 23).

5. Characterization of SWNT Alignments

The images in Figure 24 (B)-(D) show that most SWNTs on the PVA surface are not just aligned in one direction but also stretched. The feature of this SWNT combing method is the alignment of single-stranded SWNTs whose diameter is around 1.0 ~ 1.4 nm. (Figure 25) Although the successful alignments of bundled SWNTs were reported

previously,[2, 7, 9] single stranded SWNT alignment with high density was rarely reported. In addition, the alignment efficiency is quite high with more than 80 % of SWNTs aligned. (Figure 24 (B)) The characteristics of the alignment process here are similar to that of DNA combing.[19, 21] The difference, however, is that the SWNTs are combed by the strong viscous drag forces of a fast moving air-water interfacial meniscus generated by pressurized air flow after SWNTs are randomly attached to the surface, while DNA is stretched by slow air-water interface movement from hauling of a substrate.[8, 20]

(A)

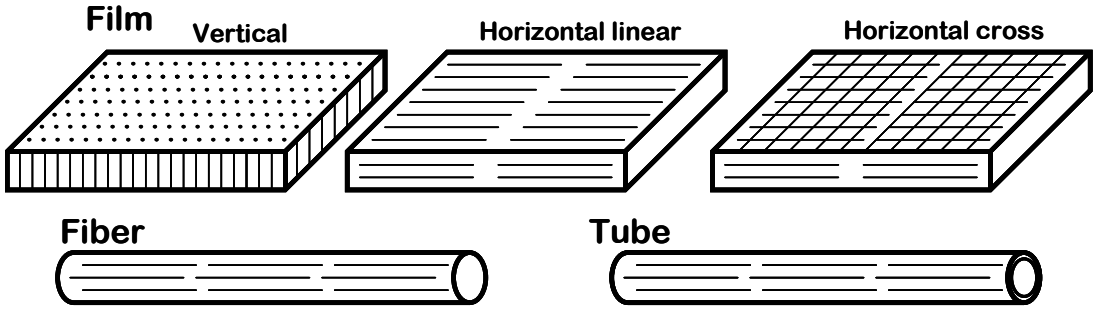

(B)

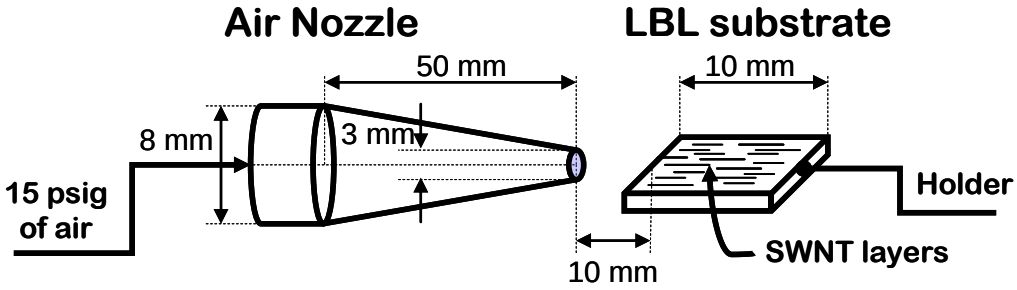

(C)

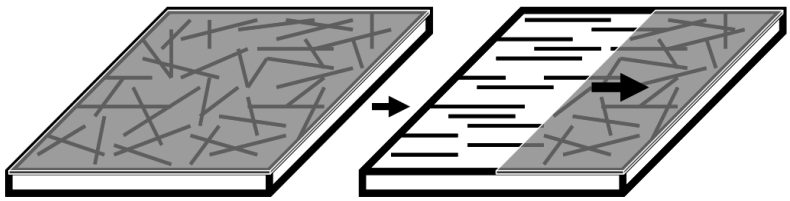

Figure 23 (A) Types of aligned SWNT composites include vertical, horizontal-linear and horizontal-cross oriented SWNT films as well as fibers and tubes. (B) Simplified experimental setup for SWNT combing, which produces a horizontal-linear alignment of SWNTs in a LBL film. Pressurized air flow with 15 psig is applied to a LBL substrate which has SWNT layers with a 10 mm gap. (C) Schematic expression of SWNT combing by air-water interfacial forces.

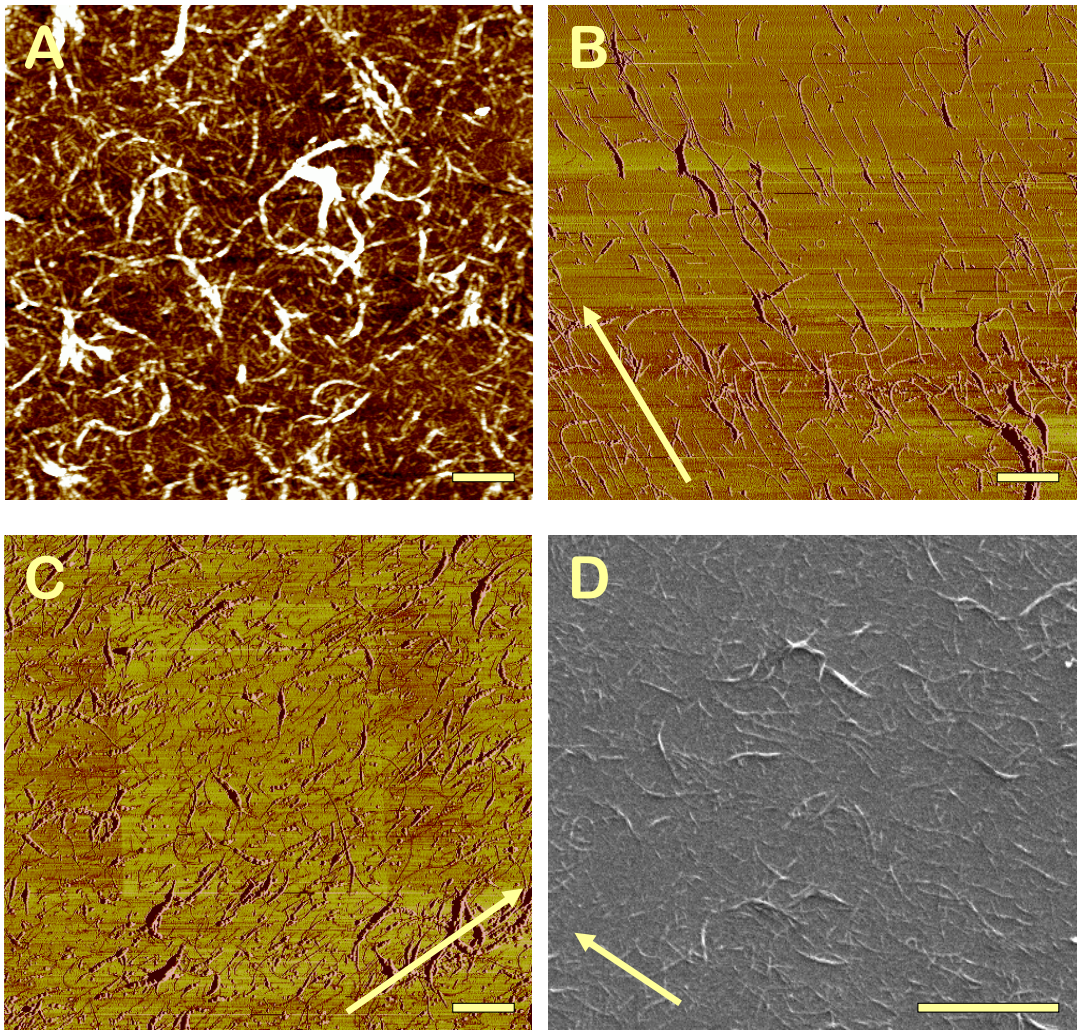

Figure 24 (A) The AFM height image of a randomly adsorbed SWNT LBL assembly, 3 layers, demonstrates the high density loading of SWNTs with single stranded dispersions. (B) The AFM phase image of aligned SWNTs by SWNT combing which changes the topography of 1 layer of $[PVA/SWNT+PSS]_1$ LBL assembly from random adsorption to stretched alignment. (C) The AFM phase image of aligned SWNT in a multiple layered LBL assembly, $[PVA/SWNT+PSS]_2$. (D) The SEM image of aligned SWNT in a multiple layered LBL assembly, $[PVA/SWNT+PSS]_3$. The bar in the images represents 1 micro-meter each.

SWNT combing method also bears similarities to the previously tested flow induced alignments of SWNTs when they start adhering to the surface.[1, 6-8] The method

described here is better suitable for the preparation of aligned flat composites mainly due to the presence of the polymer and larger amounts of SWNTs involved as well as excellent efficiency. SWNT combing after random deposition of SWNTs can achieve both the high density of SWNTs and high degree of orientation because these two processes, deposition and orientation, were performed into two distinct steps. In fluid dynamic approaches, a liquid flow driven alignment of SWNTs is less efficient[6] because the velocity in wall areas becomes zero even with high bulk flow velocity, given the height of SWNTs, 1nm, lower than the height of two water molecules. However, the surface velocity of a receding meniscus in this SWNT combing was much higher than a few cm/s although the exact measurement might need a special study.

To confirm that air-water interfacial forces is the key element in SWNT combing, we compared degree of nanotube orientation in films obtained with various LBL procedures, for instance, stagnant rinsing and drying as well as water flow rinsing. When a substrate was dipped in a stagnant SWNT dispersion, only flow of pressurized air gave aligned SWNTs; no other condition resulted in an effective orientation of SWNTs (Figure 24 (A)). Moreover, Figure 24 (C), (D) demonstrates that post LBL SWNT combing made the multilayer stacking possible because the subsequent polymer layer protected the aligned SWNTs. Immobilization of SWNT in the multilayers was previously hypothesized when discussing the reasons for significantly improved mechanical properties of SWNT LBL composites.[26] Thermal annealing (150 ^{o}C, 10 min) after each SWNT combing was adopted for increasing the alignment efficiency for obtaining aligned multilayer composites. At elevated temperature, carboxyl groups (-COOH) on

SWNTs and hydroxyl groups (-OH) on PVA can easily form ester bonds.[27] Even though the purified SWNTs were wrapped with the PSS, the ends of the SWNTs generally remain open due to higher possibility of existing carboxyl groups, which are connected to hydroxyl groups in PVA by crosslinking. Furthermore, heat treatment of an LBL film can closely pack the components, which resulted in confinement of SWNTs in their aligned states. Therefore, three layers of linearly weaved SWNTs, $[PVA/(SWNT+PSS)]_3$ preserved an almost perfect alignment of SWNTs as well as two bi-layers. (Figure 24 C, D)

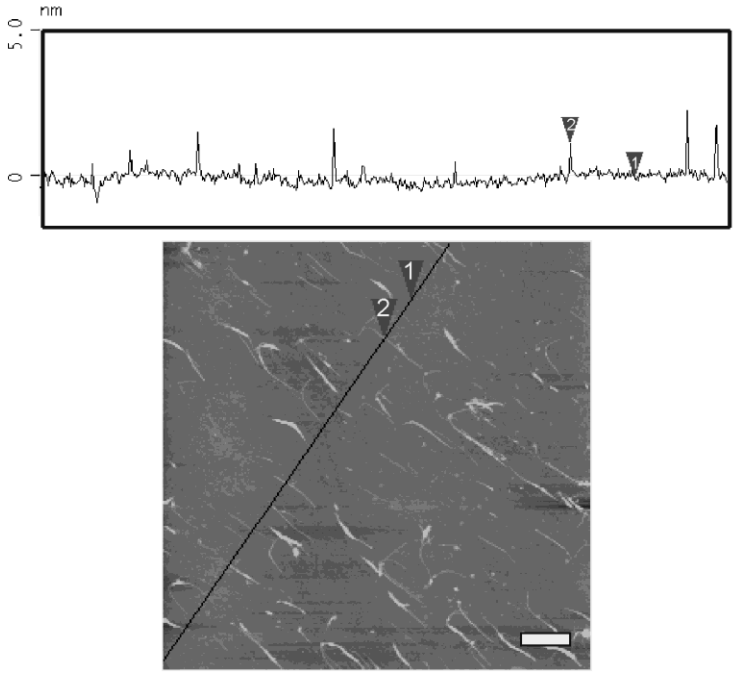

Figure 25 Height sectional analysis of aligned SWNTs. Around 1 nm of height indicates that the aligned SWNTs are well dispersed as a single stranded SWNT. The bar in the image represents 1 micro-meter.

Alignment of SWNTs is considered to be a general macro-scale process, as opposed to micro/nano-scale localized effect. This point can be supported by polarized light absorption spectroscopy measurement.[28] If the incident polarized light is parallel to the alignment direction of SWNTs, then absorbance decreases but characterized light absorption peaks of SWNTs emerge clearly. (Figure 26) These characterized peaks come from the van Hove singularities, which are the electronic transitions from the valence to conduction bands in both metallic and semiconducting SWNTs.[29]

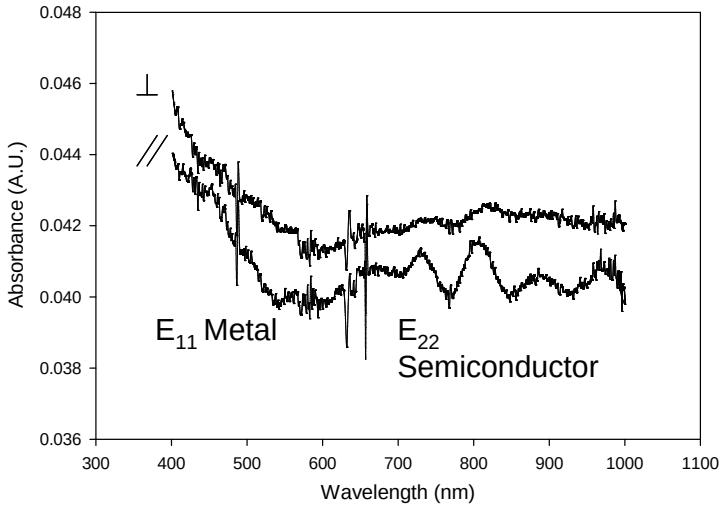

Figure 26 Polarized absorption spectra of an aligned SWNT LBL film with perpendicular and parallel to the incident polarized light.

6. Alignment Mechanism of SWNT Combing

The theory of molecular combing developed for DNA[19, 21] can be extended to the SWNT alignment presented here. The interacting alignment forces between the rod-like polymer chain, DNA, and the surface, in which the receding speed of a meniscus is slow,

300 micro-meter/s, are estimated mainly as the surface tension force.[19] However, in this SWNT combing case, the velocity of a receding meniscus should be considered by association with the hydrodynamic drag force and the rate of intrinsic dewetting along the SWNTs because the surface velocity is much higher than that of DNA combing. The hydrodynamic drag forces can be calculated by assuming a SWNT as a circular cylinder. The drag force per unit length on a cylinder of radius R is expressed by $F_D = 4\pi\mu U\varepsilon[1-0.87\varepsilon^2 + O(\varepsilon^3)]$, $\varepsilon = \left[\ln\left(\frac{4}{\mathrm{Re}}\right) + \frac{1}{2} - \omega\right]^{-1}$, where $\mathrm{Re} \equiv UR/\nu$, $\nu = \frac{\mu}{\rho}$ (kinematic viscosity), μ (viscosity), U(characteristic velocity) and $\omega(= 0.5772...)$ is the Euler's constant.[30] The intrinsic dewetting (not driven by external forces) velocity V which is related to the capillary and viscous dissipation forces is theoretically given by $V_{slip} = \frac{1}{6}\frac{\gamma}{\mu}\theta^2\frac{b}{w}$ (slipping film) or $V_{no-slip} = \frac{1}{6}\frac{\gamma}{\mu}\theta^2\frac{\theta}{L}$ (nonslipping film) with γ (surface tension), θ (contact angle), b(slippage length), w(width of the rim), and L(constant of order 10).[31] Based on these theoretical principles, the sheer force of SWNT combing effects is estimated to be the excess drag forces, which are caused by the differences between the surface velocity of the receding meniscus and the intrinsic dewetting velocity along SWNTs. Furthermore, in order to avoid detaching the SWNTs from the surface, this excess hydrodynamic force should be less than the difference in adsorption forces of SWNTs between the wet and the dry states, From this analysis, the processing variables that increase the efficiency of SWNT alignment include the viscosity of a rinsing liquid, the surface tension of the liquid, the interaction between SWNTs and the surface, and the meniscus receding velocity which can be controlled by the air blowing pressure.

7. Conclusion

In this study, a new technique for alignment of SWNT-polymer composites based on LBL assemblies and SWNT combing taking advantage of the air-water interfacial meniscus during a drying step in the LBL process was introduced. This technique is fast and efficient; it also produces SWNT-polymer nanocomposites with a single-strand quality and high density of SWNT stacking in a LBL composite. Analysis of SWNT alignment features on the basis of DNA stretching theory suggests that the excess drag force of a receding air-water meniscus and the surface velocity of an intrinsic dewetting are essential for SWNT alignment.

The controlled orientation of SWNTs in polymer composites implies the dramatic performance improvements for anisotropic SWNT-polymer composites in wide ranges of applications. For example, the oriented SWNT-polymer composite for artificial muscle or actuator application will possess improved directional electrical and mechanical properties. The biocompatibility of LBL SWNT composites[32] and other SWNT composites[33, 34] for tissue engineering applications will accommodate mammalian cells which will grow along the direction of the SWNT orientation due to directed electrical potential during culturing. Directed anisotropic response of oriented SWNTs will open new possibilities for actuation and other biomedical and electronic applications of SWNT-polymer composites.

Several recent studies of anisotropic properties driven by orientation of SWNTs in polymer nanocomposites displayed very substantial physical effects in mechanical, electrical and thermal properties.[22, 35, 36] Besides that, this area remains still mostly

unexplored due to the lack of robust fabrication techniques for aligned SWNT-polymer nanocomposites. LBL films can serve as a convenient model for such composites due to the ability of preparation of films with any thickness and immobilization of previously deposited SWNT multilayers. The investigation of deformation effects depending on the degree and the direction of SWNT alignment can answer many questions related to the dependence of mechanics of failure on composite organization.

B. Dewetting LBL Assembly

1. Summary

LBL assembly is one of the most ubiquitous coating techniques today. It also offers a pathway for multifunctional/multicomponent materials with molecular-scale control of stratified structures. However, technological applications of LBL are impeded by laborious and fluid-demanding nature of the process. It is also important to have control of lateral organization of the films. Using the deposition of SWNTs and other nanoscale colloids, we introduce a new approach to LBL based on dewetting phenomena, d-LBL. Its strengths include: (1) elimination of rinsing steps, (2) significant acceleration of the process, (3) improvement of lateral organization of the films represented by alignment of fibrous nanocolloids and creation of fractal networks and (4) ability to produce nanostructured coatings from colloids when classical LBL fails. The generality of d-LBL can compete with traditional LBL and was demonstrated for cellulose nanowires, polyelectrolyte pairs, and semiconductor nanoparticles, metal oxides, and Au nanorods.

2. Introduction

LBL assembly is a simple and versatile method for materials design with nanometer scale control over internal architecture. The technique has been already applied to a large variety of polymers and nanomaterials, such as polyelectrolytes, proteins, viruses, cells, nanoparticles, nanowires, nanotubes, etc, resulting in a palette of

remarkable materials with stratified organization.[16, 18, 24, 37, 38] Analyzing the potential directions for further development of LBL and materials made by it, we can point to three fundamental issues, which represent the bottlenecks of this technology.

(1) Adsorption of some LBL multilayers can be time consuming. Researchers have been actively looking for methods to accelerate the LBL process and techniques such as spraying,[39, 40] spin-assisted LBL,[41-44] "electrically-driven" LBL,[45] roll-to-roll process,[46] and "exponential" growth[47] had been invented/discovered. However, acceleration of the buildup often comes at a price: some loss of structural control or universality.

(2) In a typical LBL construct, each component must be adsorbed independently as a separate layer, followed by a rinsing step during which excess of the component is removed. Rinsing plays the key role in LBL assemblies because it results in precise nanoscale thickness control. However, the rinsing steps generate large amounts of waste, which is a deterrent for both practical applications especially as a technique for nanomaterials production.

(3) Besides the control of materials organization in the direction perpendicular to the substrate, it is also important to provide means of structural control laterally to the substrate. This is particularly essential for LBL materials with "made-to-order" electrical, mechanical and thermal transport properties which require organization of components in a scale of few nanometers.[48, 49 50]

In this study we want to suggest a potential resolution of these problems and a new approach to the LBL deposition.

Here, we show that the LBL cycle can be drastically accelerated by eliminating the rinsing operations. Importantly, it can be done without sacrificing other attractive features of LBL multilayers, such as simplicity, universality and stratification of the coatings. The LBL approach (d-LBL) described here takes advantage of dewetting effect, [51, 52] which occurs at solid-liquid interfaces for which the contact angle is high. This was achieved by adding small amount of dimethylformamide (DMF) to both polyelectrolyte and SWNT dipping solutions. d-LBL shortens time for the preparation of micron-scale films by ~30 times. It also produces quite unusual fishnet lateral morphology of the SWNT multilayers with fractal features, which resulted in improvement of the mechanical properties. Additionally, unique combination of d-LBL forces acting at the triple air-solid-liquid interface enables efficient alignment of the adsorbed axial species. Furthermore, d-LBL enables successful deposition of the coatings from branched SnO_2 nanowires, which failed with conventional LBL. Due to 3D nature of these wires it opens interesting possibilities for materials design. We also demonstrate that d-LBL is quite general and can be applied to other LBL materials, such as Au nanorods (NRs), cellulose nanowires, polylectrolytes and semiconducting CdTe nanoparticles (NPs). In case of Au NRs, markedly different optical properties of d-LBL and regular LBL were obtained. So, overall, the d-LBL deposition can be an essential tool that can be useful to both accelerate and organize the multilayers for a wide array of nanoscale systems with optional lateral dewetting pattern capability.[53, 54]

3. Experimental Procedure

Preparation of LBL solutions: The stable dispersion of SWNTs (Carbon Nanotechnologies Inc.) with PSS (Sigma-Aldrich, MW 1,000,000) was prepared in an ultrasonic bath (Cole-Parmer, Power 700W) for 4 hours. In a dispersion solution, PSS was varied from 0.5 %, 1 %, 2 % and SWNT concentration was adjusted to ~ 0.05 % (= 0.5 mg/ml). PVA (Sigma-Aldrich, MW 70,000), PDDA (Sigma-Aldrich, MW 400,000), PEI (Sigma-Aldrich, MW 25,000) and PSS solutions were prepared with 0.5 %, 1 %, 2 %. Preparation of CdTe semiconducting nanoparticles followed our previous article.[55, 56] The SnO_2 nanowires were provided by Prof. Wei Lu.

Film Characterization: The contact angle measurements performed on a polymer coated surface which was prepared by LBL assembly technique. We dropped 20 μl PVA and PSS solutions to measure advancing and sucked back a few μl again to observe dewetting contact angles on a PVA and PSS surface respectively. We repeated those measurements by varying contents of DMF in solutions.

The d-LBL samples for imaging were prepared on both Si substrates and glass slides depending on the measurement requirements. For d-LBL (polymer dewet), a glass slide was dipped in the polymer solution for 10 seconds and cleansed as dewetting modes. The last drops on the edges were removed by approaching Kimwipes®. Normally, dewetting mode cleansing took less than 30 seconds although these varied by contents of DMF, temperature and so on. All the conventional LBL or [polymer rinse] samples were done with 10 minutes dipping followed by rinsing in clean water for 1 min.

UV-vis spectroscopy (Agilent 8453) was performed by the sample prepared on a glass slide. SEM (FEI, Nova Nanolab Dualbeam FIB and Scanning Electron Microscope) and AFM (Digital Instruments, Nanoscope 3a) were observed the sample prepared on a Si substrate. The ellipsometry (J.A. Woollam M-44) measurements were collected 3 times with varying measurement directions of the samples on a Si substrate and then averaged. To determine the thickness increment trend is linear, not exponential in the Figure 29 a, the R-squared values were calculated to be 0.9819 for linear and 0.9036 for exponential regressions.

Adsorption morphology pattering experiments were performed in differing the position of a substrate during dewetting movements or blowing mild air. In dewetting force dominating pattern experiments, the substrate was held in horizontal plane (Figure 31 A, B). Aligning of SWNTs were performed by holding the substrate vertical position to use gravity forces to speed up dewetting movements (Figure 31 C, D) and cellulose NW alignments were done using mild air blow to guide dewetting lines (Figure 31 F).

Mechanical stretching results of the 300 layered d-LBL film were obtained by 3 times of testing (100Q model, TestResources Inc.) after the film was peeled off from the glass substrate by dipping in 1 % HF solution.

For the demonstration of generalized d-LBL assemblies, i.e., [PDDA dewet / PSS dewet] and [PEI dewet / CdTe dewet], polymer solutions were used as 0.5 wt% and 10 % DMF were added. d-LBL procedures are following; 10 sec dipping and less than 30 sec of self-cleansing by dewetting in each component adsorption. [SnO_2 nano-object dewet /

PDDA / PSS] were done by 10 sec dipping followed by dewetting in the 50% DMF SnO_2 dispersion.

4. Principles of Dewetting LBL Assembly

Typical LBL assemblies consist of series of 4 basic steps; (1) immersion of the substrate into solution of a polymer or other high molecular weight material (2) rinsing to remove excess of the first component on a substrate, (3) immersion into a solution of a different high molecular weight material, and (4) rinsing to remove excess of the second LBL component. Adsorption step of each component can take anywhere between few seconds to an hour, while rinsing steps can take between few seconds to ten minutes. These basic steps are then repeated as many times as necessary to reach a desired thickness of the film. Now let's consider the case when the LBL solutions are dewetted from the substrate surface. They are not supposed to leave appreciable amount of the solution on the surface, because this is not thermodynamically and kinetically favorable for the fluid. If the cases of extreme wetability and hydrophobicity are avoided,[57-59] rinsing steps can be completely avoided and the LBL deposition in a cycle may be reduced to only 2 steps. The question now is "*Is it possible?*" If yes, can one achieve the deposition of the multilayers in the cyclic manner similar to what we typically have in case of LBL? Are the properties of the produced material comparable to those made by conventional LBL?"

Adsorption step of SWNTs in our experience tend to require substantially longer time than that for a polymer. One can speculate that this is because of the lower charge density and/or greater rigidity of the carbon nanotube, which in turn, result in the sluggishness of molecular and nanoscale re-arrangements necessary for the successful adsorption[56]. In order to realize dewetting conditions, we added DMF to solutions of both SWNT-PSS and PVA. Advancing (wetting) contact angles and receding (dewetting) contact angles were measured for different DMF concentrations in PVA and PSS solutions (Figure 27). As DMF is added, wetting states of solutions over a surface dramatically change from stable to unstable which yields a substantial increase of receding contact angles. (Figure 27) The latter are particularly important for d-LBL from the perspective of removal of the excess of the solution, brought about by pinning of the droplets with low contact angles. Note the broad maximum in receding angle indicating existence of optimal DMF contents. Advancing contact angle is convenient for evaluation of attractive forces between the polymers in a solution and on the surface. It decreases as the attraction becomes stronger. So, the advancing contact angles between different polymers in solution and on substrate, i.e. pairs such as PVA(solution)+PSS(solid) or vice versa, are quite small regardless of DMF contents (Figure 27 E, F), which is beneficial for LBL adsorption. Simultaneously, advancing angles between same polymers, i.e. pairs such as PVA(solution)+PVA(solid) and PSS(solution)+PSS(solid), are very high (Figure 27 C, D). Altogether, it is consistent with the picture of intermolecular forces necessary for layer alternation in d-LBL and demonstrates that the balanced increase of surface tension may be achieved in this system.

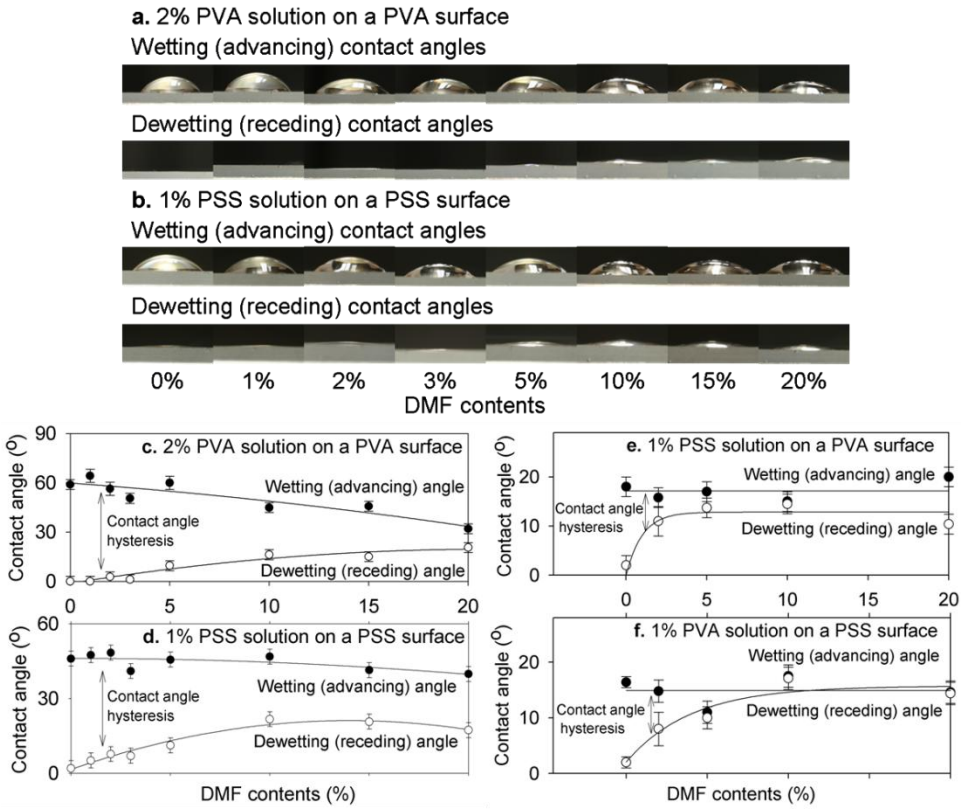

Figure 27 Contacts angle measurements. (A) The advancing and receding droplets and (C) their contact angle of 2% PVA solution on a PVA coated surface. (B) The advancing and receding droplets and (D) their contact angle of 1% PSS solution on a PSS coated surface. Contact angle measurements of (E) 1% PSS solution on a PVA coated surface, and (F) 1% PVA solution on a PSS surface. There were dramatic changes in contact angle hysteresis or wetting angles between (C, D) and (E, F). Instant droplet spreading occurs in (E, F) because there are effective attracting forces between two different LBL polymers, the driving forces for LBL assemblies. However, dewetting (receding) angles in all cases were not different much because those attraction forces of advancing droplets in (E, F) no longer exist or significantly weaken by already formed LBL polymer adsorption so that the interactions involved in all receding droplets are the same kind polymer interactions as in (C, D).

5. Self-Cleansing Effect of Dewetting LBL Assembly

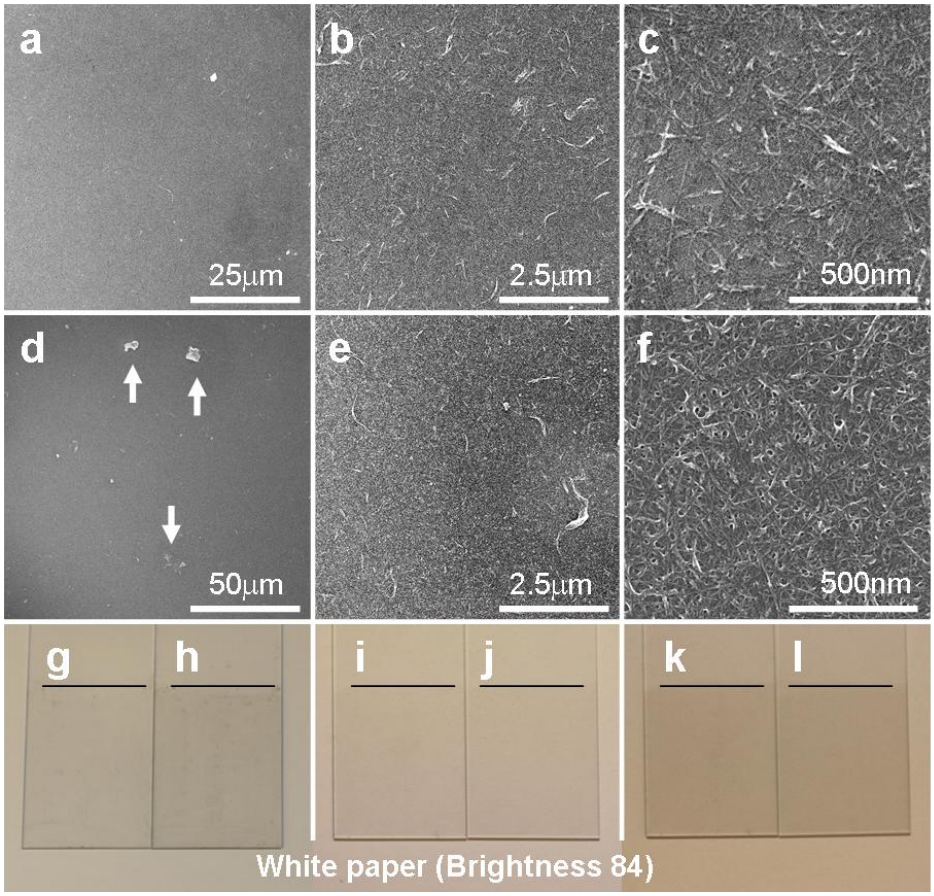

Figure 28 Comparative evaluation of basic properties of films made by dewetting and classical LBL. SEM images with different magnification of (A-C) conventional LBL ([PVA (10min) rinse / SWNT (10min) rinse]$_5$, (D-F) d-LBL ([PVA (10sec) dewet / SWNT (10sec) dewet]$_5$. The arrows in (D) indicate typical islands caused by dewetting instability. (G, H) Optical appearances of d–LBL coated films, ([PVA (10sec) dewet/SWNT (10sec) dewet]$_n$. (G) n = 2 and (H) n = 3. (I) [PVA (10sec) dewet+rinse/SWNT (10sec) dewet]$_2$, (J) [PVA (10min) rinse / SWNT (10min) rinse]$_2$, (K) [PVA (10sec) dewet+rinse/SWNT (10sec) dewet]$_3$, (L) [PVA (10min) rinse / SWNT (10min) rinse]$_3$. For all the images, the very top layer was SWNTs.

Now, let's demonstrate that dewetting (a) results in self-cleansing on the top-most LBL surface (Figure 28) and (b) does not prevent LBL growth. SWNTs are quite

convenient for characterizing the efficiency of self-cleansing by dewetting because they provide distinct micro-/nano-scale topological features. So, the cyclic d-LBL procedure was performed as described in the Experimental alternating deposition and dewetting of a substrate with solutions of PVA and SWNT-PSS both in 10% DMF/water mixture. The total adsorption time of SWNTs was reduced from 10 min to 10 sec. The surface morphology of d-LBL films as observed by SEM (Figure 28) is very similar to that of conventional LBL. There are no big aggregates of the coagulated components that should have formed when considerable quantities of solutions were left on the substrate. Note, however, that there are microscopic islands generated by receding liquid[31, 60] (Figure 28 D, SEM, marked by arrows). They are quite rare and fairly small; their overall effect on the film structure is limited mainly to adsorption curves (see below). No streaks or other large scale non-uniformities produced by moving meniscus were observed (Figure 28 G-L).

6. Efficiency of Dewetting LBL Assembly

In order to examine efficiency of the d-LBL technique, we compared the d-LBL and conventional LBL side-by-side using UV-vis absorbance. The optical density trends in d-LBL display generally larger increments and the overall trend has pronounced upward swing while conventional LBL displayed a typical linear growth. (Figure 29 A) The curve characterizing the overall accumulation of the material in d-LBL appears to be exponential, which further accelerated the growth in addition to the reduced number of steps. The linear absorbance trend was recovered when rinsing was re-introduced, for instance during the stage of PVA adsorption. (Figure 29 B) Thickness trends of the two

LBL assemblies, [PVA dewet / SWNT dewet]$_n$ and [PVA rinse / SWNT rinse]$_n$, were also compared by ellipsometry measurements. (Figure 29 A) Against expectations, the thickness increments in the ellipsometry results are clearly linear. A probable explanation of the discrepancies between exponential trend in UV-vis and linear tend in ellipsometry is that small nano- to micro-scale islands seen in SEM. (Figure 28) They are likely to completely adsorb light of He-Ne laser or Xe lamp used in UV-vis spectrophotometer. Since, ellipsometric measurements are based on reflected beam, the islands are not accounted for in ellipsometric thickness, which reflect mostly linear accumulations of the material in the dominant surfaces of the films. UV-vis data contain the contribution of the islands, and display the cumulative accumulation of the material, and hence, with the upswing.

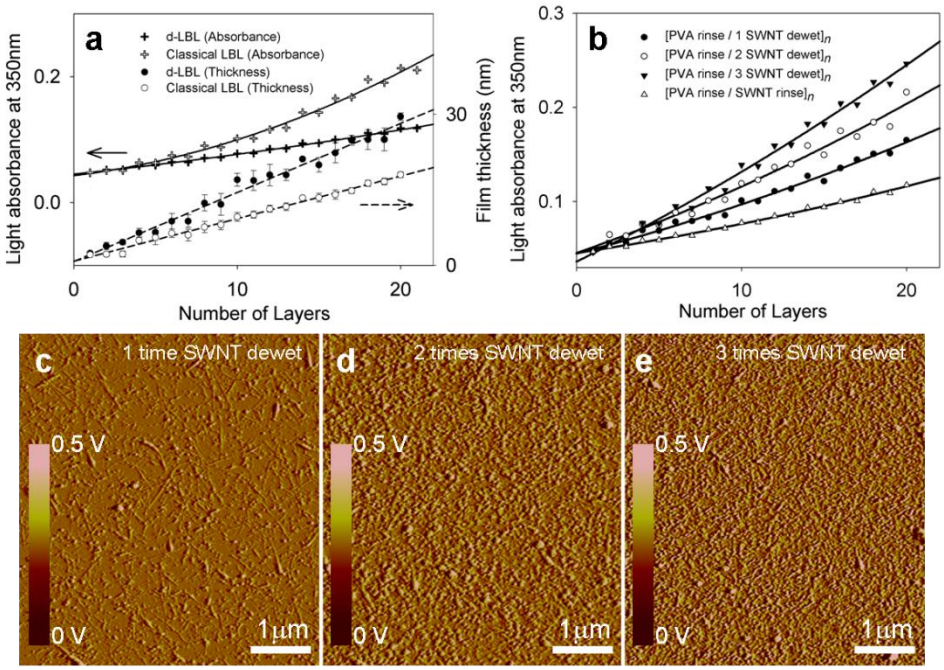

Figure 29 Adsorption trends of dewetting and classical LBL. (A) Comparison of UV-vis accumulation curves for absorbance at 350nm and ellipsometry thickness measurements of d-LBL without rinsing and classical LBL of [PVA/SWNT]n system. (B) Accumulation curves for multiple dewetting procedure, [PVA (10sec) dewet + rinse / x times SWNT dewet], (x= 1, 2, 3), and [PVA (10min) rinse / SWNT (10min) rinse]. AFM images when SWNT deposition was repeated (C) 1, (D) 2, and (E) 3 times in a row.

The efficiency of d-LBL in comparison to conventional LBL can be calculated from processing time of the films and taking into account difference in growth increments. The comparison is done for the following two settings: (1) d-LBL [PVA (10 sec) dewet (30 sec) / SWNT (10 sec) dewet (30 sec)] and (2) conventional LBL [PVA (10 min) + rinse (1 min) / SWNT (10 min) + rinse (1min)]. For d-LBL cycle length is ~80 sec while for conventional LBL it is 1320 sec. Because the ratio of slopes for the two optical density regressions (Figure 29 A, B) are 1.81, d-LBL is at least ~30 times more efficient

as applied to SWNT than conventional LBL in time-wise comparison with similar film qualities when considered total dewetting finished within much less than 30 sec.

Interestingly enough, when one simply repeats the dewetting adsorption step with the same solution without intermediate adsorption of the other component, for instance series of SWNT dewetting adsorption, greater amount of this component is accumulated on the surface. (Figure 29 B) The UV-vis data can also be confirmed by AFM. (Figure 29 C-E) This result is quite useful when one needs to increase the relative content of one of the components. In case of SWNTs, it can be used to control the nanotube loading without increasing their linear charge density, which is always connected to the greater damage of the conjugated pi-orbital system or thicker polymer coating around the graphene stem.[61]

As one can notice, adsorption steps take substantially less time in d-LBL. High density layers can be obtained substantially quicker than in conventional LBL. The slope of the material accumulation curves even in linear representation is also greater. (Figure 29) Elimination of rinsing steps, and thus, the inevitable desorption of a portion of adsorbed layer is a simple but probably an incomplete answer here because the material accumulation curves have higher slopes even when one rinsing step is used. Additionally, the time of each d-LBL cycle for SWNT is so much shorter that it must be included in consideration. Within the limit of existing knowledge of materials transfer during dewetting, this observation can be explained by acceleration of the mass transport due to vigorous convection flows in the vicinity of the interface during the dewetting movements. Furthermore, metastable adsorbed components are readily stabilized by

instant exposure to air after dewetting. Overall, dewetting eliminates the bottleneck of diffusion limiting kinetics, which is a source of process acceleration in spray deposition,[39, 40] spin-LBL,[41-44] and electro-LBL.[45] Therefore, the synergic combination of flow induced material transport and instant adsorption stabilization dramatically facilitated the adsorption reactions, but without any external devices.

7. Dewetting LBL Assembly with SWNTs

The d-LBL was further applied to fabrication of a free-standing SWNT-polymer composite film. The 300 layered d-LBL assemblies, [PVA dewet + rinse/ SWNT dewet]$_{300}$, resulted in about ~2 μm thick film (Figure 30) and displayed 229±36 MPa in tensile strength and 0.08±0.014 in strain. These mechanical properties are substantially better than those of SWNT-based composite films constructed conventional LBL assembly in several previous studies[26, 62] which indicates that dewetting process can not only accelerate the LBL procedure but also produce better materials.

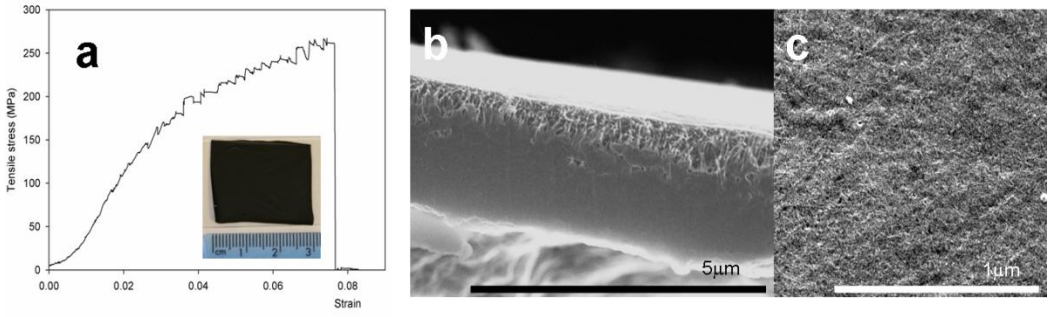

Figure 30 Mechanical testing of a SWNT film fabricated by d-LBL. (A) 300 layer d-LBL film, [PVA dewet + rinse / SWNT dewet]$_{300}$, was fabricated and tested in mechanical strength. Stress-strain curve of the d-LBL free standing film and photo-image (insert) were shown. (B) Cross-sectional and (C) in-plane view SEM images of the SWNT-polymer composite film fabricated by d-LBL technique. Densely packed and finely distributed SWNTs make inter-woven structures.

When SWNTs are being adsorbed on PVA layer, d-LBL gives an unusual 2D film morphology of the films, which can be described as the fractal network structures.[63] (Figure 31) The fractal networks can be exceptionally interesting for charge transport and mechanical properties. (Figure 30) Their extensive interconnectivity is essential in many nanotube applications, such as fuel cell membranes, and flexible electronics.[48] The fractal patterns emerge because of the dewetting movements of three-phase meniscus. They originate from the two different sets of forces exerting on SWNTs: the dewetting forces which triggers the unsteady and unstable movement of fluid along adsorbed SWNTs, and the hydrodynamic force caused by micro flows close to the substrate surface. The actual pattern is a result of SWNT adsorption during the movements combined with restructuring the film[31, 60, 64] by surface tension at the triple interface.

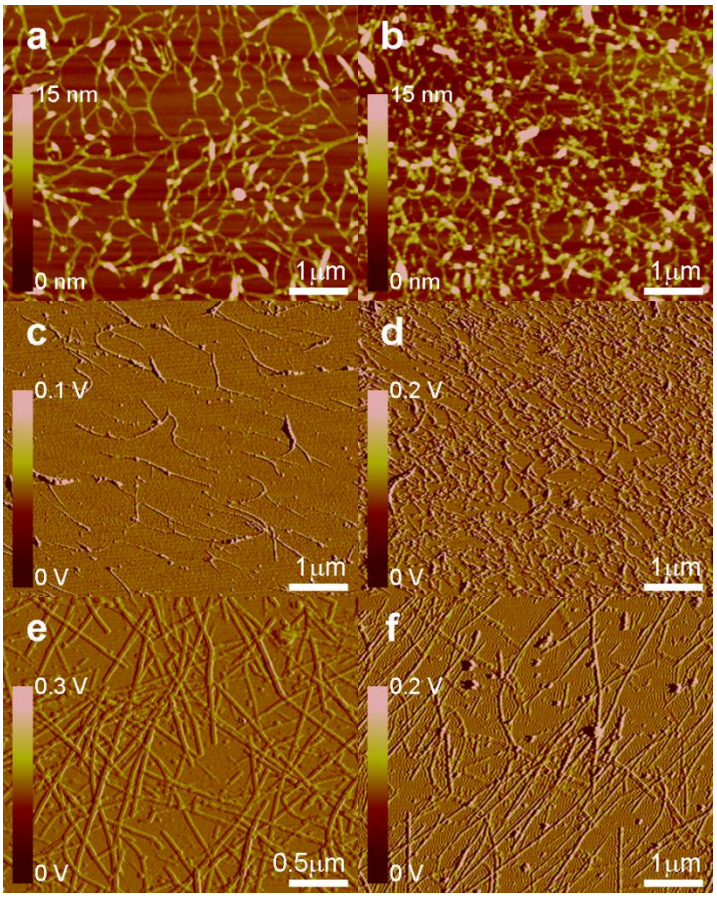

Figure 31 Lateral patterns by d-LBL. AFM images of (A) 1 bilayer and (B) 2 bilayers of [PVA rinse/SWNTs dewet] by dewetting forces dominating LBL mode, (C) 1 bilayer and (D) 2 bilayers of [PVA rinse/SWNT dewet] by hydrodynamic force controlled dewetting mode, and (E) 1 bilayer of [PVA rinse/Cellulose NWs dewet] by dewetting forces dominating LBL mode and (F) 1 bilayer of [PVA rinse/Cellulose NWs dewet] by hydrodynamic force controlled dewetting mode.

8. Morphological Control of Dewetting LBL Assembly

The dynamics of dewetting can also be used to effect a different lateral organization. When one induces a unidirectional movement of the pool of 0.5 % PSS/ 0.05 % SWNT on the surface of the substrate by gentle stream of air or simply by the effect of gravity, SWNT fibers show tendency to align as in previous study.[65] In this way,

we increase the hydrodynamic component, which dominate the other forces. Alignment of nanotubes and other axial structures is quite important for a variety of functional properties of the nanostructured materials which include mechanical properties, charge transport, and thermal conductance. We want to point out that the concentration, receding/advancing contact angles, and the speed of the fluid movement in these systems are the key structural factors determining the lateral organization of the films in d-LBL. The presented two patterns are likely to be just some examples of potentially many patterns that can exist here brought about by and the competition of forces during dewetting movements and other processes.[66]

This control of morphology is necessary for any axial nanocolloids rather than being limited only to SWNTs. Alignment of cellulose NWs in Figure 31 F shows the generality of the morphology control by d-LBL. Obtaining of aligned structures is essential for all rod- and wire-like building blocks. More complex packing motifs, such as fractal layers, are a function of not only geometry but of other the properties of nanocolloids, for instance, their mechanical compliance with the flow, surface tension and adhesion to the substrate, which will further increase the variety of potential in-plane morphologies of LBL layers.

9. Dewtting LBL Assembly with Various Materials

It is necessary to show that d-LBL is applicable to the common basic components used for preparation of nanostructured thin films. As such, d-LBL of

[poly(diallyldimethylammonium chloride), (PDDA) dewet / PSS dewet] and [poly(ethylenimine), (PEI) dewet / CdTe dewet] assemblies were performed. (Figure 32) The consistent exponential growth trends both in UV-vis absorbance and ellispometry thickness in the [PDDA dewet / PSS dewet] d-LBL were observed. No micron scale islands were observed. Instead, we saw somewhat increased roughness. In case of another standard buiding block, such nanoparticles, d-LBL of [PEI dewet / CdTe dewet]$_n$ multilayer displayed low level exponential rise in UV-vis absorbance. These observations are consistent with those for SWNTs. Overall, the key LBL characteristics, such as complete surface coverage and molecularly fine structural controls can be attributed to d-LBL as much as to the classical LBL.

Au nanorods (NRs) represent another fundamental building block in nanostructured thin films. Multilayers of Au NRs can also be easily made by d-LBL. (Figure 32 I-K) Importantly, d-LBL multilayers Au NRs display a qualitative distinction compared to the classical LBL. Greater efficiency of deposition, results in denser layers with very strong mutual coupling of electronic oscillations in An NRs absent in similar films made by classical LBL. Coupling of optical resonances in Au NRs is considered to be a prerequisite for engineering of materials with negative refractive index.

Another interesting example of d-LBL is the assembly of 20~50 nm SnO_2 nanowires which have three dimensional branched shapes with “thorns” of 1-2 micron in length. (Figure 32 G-H) These SnO_2 nanowires cannot be assembled by conventional LBL at all because of (1) limited surface charge (5mV) and (2) unfavorably small contact

area to the adsorption surface due to branching. Oppositely, d-LBL produces films with stable growth with uniform adsorption increment from one cycle to the next.

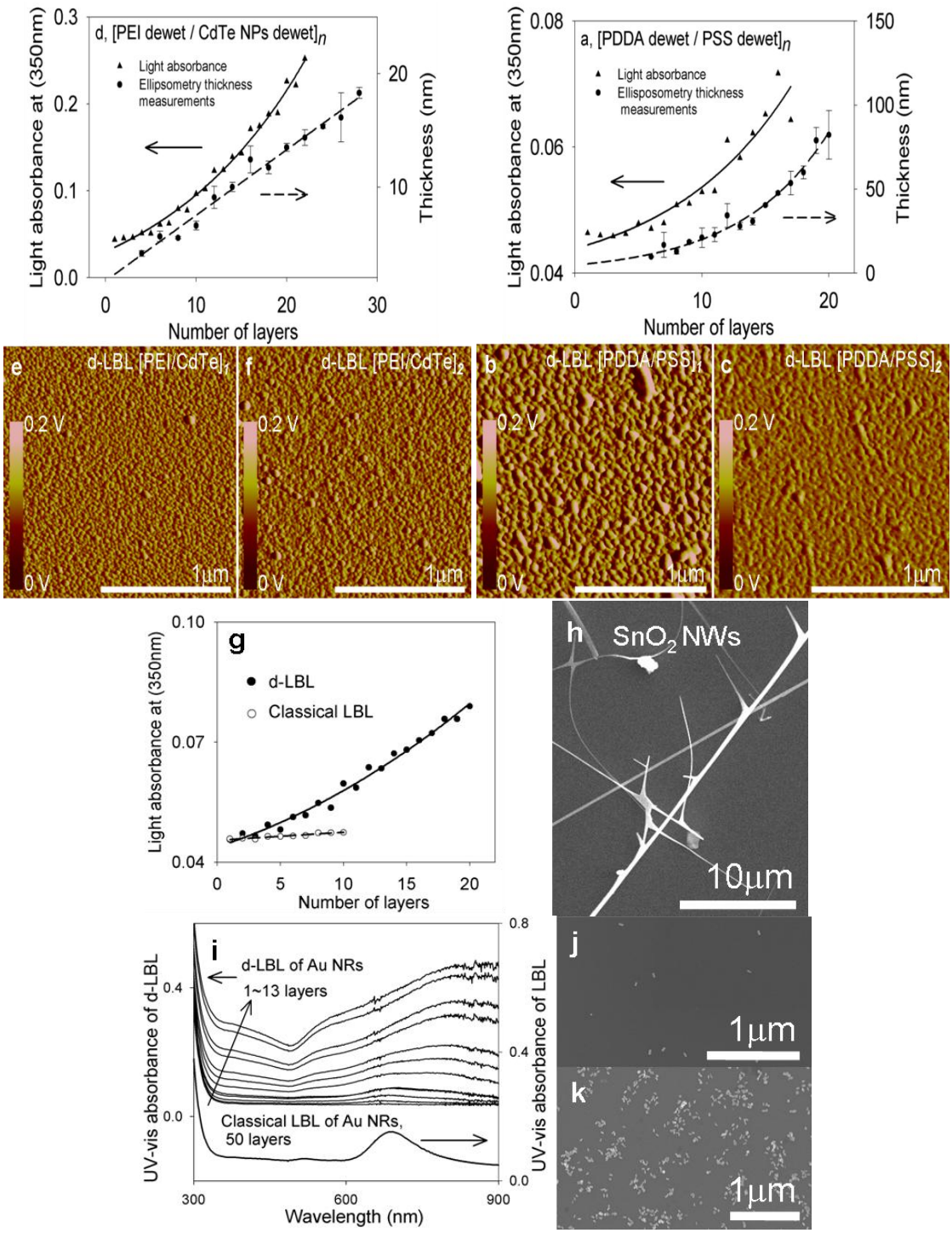

Figure 32 Applicability of d-LBL to typical nanoscale collods and polymers. (A-C) UV-vis, ellipsometry trends and AFM film topology (1 and 2 layers) for d-LBL of solely polyelectrolyte layers [PDDA dewet / PSS dewet]$_n$, (D-F) UV-vis, ellipsometry trends and AFM film topology (1 and 2 layers) for d-LBL of nanoparticles [PEI dewet / CdTe dewet]$_n$, (G-I) Comparison of UV-vis trends in d-LBL and classical LBL for branched SnO_2 nanowires [SnO_2 dewet / PDDA / PAA]$_n$ (●) and [SnO_2 / PDDA / PAA]$_n$ (○). No classical LBL deposition is observed. (H) SEM images of SnO_2 branched wires. (I) Comparison of UV-vis trends in d-LBL and classical LBL for Au NRs [Au NRs dewet / PVA]$_n$. and [Au NRs/ PVA]$_n$. Note drastically different UV spectra. (I-K) SEM images of (J) [Au NRs rinse / PVA]$_2$, (K) [Au NRs dewet / PVA]$_7$.

10. Young's Equation Analysis of Dewetting LBL Assembly

Wetting and dewetting of liquid are common phenomena which can be observed in everyday life. However, their theoretical analysis and observations still need to be fully elaborated.[67] As applied to d-LBL induced by addition of DMF the solid-liquid-gas system can be described by the Young's equation as

$$\sigma_{\alpha x} = \sigma_{\alpha\beta} \cdot \cos\theta + \sigma_{\beta x} \qquad (1)$$

where $\sigma_{\alpha x}$ is the surface tension at the gas-solid interface, $\sigma_{\alpha\beta}$ is the surface tension at the gas-liquid interface, θ is the contact angle, and $\sigma_{\beta x}$ is the surface tension at the liquid-solid interface. In this analysis, the equilibrium contact angle refers specifically to the dewetting (receding) contact angle. If we add small amount of DMF in the selected solution, then Young's equation becomes

$$\sigma_{\alpha x} = \sigma^*_{\alpha\beta} \cdot \cos\theta^* + \sigma^*_{\beta x} \qquad (2)$$

where * is used to denote properties affected by DMF. Then from (1) and (2) one can infer

$$\sigma_{\alpha\beta} \cdot \cos\theta + \sigma_{\beta x} = \sigma^*_{\alpha\beta} \cdot \cos\theta^* + \sigma^*_{\beta x} \quad (3)$$

$$\sigma_{\alpha\beta} \cdot \cos\theta - \sigma^*_{\alpha\beta} \cdot \cos\theta^* = \sigma^*_{\beta x} - \sigma_{\beta x} \quad (4)$$

Contact angle of liquid increases after adding DMF. So, $\theta < \theta^*$ and $\cos\theta > \cos\theta^*$. The surface tension of water and DMF are 72.8 mN/m and 37.1 mN/m at 20 ^{o}C respectively and that of DMF and water mixture lies between those two limits ($\sigma_{\alpha\beta} > \sigma^*_{\alpha\beta}$). Thus, we can conclude that the requirement for achieving dewetting is $(\sigma_{\alpha\beta} - \sigma^*_{\alpha\beta}) < (\sigma^*_{\beta x} - \sigma_{\beta x})$.

11. Conclusion

Two advanced LBL approaches based on dewetting phenomena were introduced in this chapter. Dewetting LBL and SWNT Combing LBL are efficient, economic, and fast. Both can also be used for creation of unique adsorption topographies including fractal networks and aligned fibers. The experiments demonstrate that it is expected to be applicable to most existing LBL assembly systems and can potentially lead to nanostructured thin films with improved structural characteristics and mechanical, electrical, and optical properties.

Appendix

Quantitative SWNT strand analysis

Various controlled adsorption morphologies of SWNTs were obtained by advanced LBL assemblies. Additional forces besides supra-molecular LBL adsorption forces were exerted for shaping alignments and fish-net networks. Therefore, quantitative analysis of these controlled geometry of SWNT strands are required for further systematic developments of advanced LBL techniques.

A. Quantitative calculation of CNT alignment effects

We have successfully demonstrated the efficient alignment of SWNT during LBL assemblies. Two methods were employed: SWNT combing and dewetting techniques. Although their alignments were easily recognized by direct microscope observations, we need to quantify the degree of alignment, which can be defined by an anisotropy parameter, $\boldsymbol{R}$.[68]

$$\boldsymbol{R} = \frac{L_{\parallel}}{L_{\perp}} = \frac{\sum_{i=1}^{N} |L_{S,i} \cdot cos\theta\ |}{\sum_{i=1}^{N} |L_{S,i} \cdot sin\theta\ |} \qquad (1)$$

where, L_s = straight segment length, θ = angle from the aligned direction

Higher value of $\boldsymbol{R}$ indicates better orientation toward the alignment direction value starting from 1 for an ideally isotropic sample. Another way to evaluate molecular orientation structures is to use 2D fast Fourier transform (FFT) of microscope images.[69]

FFT spectrum intensities by the azimuthal angle generally have a wave function. This wave function can be evaluated by the full-width at half maximum (FWHM) of FFT power intensity. The FWHM provides the quantitative information of the degree of orientation and can be further processed to calculate Hermans orientation function, $\boldsymbol{f}$.[70]

$$\boldsymbol{f} = \frac{3\langle cos^2\theta\rangle - 1}{2} \qquad (2)$$

where, θ = angle from the aligned direction

The $\boldsymbol{f}$ parameter is 0 for randomly oriented and 1 if all molecules are pure crystalline structures with perfect orientation. Here, we introduce quantitative analysis of SWNT's alignments by both the direct statistical calculation and the image processing technique.

The simplest way is to directly measure the angles of each SWNT's orientation from the aligned direction and manually count it. We did it for both SWNT combing and dewetting LBL samples as shown in figure 33. The histogram of angles and straight segments of SWNT lies were recorded in the graph. If we calculate it for our aligned SWNT samples, $\boldsymbol{R}$ becomes 3.88 for the SWNT combing and 2.68 for the dewetting mode LBL samples. These results tell us that the forced alignment by strong air blow during SWNT combing resulted more efficient orientation than the natural dewetting by gravity force.

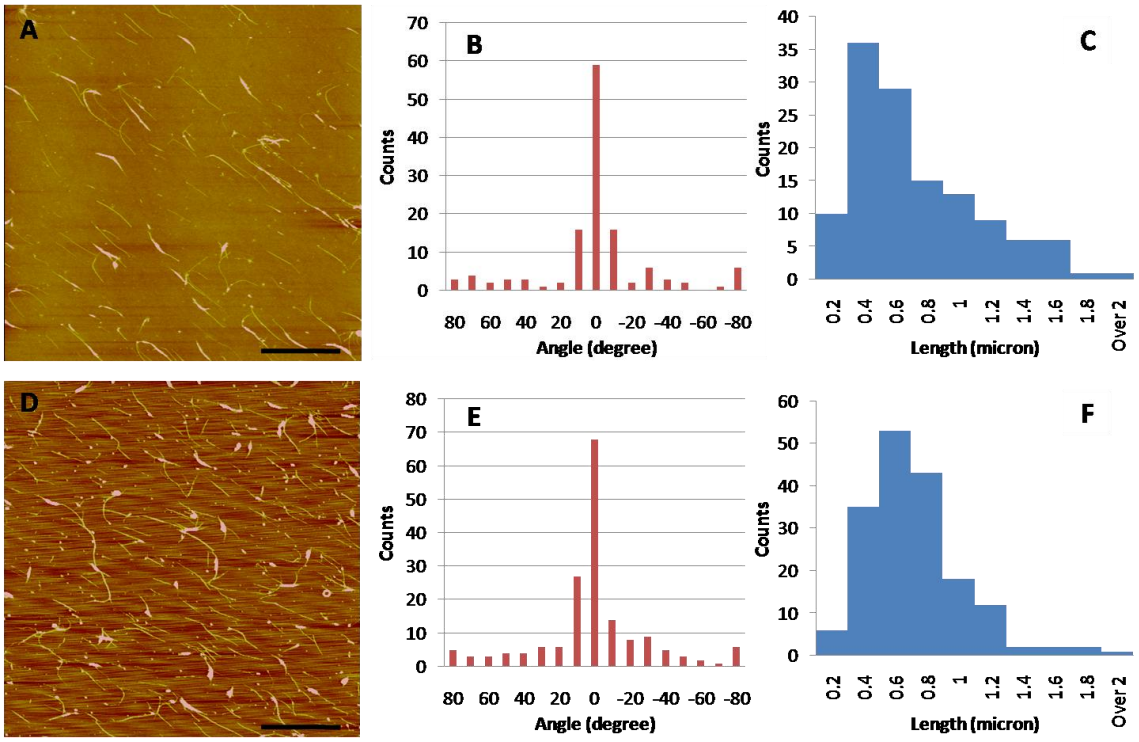

Figure 33 Calculation of anisotropy parameters of aligned SWNTs by (A-C) meniscus combing technique and (D-F) dewetting mode LBL. Aligned SWNTs shown in (A, D) AFM images were analyzed by the histograms of (B, E) angles from the alignment direction and (C, F) straight segment lengths of SWNTs. Calculated anisotropy parameters of meniscus combing and dewetting methods were 3.88 and 2.68, respectively. Each scale bar represents 2 micron.

This direct calculation is simple and reliable. However, it is critically limited to only a simple and straightforward sample because of manual counting. For more complex images, FFT is useful for assigning an objective numerical value from the spatially organized structures. The 2D FFT function converts this 2D orientation image information into a mathematically defined frequency domain. This domain maps the rate of the pixel intensity changing across the original data image.[69]

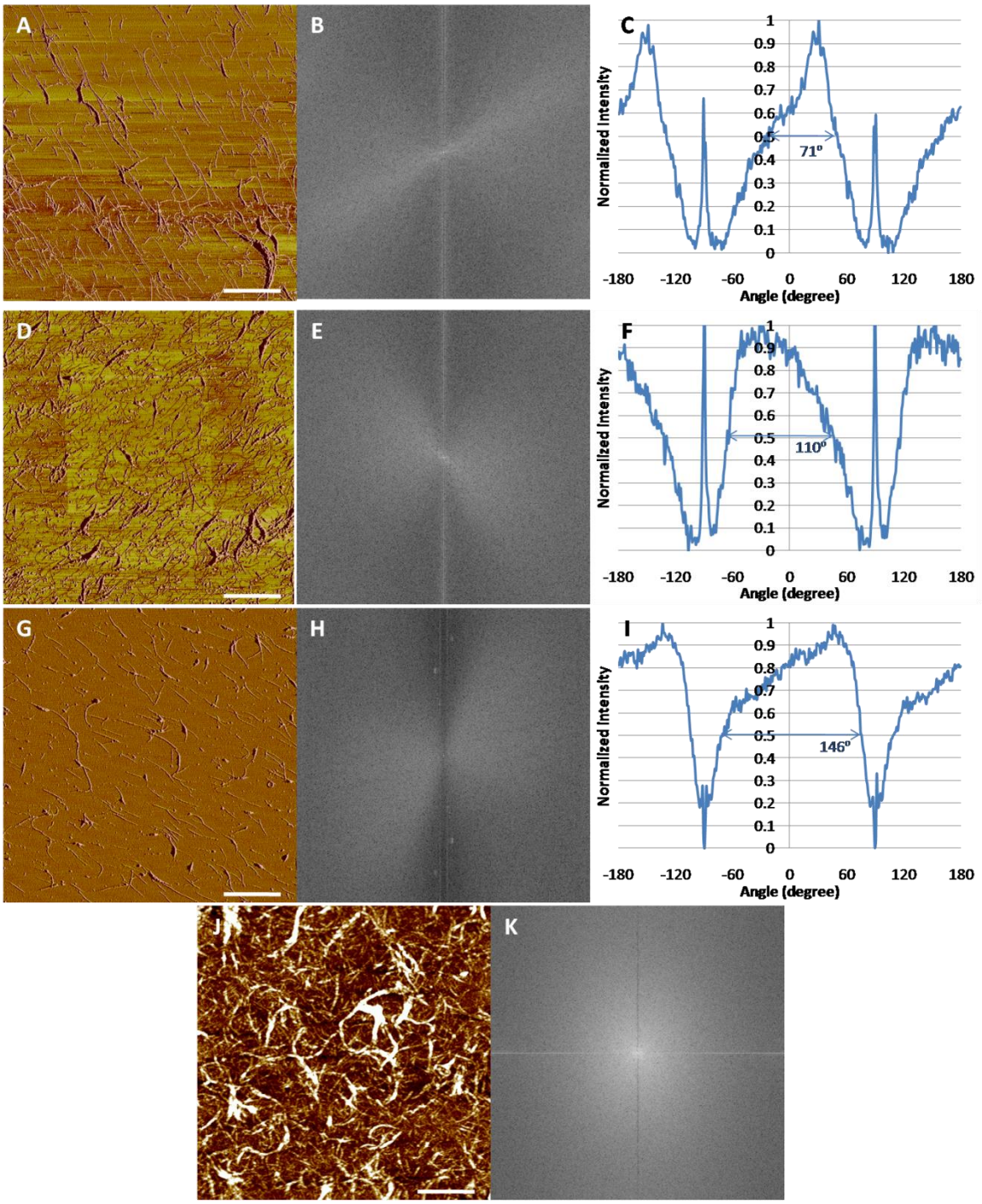

Figure 34 2D FFT processing of the AFM images showing aligned SWNTs. (A, D, G, H) original AFM images, (B, E, H, K) FFT processing of the AFM images, and (C, F, I) normalized intensity average plots vs. azimuthal angles of the FFT images were shown. The alignments of SWNTs were by (A-C) 1L SWNT combing, (D-F) 2L SWNT combing, (G-I) 1L dewetting LBL, and (J-K) random conventional LBL techniques.

The digital FFT processing of our AFM images showing SWNT alignments were done by using Image J software (http://rsb.info.nih.gov/ij/) following the detailed procedures by J. Corey *et al.*.[71] Alignments of SWNTs shown in AFM images resulted in butterfly patterns in FFT converted images. Thus, these butterfly patterns are plotted into wave-functions in the normalized intensity graph along radii at each angle (at 1° from the positive x-axis to 360°). The width of peak can be described by the FWHM, which further informs the degree of alignment information, here. Generally, smaller FWHM corresponds to higher and denser degree of alignments of SWNTs. If we performed these calculations for the LBL assembled samples, 71°, 110°, and 146° were obtained for 1L, 2L SWNT combing and dewetting LBL samples, respectively. Random orientation by conventional LBL assembly produced a broad shapeless pattern in the FFT converted images. As mentioned, this FWHM can be further processed to the orientation function if the wave-functions are well defined. However, the asymmetric bump shown in the AFM images will cause significant errors even after fitting a wave-function.

B. Persistence length of SWNTs during LBL assembly

Semi-flexible thread-like structures were represented by worm-like chain model as random-coil and rigid-rod models for flexible and stiff ones, respectively. This worm-like chain model is suitable for analyzing the behaviors of stiff polymers, double-helical DNAs, poly-peptides, and CNTs. Here, we want to analyze the SWNT's molecular

conformation in the LBL assembly by employing a worm-like chain model, which can be expressed by a persistence length.

A SWNT is one of the stiffest materials in nature. However, the thinness of SWNTs alters their molecular straightness, particularly in a nanocomposite, which can affect the reinforcement efficiencies as well as functional contributions on a hybrid structure. However, judicious estimation of the persistence length has not been widely performed in SWNT nanocomposites due to the difficulties of end-to-end distance observation for a long SWNTs. Experimentally, only limited ranges of SWNTs in a confined state were reported. Theoretically, Yakobson *et al.* calculated that the persistence length (a) of freely suspended defect-free SWNTs are a = 9.7 μm for (5,5) and a = 11 μm for (9,0) nanotubes at room temperature.[72] Experimental determinations of the persistence length were much smaller than those. Sano *et al.* observed that the persistence length of the ring-formed SWNTs were around 800 nm.[73] Their SWNTs were heavily oxidized and severely weakened by strong acid mixtures of H_2SO_4/HNO_3. Because the persistence lengths are correlated by the stiffness and the conformation of strands, their persistence length of ring SWNTs might be significantly lowered by severe chemistry.

The SWNTs adsorbed on a flat substrate by LBL assembly can be treated as a 2-dimensional topography. Thus, 2-dimensional persistence length formula can be used.[74]

$$\langle D^2 \rangle_{2D} = 4aL_c \left\{ 1 - \frac{2a}{L_c} \left[1 - \exp\left(-\frac{L_c}{2a} \right) \right] \right\} \qquad (2)$$

where, D = the end-to-end distance, a = the persistence length, L_c = the contour length of SWNTs.

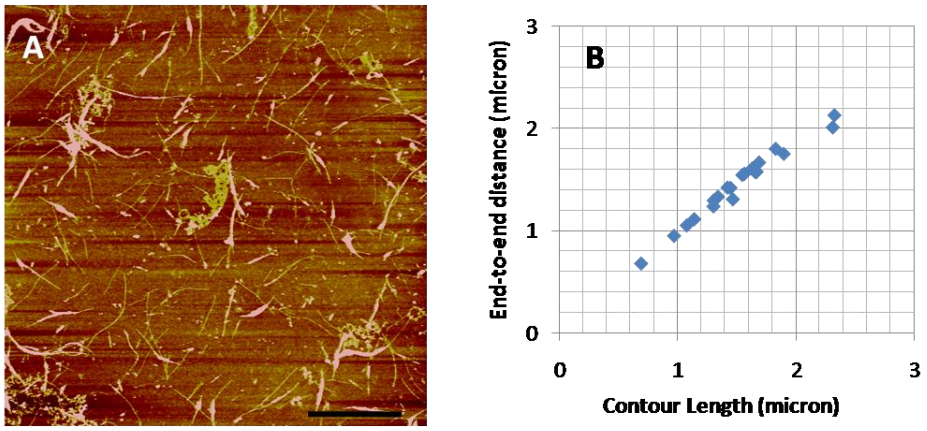

Figure 35 Calculation of SWNT's persistence length during LBL assembly. (A) AFM image of a freely dried SWNT LBL. Only well exfoliated SWNTs, whose both ends were shown, are selected to the persistence length calculation. (B) Plot of end-to-end distance (D) to contour length (L_c) of selected SWNTs.

In order to understand SWNT's conformation during LBL assembly, a freely dried LBL sample without directed forces, which usually stretch SWNTs to be straighter, was selected as shown in figure 35 A. The plot of the end-to-end distance (D) versus the contour length (L_c) indicates that the discrepancy between D and L_c generally increases by longer SWNTs. The average persistence length with selected 20 SWNTs, which were well exfoliated and clearly showed both ends, was 16.5 μm. The maximum and minimum were 168.7 and 0.99 μm. As we can easily projected, wide ranges of persistence lengths were observed because many different conformations of adsorbed SWNTs exist on a surface. Furthermore, the CNI SWNTs used here have rather perfect crystalline structures

with little defects unlike curled MWNTs, whose static bending persistence length was merely 271 nm with intrinsic structural defects.[75]

Reference

1. Huang, Y.; Duan, X.; Wei, Q.; Lieber, C. M., Directed assembly of one-dimensional nanostructures into functional networks. *Science* **2001,** 291, (5504), 630-633.
2. Vigolo, B.; Penicaud, A.; Coulon, C.; Sauder, C.; Pailler, R.; Journet, C.; Bernier, P.; Poulin, P., Macroscopic fibers and ribbons of oriented carbon nanotubes. *Science* **2000,** 290, (5495), 1331-1334.
3. Rao, S. G.; Huang, L.; Setyawan, W.; Hong, S., Nanotube electronics: large-scale assembly of carbon nanotubes. *Nature* **2003,** 425, (6953), 36-37.
4. Dresselhaus, M. S.; Dresselhaus, G.; Jorio, A., Unusual properties and structure of carbon nanotubes. *Annual Review of Materials Research* **2004,** 34, 247-278.
5. Xin, H.; Woolley, A. T., Directional Orientation of Carbon Nanotubes on Surfaces Using a Gas Flow Cell. *Nano Letters* **2004,** 4, (8), 1481-1484.
6. Guldi, D. M.; Mamedov, A.; Crisp, T.; Kotov, N. A.; Hirsch, A.; Prato, M., Ring-Ribbon Transition and Parallel Alignment in SWNT Films on Polyelectrolytes. *Journal of Physical Chemistry B* **2004,** 108, (26), 8770-8772.
7. Ko, H.; Peleshanko, S.; Tsukruk, V. V., Combing and bending of carbon nanotube arrays with confined microfluidic flow on patterned surfaces. *Journal of Physical Chemistry B* **2004,** 108, (14), 4385-4393.
8. Tsukruk, V. V.; Ko, H.; Peleshanko, S., Nanotube surface arrays: weaving, bending, and assembling on patterned silicon. *Physical Review Letters* **2004,** 92, (6), 065502/1-065502/4.
9. Smith, B. W.; Benes, Z.; Luzzi, D. E.; Fischer, J. E.; Walters, D. A.; Casavant, M. J.; Schmidt, J.; Smalley, R. E., Structural anisotropy of magnetically aligned single wall carbon nanotube films. *Applied Physics Letters* **2000,** 77, (5), 663-665.
10. Kamat, P. V.; Thomas, K. G.; Barazzouk, S.; Girishkumar, G.; Vinodgopal, K.; Meisel, D., Self-assembled linear bundles of single wall carbon nanotubes and their alignment and deposition as a film in a d.c. field. *Journal of the American Chemical Society* **2004,** 126, (34), 10757-10762.
11. Gao, J.; Yu, A.; Itkis, M. E.; Bekyarova, E.; Zhao, B.; Niyogi, S.; Haddon, R. C., Large-Scale Fabrication of Aligned Single-Walled Carbon Nanotube Array and Hierarchical Single-Walled Carbon Nanotube Assembly. *Journal of the American Chemical Society* **2004,** 126, (51), 16698-16699.
12. Shimoda, H.; Oh, S. J.; Geng, H. Z.; Walker, R. J.; Zhang, X. B.; McNeil, L. E.; Zhou, O., Self-assembly of carbon nanotubes. *Advanced Materials* **2002,** 14, (12), 899-901.
13. Chen, J. H.; Huang, Z. P.; Wang, D. Z.; Yang, S. X.; Wen, J. G.; Ren, Z. F., Electrochemical synthesis of polypyrrole/carbon nanotube nanoscale composites using well-aligned carbon nanotube arrays. *Applied Physics A: Materials Science & Processing* **2001,** 73, (2), 129-131.
14. He, P.; Shi, D.; Lian, J.; Wang, L. M.; Ewing, R. C.; van Ooij, W.; Li, W. Z.; Ren, Z. F., Plasma deposition of thin carbonfluorine films on aligned carbon nanotube. *Applied Physics Letters* **2005,** 86, (4), 043107/1-043107/3.

15. Fischer, J. E.; Zhou, W.; Vavro, J.; Llaguno, M. C.; Guthy, C.; Haggenmueller, R.; Casavant, M. J.; Walters, D. E.; Smalley, R. E., Magnetically aligned single wall carbon nanotube films: Preferred orientation and anisotropic transport properties. *Journal of Applied Physics* **2003,** 93, (4), 2157-2163.
16. Decher, G., Fuzzy nanoassemblies: toward layered polymeric multicomposites. *Science* **1997,** 277, (5330), 1232-1237.
17. Kotov, N. A., Ordered layered assemblies of nanoparticles. *MRS Bulletin* **2001,** 26, (12), 992-997.
18. Hammond, P. T., Form and function in multilayer assembly: New applications at the nanoscale. *Advanced Materials* **2004,** 16, (15), 1271-1293.
19. Bensimon, A.; Simon, A.; Chiffaudel, A.; Croquette, V.; Heslot, F.; Bensimon, D., Alignment and sensitive detection of DNA by a moving interface. *Science* **1994,** 265, (5181), 2096-2098.
20. Michalet, X.; Ekong, R.; Fougerousse, F.; Rousseaux, S.; Schurra, C.; Hornigold, N.; van Slegtenhorst, M.; Wolfe, J.; Povey, S.; Beckmann, J. S.; Bensimon, A., Dynamic molecular combing: stretching the whole human genome for high-resolution studies. *Science* **1997,** 277, (5331), 1518-1523.
21. Bensimon, D.; Simon, A. J.; Croquette, V.; Bensimon, A., Stretching DNA with a receding meniscus: experiments and models. *Physical Review Letters* **1995,** 74, (23), 4754-4757.
22. Hone, J.; Llaguno, M. C.; Nemes, N. M.; Johnson, A. T.; Fischer, J. E.; Walters, D. A.; Casavant, M. J.; Schmidt, J.; Smalley, R. E., Electrical and thermal transport properties of magnetically aligned single wall carbon nanotube films. *Applied Physics Letters* **2000,** 77, (5), 666-668.
23. O'Connell, M. J.; Boul, P.; Ericson, L. M.; Huffman, C.; Wang, Y.; Haroz, E.; Kuper, C.; Tour, J.; Ausman, K. D.; Smalley, R. E., Reversible water-solubilization of single-walled carbon nanotubes by polymer wrapping. *Chemical Physics Letters* **2001,** 342, (3,4), 265-271.
24. Kovtyukhova, N. I.; Mallouk, T. E., Ultrathin Anisotropic Films Assembled from Individual Single-Walled Carbon Nanotubes and Amine Polymers. *Journal of Physical Chemistry B* **2005,** 109, (7), 2540-2545.
25. Tang, Z.; Kotov, N. A.; Magonov, S.; Ozturk, B., Nanostructured artificial nacre. *Nature Materials* **2003,** 2, (6), 413-418.
26. Mamedov, A. A.; Kotov, N. A.; Prato, M.; Guldi, D. M.; Wicksted, J. P.; Hirsch, A., Molecular design of strong single-wall carbon nanotube/polyelectrolyte multilayer composites. *Nature Materials* **2002,** 1, (3), 190-194.
27. Kumeta, K.; Nagashima, I.; Matsui, S.; Mizoguchi, K., Crosslinking reaction of poly(vinyl alcohol) with poly(acrylic acid) (PAA) by heat treatment: Effect of neutralization of PAA. *J.Appl.Polym.Sci.* **2003,** 90, (9), 2420-2427.
28. Kim, Y.; Minami, N.; Kazaoui, S., Highly polarized absorption and photoluminescence of stretch-aligned single-wall carbon nanotubes dispersed in gelatin films. *Applied Physics Letters* **2005,** 86, (7), 073103/1-073103/3.
29. Strano, M. S.; Dyke, C. A.; Usrey, M. L.; Barone, P. W.; Allen, M. J.; Shan, H.; Kittrell, C.; Hauge, R. H.; Tour, J. M.; Smalley, R. E., Electronic structure control of

single-walled carbon nanotube functionalization. *Science (Washington, DC, United States)* **2003,** 301, (5639), 1519-1522.
30. William, M. D., *Analysis of Transport Phenomena*. Oxford University Press: 1998; p 323.
31. Reiter, G.; Sharma, A., Auto-Optimization of Dewetting Rates by Rim Instabilities in Slipping Polymer Films. *Physical Review Letters* **2001,** 87, (16), 166103/1-166103/4.
32. Gheith, M. K.; Sinani, V. A.; Wicksted, J. P.; Matts, R. L.; Kotov, N. A., Single-walled carbon nanotube polyelectrolyte multilayers and freestanding films as a biocompatible platformfor neuroprosthetic implants. *Advanced Materials* **2005,** 17, (22), 2663-+.
33. Hu, H.; Ni, Y.; Mandal, S. K.; Montana, V.; Zhao, B.; Haddon, R. C.; Parpura, V., Polyethyleneimine Functionalized Single-Walled Carbon Nanotubes as a Substrate for Neuronal Growth. *Journal of Physical Chemistry B* **2005,** 109, (10), 4285-4289.
34. Hu, H.; Ni, Y.; Montana, V.; Haddon, R. C.; Parpura, V., Chemically functionalized carbon nanotubes as substrates for neuronal growth. *Nano Letters* **2004,** 4, (3), 507-511.
35. Dalton, A. B.; Collins, S.; Munoz, E.; Razal, J. M.; Ebron, V. H.; Ferraris, J. P.; Coleman, J. N.; Kim, B. G.; Baughman, R. H., Super-tough carbon-nanotube fibres. *Nature* **2003,** 423, (6941), 703.
36. Ericson, L. M.; Fan, H.; Peng, H.; Davis, V. A.; Zhou, W.; Sulpizio, J.; Wang, Y.; Booker, R.; Vavro, J.; Guthy, C.; Parra-Vasquez, A. N.; Kim, M. J.; Ramesh, S.; Saini, R. K.; Kittrell, C.; Lavin, G.; Schmidt, H.; Adams, W. W.; Billups, W. E.; Pasquali, M.; Hwang, W. F.; Hauge, R. H.; Fischer, J. E.; Smalley, R. E., Macroscopic, Neat, Single-Walled Carbon Nanotube Fibers. *Science* **2004,** 305, (5689), 1447-1450.
37. Jiang, C. Y.; Markutsya, S.; Pikus, Y.; Tsukruk, V. V., Freely suspended nanocomposite membranes as highly sensitive sensors. *Nature Materials* **2004,** 3, (10), 721-728.
38. Wu, Z. Z.; Walish, J.; Nolte, A.; Zhai, L.; Cohen, R. E.; Rubner, M. F., Deformable antireflection coatings from polymer and nanoparticle multilayers. *Advanced Materials* **2006,** 18, (20), 2699-+.
39. Schlenoff, J. B.; Dubas, S. T.; Farhat, T., Sprayed polyelectrolyte multilayers. *Langmuir* **2000,** 16, (26), 9968-9969.
40. Izquierdo, A.; Ono, S. S.; Voegel, J. C.; Schaaff, P.; Decher, G., Dipping versus spraying: Exploring the deposition conditions for speeding up layer-by-layer assembly. *Langmuir* **2005,** 21, (16), 7558-7567.
41. Jiang, C.; Markutsya, S.; Tsukruk, V. V., Collective and Individual Plasmon Resonances in Nanoparticle Films Obtained by Spin-Assisted Layer-by-Layer Assembly. *Langmuir* **2004,** 20, (3), 882-890.
42. Lee, S. S.; Hong, J. D.; Kim, C. H.; Kim, K.; Koo, J. P.; Lee, K. B., Layer-by-layer deposited multilayer assemblies of ionene-type polyelectrolytes based on the spin-coating method. *Macromolecules* **2001,** 34, (16), 5358-5360.

43. Cho, J.; Char, K.; Hong, J. D.; Lee, K. B., Fabrication of highly ordered multilayer films using a spin self-assembly method. *Advanced Materials* **2001,** 13, (14), 1076-1078.
44. Chiarelli, P. A.; Johal, M. S.; Casson, J. L.; Roberts, J. B.; Robinson, J. M.; Wang, H. L., Controlled fabrication of polyelectrolyte multilayer thin films using spin-assembly. *Advanced Materials* **2001,** 13, (15), 1167-1171.
45. Sun, J.; Gao, M.; Feldmann, J., Electric field directed layer-by-layer assembly of highly fluorescent CdTe nanoparticles. *Journal of Nanoscience and Nanotechnology* **2001,** 1, (2), 133-136.
46. Fujimoto, K.; Fujita, S.; Ding, B.; Shiratori, S., Fabrication of layer-by-layer self-assembly films using roll-to-roll process. *Japanese Journal of Applied Physics, Part 2: Letters & Express Letters* **2005,** 44, (1-7), L126-L128.
47. Picart, C.; Mutterer, J.; Richert, L.; Luo, Y.; Prestwich, G. D.; Schaaf, P.; Voegel, J. C.; Lavalle, P., Molecular basis for the explanation of the exponential growth of polyelectrolyte multilayers. *Proceedings of the National Academy of Sciences of the United States of America* **2002,** 99, (20), 12531-12535.
48. Nam, K. T.; Kim, D. W.; Yoo, P. J.; Chiang, C. Y.; Meethong, N.; Hammond, P. T.; Chiang, Y. M.; Belcher, A. M., Virus-enabled synthesis and assembly of nanowires for lithium ion battery electrodes. *Science* **2006,** 312, (5775), 885-888.
49. Maheshwari, V.; Saraf, R. F., High-Resolution Thin-Film Device to Sense Texture by Touch. *Science* **2006,** 312, (5779), 1501-1504.
50. Ko, H.; Jiang, C.; Shulha, H.; Tsukruk, V. V., Carbon Nanotube Arrays Encapsulated into Freely Suspended Flexible Films. *Chemistry of Materials* **2005,** 17, (10), 2490-2493.
51. Reiter, G., Dewetting of thin polymer films. *Physical Review Letters* **1992,** 68, (1), 75-78.
52. Reiter, G.; Demirel, A. L.; Granick, S., From static to kinetic friction in confined liquid films. *Science* **1994,** 263, (5154), 1741-1744.
53. Lu, N.; Chen, X.; Molenda, D.; Naber, A.; Fuchs, H.; Talapin, D. V.; Weller, H.; Mueller, J.; Lupton, J. M.; Feldmann, J.; Rogach, A. L.; Chi, L., Lateral Patterning of Luminescent CdSe Nanocrystals by Selective Dewetting from Self-Assembled Organic Templates. *Nano Letters* **2004,** 4, (5), 885-888.
54. Huang, J.; Kim, F.; Tao, A. R.; Connor, S.; Yang, P., Spontaneous formation of nanoparticle stripe patterns through dewetting. *Nature Materials* **2005,** 4, (12), 896-900.
55. Gaponik, N.; Talapin, D. V.; Rogach, A. L.; Hoppe, K.; Shevchenko, E. V.; Kornowski, A.; Eychmueller, A.; Weller, H., Thiol-Capping of CdTe Nanocrystals: An Alternative to Organometallic Synthetic Routes. *Journal of Physical Chemistry B* **2002,** 106, (29), 7177-7185.
56. Tang, Z.; Kotov, N. A.; Giersig, M., Spontaneous organization of single CdTe nanoparticles into luminescent nanowires. *Science* **2002,** 297, (5579), 237-240.
57. Cebeci, F. C.; Wu, Z.; Zhai, L.; Cohen, R. E.; Rubner, M. F., Nanoporosity-Driven Superhydrophilicity: A Means to Create Multifunctional Antifogging Coatings. *Langmuir* **2006,** 22, (6), 2856-2862.

58. Serizawa, T.; Kamimura, S.; Kawanishi, N.; Akashi, M., Layer-by-Layer Assembly of Poly(vinyl alcohol) and Hydrophobic Polymers Based on Their Physical Adsorption on Surfaces. *Langmuir* **2002,** 18, (22), 8381-8385.
59. Blossey, R., Self-cleaning surfaces - virtual realities. *Nature Materials* **2003,** 2, (5), 301-306.
60. Yerushalmi-Rozen, R.; Kerle, T.; Klein, J., Alternative dewetting pathways of thin liquid films. *Science* **1999,** 285, (5431), 1254-1256.
61. Sinani, V. A.; Gheith, M. K.; Yaroslavov, A. A.; Rakhnyanskaya, A. A.; Sun, K.; Mamedov, A. A.; Wicksted, J. P.; Kotov, N. A., Aqueous dispersions of single-wall and multiwall carbon nanotubes with designed amphiphilic polycations. *Journal of the American Chemical Society* **2005,** 127, (10), 3463-3472.
62. Olek, M.; Ostrander, J.; Jurga, S.; Mohwald, H.; Kotov, N.; Kempa, K.; Giersig, M., Layer-by-layer assembled composites from multiwall carbon nanotubes with different morphologies. *Nano Letters* **2004,** 4, (10), 1889-1895.
63. Thiele, U.; Mertig, M.; Pompe, W., Dewetting of an evaporating thin liquid film: heterogeneous nucleation and surface instability. *Physical Review Letters* **1998,** 80, (13), 2869-2872.
64. Ghatak, A.; Khanna, R.; Sharma, A., Dynamics and Morphology of Holes in Dewetting of Thin Films. *Journal of Colloid and Interface Science* **1999,** 212, (2), 483-494.
65. Shim, B. S.; Kotov, N. A., Single-Walled Carbon Nanotube Combing during Layer-by-Layer Assembly: From Random Adsorption to Aligned Composites. *Langmuir* **2005,** 21, (21), 9381-9385.
66. Deegan, R. D.; Bakajin, O.; Dupont, T. F.; Huber, G.; Nagel, S. R.; Witten, T. A., Capillary flow as the cause of ring stains from dried liquid drops. *Nature* **1997,** 389, (6653), 827-829.
67. Herminghaus, S., Wetting: Introductory note. *Journal of Physics: Condensed Matter* **2005,** 17, (9), S261-S263.
68. Kocabas, C.; Pimparkar, N.; Yesilyurt, O.; Kang, S. J.; Alam, M. A.; Rogers, J. A., Experimental and theoretical studies of transport through large scale, partially aligned arrays of single-walled carbon nanotubes in thin film type transistors. *Nano Letters* **2007,** 7, (5), 1195-1202.
69. Ayres, C. E.; Jha, B. S.; Meredith, H.; Bowman, J. R.; Bowlin, G. L.; Henderson, S. C.; Simpson, D. G., Measuring fiber alignment in electrospun scaffolds: a user's guide to the 2D fast Fourier transform approach. *Journal of Biomaterials Science-Polymer Edition* **2008,** 19, (5), 603-621.
70. Du, N.; Liu, X. Y.; Narayanan, J.; Li, L. A.; Lim, M. L. M.; Li, D. Q., Design of superior spider silk: From nanostructure to mechanical properties. *Biophysical Journal* **2006,** 91, (12), 4528-4535.
71. Corey, J. M.; Lin, D. Y.; Mycek, K. B.; Chen, Q.; Samuel, S.; Feldman, E. L.; Martin, D. C., Aligned electrospun nanofibers specify the direction of dorsal root ganglia neurite growth. *Journal of Biomedical Materials Research Part A* **2007,** 83A, 636-645.
72. Yakobson, B. I.; Couchman, L. S., Persistence length and nanomechanics of random bundles of nanotubes. *Journal of Nanoparticle Research* **2006,** 8, (1), 105-110.

73. Sano, M.; Kamino, A.; Okamura, J.; Shinkai, S., Ring closure of carbon nanotubes. *Science* **2001,** 293, (5533), 1299-1301.
74. Kaji, N.; Ueda, M.; Baba, Y., Direct measurement of conformational changes on DNA molecule intercalating with a fluorescence dye in an electrophoretic buffer solution by means of atomic force microscopy. *Electrophoresis* **2001,** 22, (16), 3357-3364.
75. Lee, H. S.; Yun, C. H.; Kim, H. M.; Lee, C. J., Persistence length of multiwalled carbon nanotubes with static bending. *Journal of Physical Chemistry C* **2007,** 111, (51), 18882-18887.

Chapter V

Next Generation Electronic Materials

A. Smart Electronic Yarns and Wearable Fabrics Made by CNT Coating

1. Summary

The idea of electronic yarns and textiles appeared quite some time, but their properties often do not meet practical expectations.[1-3] In addition to chemical/mechanical durability and high electrical conductivity, important materials qualifications include weavablity, wearability, light weight, and "smart" functionalities. Here we demonstrate a simple process of transforming general commodity cotton threads into intelligent e-textiles using a polyelectrolyte-based coating with CNTs. Efficient charge transport through the network of nanotubes (20 Ω/cm) and the possibility to engineer tunneling junctions make them promising materials for many high knowledge-content garments. Along with integrated humidity sensing, we demonstrate that CNT/cotton threads can be used to detect albumin, the key protein of blood, with high sensitivity and selectivity. Notwithstanding future challenges, these proof-of-concept demonstrations provide a direct pathway for the application of these materials as wearable biomonitoring and telemedicine sensors, which are simple, sensitive, selective, and versatile.

2. Introduction

Nanocomposites have the potential to significantly surpass the properties of conventional bulk materials such as ceramics and metals.[4] Among widespread nanoscale building blocks, such as organic or inorganic nanowires and nanodots, CNTs are regarded as one of the most versatile because of their superior mechanical and electrical properties and geometrical perfection.[5] CNT composites have been made in the form of bulk monoliths,[6] sheets, fibers,[7, 8] and yarns[9] for subsequent manufacturing of high-strength composites and laminates. Dilute CNT solutions have also been used to prepare transparent flexible conductive films[10] and electronic inks[11] for printed electronics[12] and optoelectronic devices[13]. CNT yarns have also been applied in electronics applications such as field-emission filaments.[14] However, Atkinson *et al.* have reported that current CNT-based yarns are not very suitable for general electronic textile (e-textile) applications because of basic scaling issues when moving from micron-/nano-sized single CNT fibers and yarns to mm–thick, multi-strand forms.[15] In textile-related applications, CNT yarns have been made by direct drawing from CNT forests[9, 16] and, in some cases, dyeing process have been applied to commercial fabrics in order to impregnate them with nanotubes.[17, 18] However, vast majority of the studies on textile modification with nanomaterials was carried with nanoparticles.[19-23] The reasons for addition of metal and semiconductor nanoparticles to fabrics were the following: fashionably glittering colors, antimicrobial function; UV protection, wrinkle resistance and anti odor function.[19-23] Development of smart fabrics with biomonitoring functionalities has great importance for

a variety of health conditions and professions, which was so far accomplished only with quite clumsy, heavy, and complex optical detectors integrated in the fabric.[24]

The essential qualities of e-textiles include wearability, weaveability, and flexibility as well as electrical conductivity.[1-3] The combination of these properties can lead to tremendous changes in the technology and functionality of apparel, starting with advanced clothing for high-risk professions, medical monitoring, and integrated communication.[25] Conductive metal wires and other rigid fibers have been used in the past to demonstrate proof-of-concept wearable electronics.[26] Unfortunately, these materials do not provide textiles with sufficient biological compatibility, flexibility, durability, and mobile comfort as well as intelligent functionalities like integrated smart sensing.[27] The manufacturing process of these fibers is also quite complex.

In this chapter, cotton yarn has been coated with CNTs and polyelectrolytes. This method provides a fast, simple, robust, low-cost, and readily scalable process for making e-textiles, reminiscent of LBL assembly processes used before.[19, 28] The resulting CNT/cotton yarns showed high electrical conductivities as well as some functionality due to biological modification of inter-nanotube tunneling junctions. When the CNT/cotton yarn incorporated anti-albumin, it became an e-textile biosensor that quantitatively and selectively detected albumin, the essential protein in blood. The same sensing approach can easily be extended to many other proteins and biomolecules.

3. Preparation and Characterization of E-Textiles

SWNTs and MWNTs were dispersed in dilute Nafion^{TM}-ethanol[29] or PSS-water solutions. A general commodity cotton thread (1.5 mm in diameter) was dipped in the prepared CNT dispersions and dried (Figure 36 A, B). Dipping technique for modifying fabric is the most convenient way of processing of fabric and should be considered as a great advantage of the described method because of simplicity and simple integration with existing processing steps. After several repetitive dips, the cotton thread became conductive with a resistivity as low as 20 Ω/cm. (Note that the units of resistivity used here are Ω/cm which is reflective of the one-dimensional nature of threads. Calculation of the resistivity in the form similar to metal wires is impossible for the case of coated fibers because of uncertainty with the total volume and cross-sectional area of the conductive layers). As a demonstration of the conductivity, we easily powered an LED device connected to a battery by the prepared threads (Figure 36 C).

Once the adsorbed CNT/cotton threads were dried, it was impossible to remove the adsorbed CNTs from the fibers by exposure to solvents, heat, or a combination of both. The incorporation of CNTs into the cotton yarn was much more efficient than their adsorption into carbon fibers, which was tried elsewhere.[30] This could be a result of the efficient interaction of polyelectrolytes with cotton and other natural polysaccharide- and cellulose-based materials, such as paper,[31] which is well known in industry.[32] Additionally, the flexibility of the CNTs allowed them to conform to the surface of the cotton fibers.

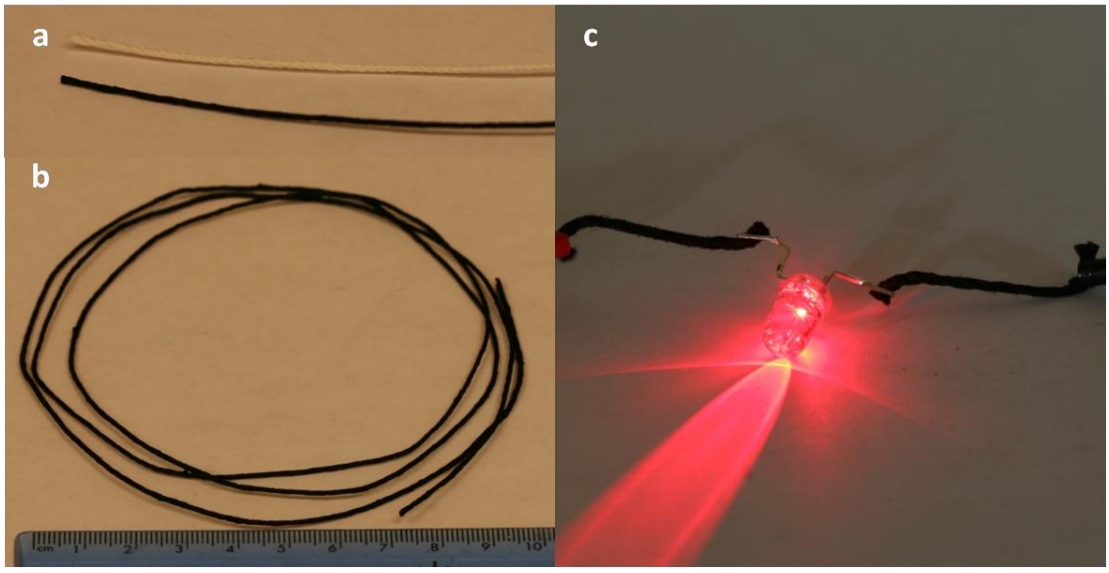

Figure 36 Photographs of SWNT-cotton yarn. (A) Comparison of the original and surface modified yarn. (B) 1 m-long piece as made. (C) Demonstration of LED emission with the current passing through the yarn.

The morphology of CNT/cotton yarns were observed by SEM (Figure 37). Both SWNTs and MWNTs stabilized in Nafion™ seamlessly cover the exterior of every strand of cotton yarn so that numerous electrical carrier paths can be formed. The weight ratio of CNTs and Nafion™ in the dispersion was 1:1 in both cases, which is well above than percolation threshold of the solid composites. The lower limit of CNT loading in polymers is around 0.002 wt%, although it significantly varies with the molecular distribution in composite structures and the degree of CNT exfoliation.[33] The differences between SWNT and MWNT coatings can also be seen. SWNTs form a tighter and more dispersed network than large and rigid MWNTs, easily recognizable even at fairly low magnifications (Figure 37 D). One should expect substantially different electrical

transport properties because it has been demonstrated that the uniformity of nanotube distribution strongly affects both strength and conductivity of CNT composites.[34]

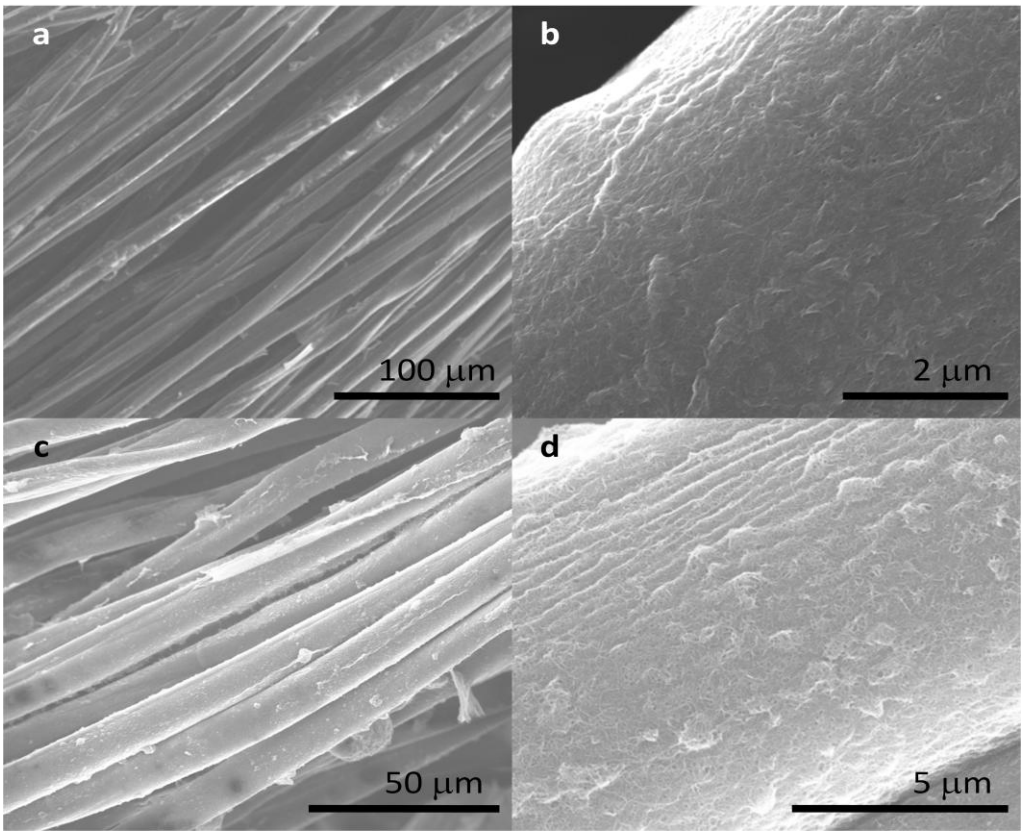

Figure 37 SEM images of e-textiles. SWNT-Nafion™ coated (A, B) and MWNT-Nafion™ coated (C, D) cotton threads after one dipping cycle.

We tested the dependence of the conductivity of the prepared CNT/cotton yarns on several experimental parameters: the type of CNT and polymer, CNT-polymer ratio, and deposition technique (Figure 38 A). For the same CNT-polymer ratio, yarn made from Nafion™-stabilized CNTs in ethanol is 2 orders of magnitude more

conductive than that made from PSS-stabilized CNTs in water. In more quantitative terms, MWNT-Nafion™ yarn obtained after 10 deposition cycles exhibited a resistivity of 118 Ω/cm. Similarly processed yarn comprised of SWNTs exhibited resistivities as low as 25 Ω/cm. Post-processing acid treatment[35] and thermal annealing[34] reduced the resistivity of SWNT-Nafion™ yarn even further, 40% (15 Ω/cm) and 23% (19 Ω/cm), respectively. In comparison with other electronic textiles, fabrics, and threads, the resistivity of the yarn in Figure 36 is two orders of magnitude lower than the resistivity of comparable CNT-dyed textiles (7.8 kΩ/cm).[17] Furthermore, the reported resistivity of 1 cm-long yarn drawn from CNT forests is at best, if converted to the scale used here, in the range of a few kΩ/cm.[14, 36]

The strength of the CNT/cotton yarn is more than 2 times higher than that of the original cotton thread due to a reduction of the overall diameter, densification and stronger adhesion of the fibers to each other by the polymer material. The mechanical property data of the original cotton and CNT-coated yarn are: ultimate yield strength, 41.6 MPa and 87.8 MPa; initial modulus, 140 MPa and 342 MPa; and tensile breaking strain, 0.36 and 0.28, respectively. The density-normalized breaking energy is 65 kJ/kg for both threads, which indicates that most of the energy is absorbed by the structural cotton backbone. Even though the cotton yarn became slightly harder after being coated with SWNTs, it is still very flexible and soft, both of which are important for the wearability of electronic fabric. Single exposure of the produced yarn to different solvents imitating washing did not appreciably affect the electrical properties.

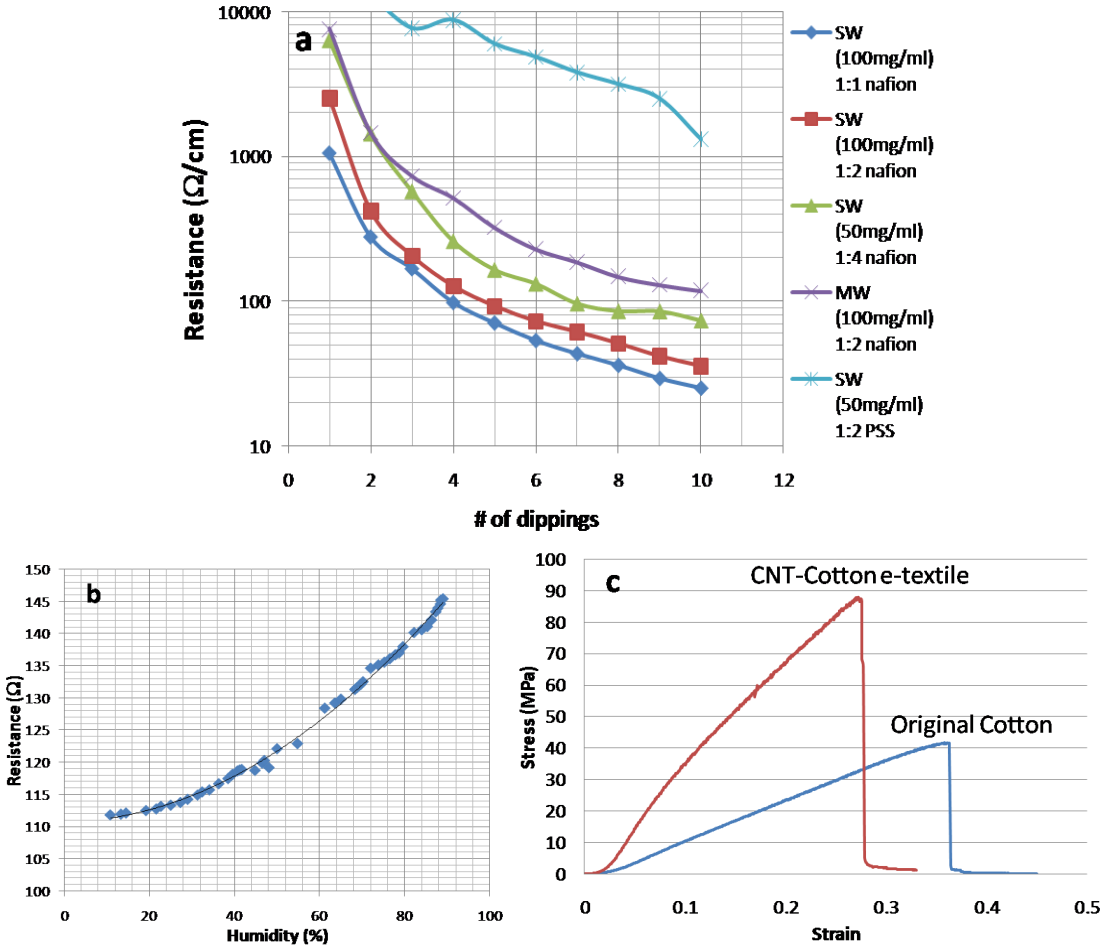

Figure 38 Physical properties of CNT-cotton yarn. (A) Dependence of electrical resistance on the CNT nature, polymer structure, and number of dipping cycles. (B) Effect of humidity on electrical resistance (tested at 20°C). (C) Stress-strain curves for the CNT-cotton yarn and the original cotton thread.

4. Humidity Sensor Application of E-Textiles

The fairly low electrical resistance of CNT/cotton yarn allows for convenient sensing applications which may not require any additional electronics or converters. At the same time, too high metallic conductance will be a disadvantage for sensing because

it will reduce dynamic range and increase the power control accuracy necessary for sensing. If the high conductivity fabrics made here becomes a problem, it can always be reduced to the necessary values as described in Figure 38 A. When considering sensing applications, we also need to take into account the polymer's characteristics in order to maximize the signal-to-noise ratio and sensing linearity in different environments. PSS is more hydrophilic than Nafion™, and, thus, CNT-Nafion™ is more advantageous for dry-state sensing while CNT-PSS will be more advantageous in humid conditions. For intelligent fabric demonstrations, the CNT-Nafion™ yarn was tested as a humidity sensor in a dry state while CNT-PSS yarn served as a wet-state bio-sensor platform.

The electrical resistance of 5 cm-long SWNT-Nafion™ yarn was measured in air by varying the humidity between 10 and 90% (Figure 38 B). As the humidity was raised, the resistance increased. This is most likely a result of reversible hygroscopic swelling of both Nafion™ and cotton, which readily disrupts the electron transport between CNTs. The change in the resistance was almost instantaneous, and the signal was strong even in the very dry conditions of 20% humidity. Sensitivity to humidity changes also gives a good indication of the so-called "breathability" of the material, which is also an important parameter for smart fabrics.

5. Bio-Sensor Application of E-Textiles

Another example of an integrated, functional biosensor was demonstrated using SWNT-PSS yarn. We chose the antigen/antibody reaction between human serum albumin

(HSA) and its respective immunoglobulin (IgG) anti-HSA for several reasons: (1) this is a model system that can be generalized to many other relevant antigen/antibody systems of interest; (2) albumin is the key protein of blood and can be used to sense bleeding, which in extreme situations may be impossible to detect by any other method, which is of key importance for many high-risk occupations; and (3) monitoring physiological health conditions should be one of the key functions of smart clothes.

PSS is known as an excellent stabilizer of proteins and can be used to form a LBL film with IgG antibodies.[37, 38] We added anti-HSA directly to the SWNT-PSS solution and coated the cotton yarn as before. The CNT-IgG/cotton yarn was frozen and then dried under vacuum in order to minimize antibody denaturation. This cycle was repeated three times before use. For sensing experiments, two different albumin proteins were used; human serum albumin (HSA, 67 kDa) and bovine serum albumin (BSA, 66 kDa). Each experiment involved the measurements of conductivity of yarns being in contact with a 500 μl aqueous volume of water. 50 μl aliquots of bovine and human albumins at different concentration were added to this starting volume. Different concentrations of albumin were obtained by ×1000, ×100, and ×10 dilution of the stock solution (denoted as x1 dilution) of corresponding albumins: 11.9 μM for HSA and 30 μM for BSA. Detection of the antigen with CNT-IgG/cotton yarn was very sensitive and selective. The presence of analyte around the CNT-IgG/cotton yarn was indicated by an increase in conductivity (Figure 39 A, B). The detectable concentration of HSA was as low as 119 nM (Figure 38 A, ×100), producing a signal drop of 2980 Ω, which is a 2.5% change from the baseline. As a reference, the HSA concentration in our blood ranges from 446

μM to 746 μM. The high sensitivity obtained in these experiments is comparable or exceeds that of sensing devices based on surface modified cantilevers similar to those used in AFM.[39] Needles to say that the SWNT yarns are much simpler and possibly a more affordable system than nanomechanical sensor arrays. At the same time, the selectivity of the SWNT-cotton yarn sensor was also high. Structurally similar BSA at a concentration as high as 30 μM (Figure 39 B, ×1) produced only a small signal change of 1100 Ω (0.49% of the base) in the sensor aimed for detection of human albumin. It is also important to highlight the fact that we used in this work electrical methods of analyte detection as opposed to optical means as being done in other approaches to biomonitoring with smart fabric being developed in several European institutions.[24] Optical components are more expensive, complex, and have greater power requirements.

The signal transduction mechanism is believed to involve the release or significant rearrangement of IgGs from the CNT/cotton yarn. Negatively-charged HSA reacts with anti-albumin, which is followed by the process of expulsion from the SWNT-cotton matrix by the negatively charged polyelectrolyte, such as PSS. As a result, more extensive SWNT contacts are formed producing a more conductive network, resulting in the drop of the resistance. Because the contact resistance between SWNTs is affected by changes in the tunneling junction as small as a few angstroms, the removal or rearrangement of large protein macromolecules with diameters of a few nanometer results in a very substantial change in resistivity as one can see above from exceptional sensitivity obtained. SEM observations and cyclic voltammetry (CV) measurements corroborate the suggested signal transduction mechanism. SEM images show substantial

restructuring upon exposure to the target protein. Before the biosensing reaction, the SWNT-PSS-anti-HSA coating displays a wavy morphology (Figure 39 F, G), which likely originates from the drying of frozen SWNT-PSS-anti-HSA yarn under vacuum. After HSA detection, the wavy structures have disappeared; flat coatings with clearly visible SWNT networks can be seen. While we cannot distinguish whether the reacted antibody was released from the nanocomposite or simply rearranged, it is evident that after reaction with HSA, the SWNTs formed a more compact phase and, thus, more efficient percolation routes. These observations were further validated by CV measurements in which the anti-HSA coated smart yarn was set as a working electrode. CV data indicate a clear increase of conductivity of the smart fabric upon the less diluted antigen proteins (Figure 39 C) in solution confirming the partial removal of the insulating spacing between the SWNTs. This effect is clearly absent when no antibody was incorporated between the nanotubes (Figure 39 D).

The suggested signal transduction mechanism implies one-time sensing upon complete removal of the antibodies, or cumulative sensing of the protein until it has been completely removed. From a fundamental standpoint, it would be interesting to engineer a coating with reversible sensing functionality. From a practical standpoint, however, which must consider (1) the limited life-time of antibodies and (2) the actual circumstances that can result in the appearance of blood, the multiple use of this sensor is unlikely. So, the reversible sensor to HSA might be interesting from academic point of view but its practicality is questionable.

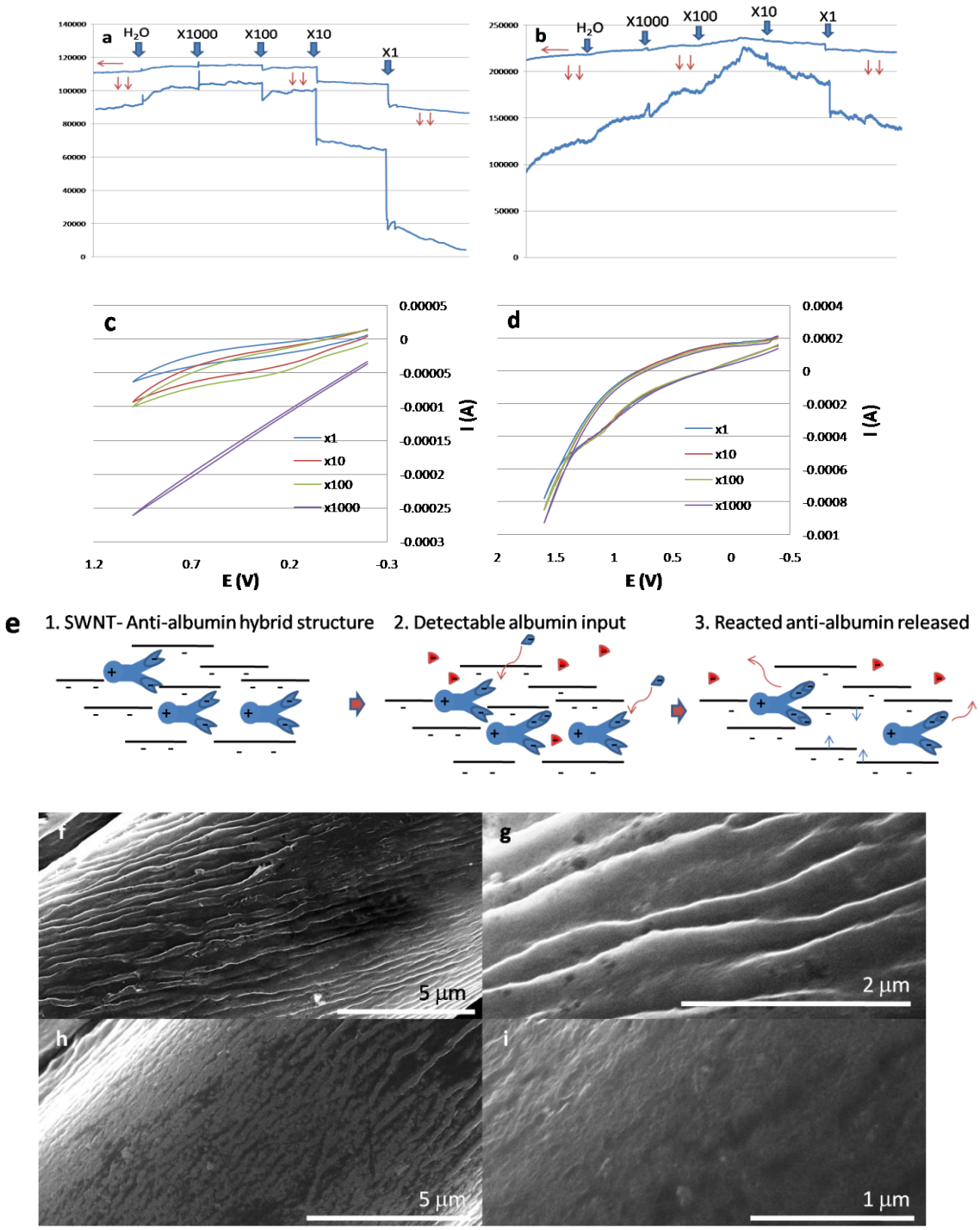

Figure 39 Demonstration of the biosensing functionality of SWNT-modified yarn using a generic antibody-antigen reaction. (A) Effect of the concentration of HSA (11.9 µM at ×1 dilution) and (B) BSA (30 µM at ×1 dilution) on conductivity of a CNT-PSS-anti-HSA coated yarn. (C, D) Cyclic voltammetry measurements of HSA (11.9 µM at ×1 dilution) on (C) a CNT-PSS-anti-HSA coated yarn and (D) a CNT-PSS yarn (E)

Suggested detection mechanism of antibody-antigen reaction. SEM images before (F, G) and after (H, I) the antibody/antigen reaction.

6. Conclusion

In summary, the conductive SWNT-modified cotton yarn obtained as described here offers a uniquely simple yet remarkably functional solution for wearable electronics and smart textiles, with many parameters exceeding the existing technological solutions, including those using carbon materials. From the proof-of-concept biosensor demonstrated here, we believe that further development of these materials could potentially include (1) reversible sensing schemes for relevant biological compounds/markers, (2) various sensors for body functions including monitoring of degree of contusion/blast damage, and (3) multiplexed sensing of 5-6 analytes with yarns modified in different ways. We also might add that energy harvesting materials and fabrics with charge storage capabilities are also possible for the fabrics described here. The latter goal could be the most challenging but nevertheless suitable for the SWNT-cotton composite because of the nature of CNTs, the fairly high conductivity obtained, and supercapacitor properties of carbon nanotubes. As a final note, we also need to note that the toxicological issues of CNTs, extensive cell-culture data indicates that the solid CNT-polymer composites are largely benign.[40, 41] Nevertheless, the question of long-term contact between skin and SWNTs should be investigated further.

Reference

1. Post, E. R.; Orth, M.; Russo, R. R.; Gershenfeld, N., E-broidery: Design and fabrication of textile-based computing. *IBM SYSTEMS JOURNAL* **2000,** 39, (3&4), 840-860.
2. Service, R. F., Technology: Electronic textiles charge ahead. *Science* **2003,** 301, (5635), 909-911.
3. Coyle, S.; Wu, Y.; Lau, K. T.; De Rossi, D.; Wallace, G.; Diamond, D., Smart nanotextiles: a review of materials and applications. *MRS Bull.* **2007,** 32, (5), 434-442.
4. Hogg, P. J., Composites in armor. *Science* **2006,** 314, (5802), 1100-1101.
5. Baughman, R. H.; Zakhidov, A. A.; de Heer, W. A., Carbon nanotubes-the route toward applications. *Science* **2002,** 297, (5582), 787-792.
6. Cao, A. Y.; Dickrell, P. L.; Sawyer, W. G.; Ghasemi-Nejhad, M. N.; Ajayan, P. M., Super-compressible foamlike carbon nanotube films. *Science* **2005,** 310, (5752), 1307-1310.
7. Dalton, A. B.; Collins, S.; Munoz, E.; Razal, J. M.; Ebron, V. H.; Ferraris, J. P.; Coleman, J. N.; Kim, B. G.; Baughman, R. H., Super-tough carbon-nanotube fibres. *Nature* **2003,** 423, (6941), 703.
8. Koziol, K.; Vilatela, J.; Moisala, A.; Motta, M.; Cunniff, P.; Sennett, M.; Windle, A., High-Performance Carbon Nanotube Fiber. *Science* **2007,** 318, 1892-1895.
9. Zhang, M.; Atkinson, K. R.; Baughman, R. H., Multifunctional Carbon Nanotube Yarns by Downsizing an Ancient Technology. *Science* **2004,** 306, (5700), 1358-1361.
10. Wu, Z.; Chen, Z.; Du, X.; Logan, J. M.; Sippel, J.; Nikolou, M.; Kamaras, K.; Reynolds, J. R.; Tanner, D. B.; Hebard, A. F.; Rinzler, A. G., Transparent, conductive carbon nanotube films. *Science* **2004,** 305, (5688), 1273-1277.
11. Park, J. U.; Hardy, M.; Kang, S. J.; Barton, K.; Adair, K.; Mukhopadhyay, D. k.; Lee, C. Y.; Strano, M. S.; Alleyne, A. G.; Georgiadis, J. G.; Ferreira, P. M.; Rogers, J. A., High-resolution electrohydrodynamic jet printing. *Nat.Mater.* **2007,** 6, (10), 782-789.
12. Beecher, P.; Servati, P.; Rozhin, A.; Colli, A.; Scardaci, V.; Pisana, S.; Hasan, T.; Flewitt, A. J.; Robertson, J.; Hsieh, G. W.; Li, F. M.; Nathan, A.; Ferrari, A. C.; Milne, W. I., Ink-jet printing of carbon nanotube thin film transistors. *J.Appl.Phys.* **2007,** 102, (4), 043710/1-043710/7.
13. Hatton, R. A.; Miller, A. J.; Silva, S. R. P., Carbon nanotubes: a multi-functional material for organic optoelectronics. *Journal of Materials Chemistry* **2008,** 18, (11), 1183-1192.
14. Zakhidov, A.; Nanjundaswamy, R.; Obraztsov, A. N.; Zhang, M.; Fang, S.; Klesch, V. I.; Baughman, R. H.; Zakhidov, A. A., Field emission of electrons by carbon nanotube twist-yarns. *Appl.Phys.A: Mater.Sci.Process.* **2007,** 88, (4), 593-600.
15. Atkinson, K. R.; Hawkins, S. C.; Huynh, C.; Skourtis, C.; Dai, J.; Zhang, M.; Fang, S.; Zakhidov, A. A.; Lee, S. B.; Aliev, A. E.; Williams, C. D.; Baughman, R. H., Multifunctional carbon nanotube yarns and transparent sheets: Fabrication, properties, and applications. *Phys.B* **2007,** 394, (2), 339-343.

16. Jiang, K.; Li, Q.; Fan, S., Spinning continuous carbon nanotube yarns. *Nature* **2002,** 419, (6909), 801.
17. in het Panhuis, M.; Wu, J.; Ashraf, S. A.; Wallace, G. G., Conducting textiles from single-walled carbon nanotubes. *Synth.Met.* **2007,** 157, (8-9), 358-362.
18. Liu, Y.; Tang, J.; Wang, R.; Lu, H.; Li, L.; Kong, Y.; Qi, K.; Xin, J. H., Artificial lotus leaf structures from assembling carbon nanotubes and their applications in hydrophobic textiles. *J.Mater.Chem.* **2007,** 17, (11), 1071-1078.
19. Hyde, K.; Rusa, M.; Hinestroza, J., Layer-by-layer deposition of polyelectrolyte nanlayers on natural fibres: cotton. *Nanotechnology* **2005,** 16, (7), S422-S428.
20. Hyde, G. K.; Park, K. J.; Stewart, S. M.; Hinestroza, J. P.; Parsons, G. N., Atomic layer deposition of Conformal inorganic nanoscale coatings on three-dimensional natural fiber systems: Effect of surface topology on film growth characteristics. *Langmuir* **2007,** 23, (19), 9844-9849.
21. Perelshtein, I.; Applerot, G.; Perkas, N.; Guibert, G.; Mikhailov, S.; Gedanken, A., Sonochemical coating of silver nanoparticles on textile fabrics (nylon, polyester and cotton) and their antibacterial activity. *Nanotechnology* **2008,** 19, (24).
22. Becheri, A.; Durr, M.; Lo Nostro, P.; Baglioni, P., Synthesis and characterization of zinc oxide nanoparticles: application to textiles as UV-absorbers. *Journal of Nanoparticle Research* **2008,** 10, (4), 679-689.
23. Yuen, C. W. M.; Ku, S. K. A.; Kan, C. W.; Cheng, Y. F.; Choi, P. S. R.; Lam, Y. L., Using nano-TiO2 as co-catalyst for improving wrinkle-resistance of cotton fabric. *Surface Review and Letters* **2007,** 14, (4), 571-575.
24. Pasche, S.; Angeloni, S.; Ischer, R.; Liley, M.; Lupranoe, J.; Voirinf, G., Wearable Biosensors for Monitoring Wound Healing. *Advances in Science and Technology* **2008,** 57, 80-87.
25. Carpri, F.; De Rossi, D., Electroactive Polymer-Based Devices for e-Textiles in Biomedicine. *IEEE Transactions on Information Technology in Biomedecine* **2005,** 9, (3), 295-318.
26. Billinghurst, M.; Starner, T., Wearable Devices: New Ways to Manage Information. *Computer* **1999,** 32, (1), 57-64.
27. Winterhalter, C. A.; Teverovsky, J.; Wilson, P.; Slade, J.; Farell, B.; Horowitz, W.; Tierney, E., Development of electronic textiles to transport data and power in future U.S. military protective clothing systems. *J.ASTM Int.* **2005,** 2, (7), No.
28. Hyde, K.; Dong, H.; Hinestroza, J. P., Effect of surface cationization on the conformal deposition of polyelectrolytes over cotton fibers. *Cellulose* **2007,** 14, (6), 615-623.
29. Wang, J.; Musameh, M.; Lin, Y., Solubilization of carbon nanotubes by nafion toward the preparation of amperometric biosensors. *J.Am.Chem.Soc.* **2003,** 125, (9), 2408-2409.
30. Bekyarova, E.; Thostenson, E. T.; Yu, A.; Kim, H.; Gao, J.; Tang, J.; Hahn, H. T.; Chou, T. W.; Itkis, M. E.; Haddon, R. C., Multiscale Carbon Nanotube-Carbon Fiber Reinforcement for Advanced Epoxy Composites. *Langmuir* **2007,** 23, (7), 3970-3974.

31. Zheng, Z.; McDonald, J.; Khillan, R.; Su, Y.; Shutava, T.; Grozdits, G.; Lvov, Y. M., Layer-by-layer nanocoating of lignocellulose fibers for enhanced paper properties. *J.Nanosci.Nanotechnol.* **2006,** 6, (3), 624-632.
32. Blackburn, R. S.; Burkinshaw, S. M., A greener approach to cotton dyeings with excellent wash fastness. *Green Chem.* **2002,** 4, (1), 47-52.
33. Yao, S. H.; Dang, Z. M.; Jiang, M. J.; Xu, H. P., Influence of aspect ratio of carbon nanotube on percolation threshold in ferroelectric polymer nanocomposite. *Applied Physics Letters* **2007,** 91, (21).
34. Shim, B. S.; Tang, Z.; Morabito, M. P.; Agarwal, A.; Hong, H.; Kotov, N. A., Integration of Conductivity, Transparency, and Mechanical Strength into Highly Homogeneous Layer-by-Layer Composites of Single-Walled Carbon Nanotubes for Optoelectronics. *Chem.Mater.* **2007,** 19, (23), 5467-5474.
35. Geng, H. Z.; Kim, K. K.; So, K. P.; Lee, Y. S.; Chang, Y.; Lee, Y. H., Effect of Acid Treatment on Carbon Nanotube-Based Flexible Transparent Conducting Films. *J.Am.Chem.Soc.* **2007,** 129, (25), 7758-7759.
36. Aliev, A. E.; Guthy, C.; Zhang, M.; Fang, S.; Zakhidov, A. A.; Fischer, J. E.; Baughman, R. H., Thermal transport in MWCNT sheets and yarns. *Carbon* **2007,** 45, (15), 2880-2888.
37. Caruso, F.; Niikura, K.; Furlong, D. N.; Okahata, Y., Assembly of Alternating Polyelectrolyte and Protein Multilayer Films for Immunosensing. *Langmuir* **1997,** 13, (13), 3427-3433.
38. Lvov, Y.; Ariga, K.; Ichinose, I.; Kunitake, T., Assembly of Multicomponent Protein Films by Means of Electrostatic Layer-by-Layer Adsorption. *J.Am.Chem.Soc.* **1995,** 117, (22), 6117-6123.
39. Fritz, J.; Baller, M. K.; Lang, H. P.; Rothuizen, H.; Vettiger, P.; Meyer, E.; Guntherodt, H. J.; Gerber, C.; Gimzewski, J. K., Translating biomolecular recognition into nanomechanics. *Science* **2000,** 288, (5464), 316-318.
40. Jan, E.; Kotov, N. A., Successful differentiation of mouse neural stem cells on layer-by-layer assembled single-walled carbon nanotube composite. *Nano Letters* **2007,** 7, (5), 1123-1128.
41. Gheith, M. K.; Pappas, T. C.; Liopo, A. V.; Sinani, V. A.; Shim, B. S.; Motamedi, M.; Wicksted, J. P.; Kotov, N. A., Stimulation of neural cells by lateral currents in conductive layer-by-layer films of single-walled carbon nanotubes. *Advanced Materials* **2006,** 18, (22), 2975-2979.

Chapter VI

Conclusion and Future Research Direction

A. Conclusion of Thesis

In this thesis, I presented LBL assembly of CNT materials design with emphasis of bridging the properties of CNTs to the real world applications. Combinations of superior properties of SWNTs and excellent nanostructural controllability of LBL assembly provided great opportunities to create new class of materials. Indeed, SWNTs and LBL assemblies have shown many 'Miracles of Science', and I am the one who observed those. One SWNT LBL assembled nanocomposite has demonstrated their stronger, tougher, and stiffer properties simultaneously. Another LBL coating with black SWNTs has displayed more conductive, more transparent, and stronger properties at a same time. I should indicate that, however, the potential of this CNT LBL assembly has not yet been fully developed. This thesis provides only a little starting point of the quest to a big 'Blue Ocean' of this nanotechnology: Molecularly controlled LBL assembly with multi-functional CNTs.

I also hope that this thesis presented right understandings, opportunities, and promises of LBL assembly to search the next generation multi-component functional

materials. Molecular-scale structural tuning and wide ranges of materials option of LBL assembly will further enrich our materials life in future world. Surely, this LBL assembly of multi-component functional materials allows anyone to have the most powerful tools to probe challenging future complex materials design and process.

B. Future Research Direction

My future research aim is to bridge nano-scale functional properties to real world applications by molecularly controlled assemblies. This research is one of the most crucial parts of the next generation complex material systems because of the difficulty and insufficiency of transferring superior nanomaterials' properties to the macro-scale applications. The strategies are focusing on the experimental preparations of (1) ***thermoelectric (TE) energy conversion material systems,*** (2) ***transparent, stretchable, electronic materials***, and fundamental studies of (3) ***macro-scale materials properties tailored by nanostructures***. The emphasis of my research will be low-cost, large-scale, high-throughput, and robust materials processing in which I am specialized.

More explicitly, my future research will have the following directions:

- Preparation of soft TE nanocomposites from one-dimensional nanowires (NWs). This requires the fundamental understanding of phonon scattering and electron conduction at the interfaces of NWs as well as precise assembly techniques enabling molecular scale control. The nanocomposites will be fabricated towards

a light weight, flexible, and high efficient TE energy generator for replacing batteries in micro-scale prosthetics and robots, as well as for processing of large-scale flexible thin film energy generators.

- Preparation of the next generation transparent, stretchable, electronic materials for the applications of smart windows, roll-to-roll solar cells, biomedical devices, and many emerging flexible electronics. Furthermore, doping and buckling conditions of CNTs and wide range of polymeric matrix will add smart functionality such as environmental condition monitoring, responsive optical and mechanical transduction.
- Fundamental studies of micro-/nano- structures and material components for improving functional performances such as thermoelectric, mechanical, electrical, thermal, optical, and photovoltaic properties. The expertise on advanced LBL processes such as combing, dewetting, spin-assisted, and all-nanomaterial methods will be benefited in verifying the effects of the complex nanostructures. Furthermore, the nanocomposite design will be extended to biomimetic material approaches, inspired by biological materials where their versatility, adaptability, and performance are often superior to many man-made ceramics and composites.